Alma Mater Studiorum – Università di Bologna

DOTTORATO DI RICERCA IN

GEOFISICA

Ciclo XXVI

Settore Concorsuale di afferenza: 04 / A4 – Geofisica

Settore Scientifico disciplinare: GEO / 10 – Geofisica della Terra Solida

GROUND PENETRATING RADAR EARLY-TIME TECHNIQUE FOR SOIL ELECTROMAGNETIC PARAMETERS ESTIMATION

Presentata da: **Carlotta Ferrara**

Coordinatore Dottorato **Relatore**

Prof. Michele Dragoni **Prof. Elena Pettinelli**

Esame finale anno 2014

Abstract

In recent years, thanks to the technological advances, electromagnetic methods for non-invasive shallow subsurface characterization have been increasingly used in many areas of environmental and geoscience applications. The quantitative evaluation of the electromagnetic properties of a material is an important goal for multiple purposes in many fields of application such as environmental physics, geophysical and hydro-geophysical investigations, civil engineering, precision agriculture and forestry, forensics, military and rescue uses, archaeology and planetary exploration.

One of the most interesting aspects of the methodological development of electromagnetic techniques is to use multi-technology integrated approaches, which allows to monitor different physical parameters. In particular, the geophysical electromagnetic methods are strongly sensitive to the volumetric water content (permittivity of liquid water is much higher than other geological constituents) and, in general, to water content variations, responding primarily to the bulk dielectric permittivity of the medium.

As well known, electromagnetic techniques are based on the propagation of a signal in an investigated medium, detecting and recording the anomaly with different modalities depending on the chosen technique. Among all the geophysical electromagnetic methods, the Ground Penetrating Radar (GPR) has received unprecedented attention over the last few decades due to its capability to obtain, spatially and temporally, high-resolution electromagnetic parameter information. Moreover, GPR is a particular technique well suited to different types of research in multiple areas for its versatility, its handling, its non-invasive nature, its high resolving power, and its fast implementation.

The main focus of this thesis is to perform a dielectric site characterization in a quick, efficient and accurate way studying in-depth a physical phenomenon behind a recent developed GPR approach, the so-called early-time technique, which infers the electrical properties of the soil in the proximity of the antennas. Moreover, the GPR results obtained with this alternative early-time GPR method were compared with the results coming from other more usual techniques, such as NMR (Nuclear Magnetic Resonance), TDR (Time Domain Reflectometry), gravimetric measurements, more conventional GPR data analysis (e.g., CMP - Common Mid Point, etc.), and also with a theoretical model, which numerically simulates the GPR response.

In particular, the early-time approach is based on the amplitude analysis of the early-time portion of the GPR waveform using a fixed-offset ground-coupled antenna configuration where the separation between the transmitting and receiving antenna is on the order of the dominant pulse-wavelength. Under these conditions, the early-time signal is a complex superposition of the air and ground

waves, whereby the ground wave velocity cannot be measured using traditional GPR travel time techniques. However, other measurable attributes of the transmitted signal, such as the wavelet amplitude, duration, and shape, contain information about the physical properties of the near-surface material. Amplitude information can be extracted from the early-time signal through complex trace analysis, computing the instantaneous-amplitude attributes over a selected time-duration of the early-time signal. Basically, if the acquired GPR signals are considered to represent the real part of a complex trace, and the imaginary part is the quadrature component obtained by applying a Hilbert transform to the GPR trace, the amplitude envelope is the absolute value of the resulting complex trace (also known as the instantaneous-amplitude).

As mentioned above, to test this novel approach, a first controlled laboratory experiment was specifically designed to study the effect of the electromagnetic properties variations on the antenna-material coupling, minimizing the influence of both surface roughness and heterogeneity. Not only the early-time GPR signal was used to map the near surface lateral distribution of the dielectric parameters, induced by changing the shallow water content on the tested material, but such results were also compared to a portable unilateral NMR sensor, which is able to determine the water content variation in the material on the basis of the measured proton density. The direct comparison was possible because the NMR exposes the object to the coil stray field in a configuration similar to the one used to radiate the EM field from GPR antennas. First of all, the results show a matching pattern of the physical parameters measured with the two different techniques, and a very high degree of correlation between the radar early-time signal average amplitude and the intensity of the NMR signal which is proportional to the proton density, i.e. to the water content. Then, this experiment suggests that the early-time technique can be used as a fast and high spatial resolution tool for qualitatively mapping dielectric permittivity variations in a material at shallow depth.

Based on these encouraging results, numerical analyses and more experimental investigations were performed with the aim of analysing the features related to the early-time method.

Primarily, the possibility to evaluate the soil dielectric parameters features from the first-arrival signal attributes in ground-coupled radars is studied together with a numerical analysis derived by implementing suitably a full-wave numerical modelling. Moreover, till this stage, the early-time technique has been tested on GPR data only with the aim of evaluating the effect of permittivity; the influence of conductivity has been never analysed. Therefore, a specific second laboratory experiment was design with the aim of detecting the variations of the electric conductivity in a porous medium having a uniform permittivity, and comparing the early-time results with the conductivity measured in parallel with TDR. Both experimental and numerical data have obtained a very strong correlation between the early-wavelet amplitudes and the shallow-soil dielectric conductivity derived from TDR measurements, indicating, once more, that the near-surface

electromagnetic properties of the material can be directly extracted from the GPR early-time amplitude technique.

It is worth noticing that both controlled experiments and numerical simulations, conducted to study the effects of dielectric parameters variations on the antenna-material coupling, have considered a limited range of dielectric properties variations, only ideal material (without taking into account irregularity, lateral and vertical heterogeneities, or roughness), and not considering highly dynamic shallow moisture responses encountered under natural field conditions. For these reasons, general acceptance of this new method requires that it be tested in 'real life' applications.

The latter part of the present thesis is dedicated to evaluate the early-time GPR technique under natural field conditions where surface roughness, lithology, lateral heterogeneities, vegetation and water content dynamics are not controlled. In particular, it is been assessed the capacity of the early-time amplitude technique over a complete annual cycle of soil moisture conditions at three different textural sites. Principally, this unique data set has permitted an evaluation of the sensitivity of the early-time amplitudes to subsurface water content variations. In particular, comparing the results obtained from the first part enveloped amplitude of GPR signals both with the bulk dielectric permittivity obtained from a more established GPR data analysis (the CMP), and with gravimetric water content measurements, it is clear that the early-time method can provide accurate predictions of shallow soil electromagnetic parameters conditions.

Analysing laboratory information, numerical simulations and natural field conditions, and summarising the overall results embodied in this thesis, it is possible to suggest the early-time GPR technique as an effective method to estimate physical properties of the soil in a fast and non-invasive way.

Acknowledgements

I would especially like to thank my supervisor prof. Elena Pettinelli that believed, supported, inspired and corrected this work. I would like to thank her for her guidance on developing this thesis further. I thank also my labmates with whom I have shared experiences, field works, travels, conferences, enthusiasms, questions, problems and discussions. I would like to thank all the people that supported me in the department either academically or in form of friendship.

I would like also to convey my gratitude towards prof. Tony Endres, who welcomed me and guided me through this project during the moths that I spent as a visiting Ph.D. student in Canada. Also I would like to thank his entire laboratory, with a special mention to dr. Colby Steelman that supported my work with advices, reviews and constructive comments.

I would like to deeply thank Peter Annan, Dave Redman, the R&D lab, and all the Sensors&Sofware Inc. for the opportunity to meet exceptional people/scientists supporting me both with operational and theoretical explanation, not only in Canada, but also during the entire thesis work. Thank you for the experiences in the field measurements and in our priceless meetings.

A precious thank to my father, prof. Agostino Ferrara, who have guided me in so many ways throughout the entirety of my education and also through this thesis work.

I would like to thank all the people who directly or indirectly sustained me during this period, with whom I have shared my space and spent my time. I would like to thank all my family, particularly my mother, my parent-in-law, my sister, and my beloved granddaughter. All my friends. My two wonderful dogs.

Finally, a really special thanks to my husband, prof. Pier Matteo, who throughout the entirety of this PhD supported me, believed me, marry me (!), encourage me, comforted me, both in the work and in my life. This thesis would not have happened without you. Our daughter, Ofelia, with all my possible love.

Table of Contents

List of Figures

line. The real signals and the envelopes are expressed in arbitrary units (a.u.). Moreover, figure 3.2b shows the time delay Δt, between the direct and reflected envelope maxima.

Figure 3.4. Figure 3.4a shows an example of the radargram in dry condition; whilst figure 3.4b illustrates the radargram in wet condition. Here it is well visible the step due to the presence of the water effects and the signal time-stretching.

Figure 3.5. (a) Echo envelopes obtained by applying the CPMG pulse sequence to bulk water (circles) and to water saturated specimen (squares). (b) Transverse relaxation time distributions measured in a water saturated concrete specimen at 3.5 mm, 4 mm, and 5 mm depths.

Figure 3.6. Water content distribution measured with GPR (on the top) and NMR (on the bottom). The GPR data are expressed in arbitrary units (a.u.) and the NMR-estimated water contents are expressed in weight percentage. Note that both the GPR and NMR maps have the same origin which correspond to 0,0 in Figure 3.1.

Figure 3.7. XY scatter plot of GPR average envelope amplitude vs. NMR signal intensity with the experimental uncertainties. The trend is clearly linear and the coefficient r=0.97 indicates a high degree of correlation. The GPR and NMR data are expressed in arbitrary units (a.u.).

Figure 4.1. Typical TDR waveforms as a function of time (ns), for deionised water, solid line, and air, dotted line. In the figure are indicated the signal travel times in water (AC) and in air (AB) and the initial (V_0) and final (V_F) TDR voltage.

Figure 4.2. GPR numerical setup: half-wavelength dipole antenna in a bistatic configuration. (a) The scenario under analysis (with a coordinate system) consisting of two half-space media (e.g., an air/soil environment, described by the EM parameters ε_r, μ_r, σ) where a fixed bistatic ground-coupled Tx/Rx antenna system is located. Resistively-loaded folded dipoles are chosen in this case. (b) Radiation features of the loaded dipole antenna (in the cross *xy* plane): a far-field pattern in free space (left) and a near-field pattern at close distance (r = 20 cm) from the interfacial ground-coupled dipole (right).

Figure 4.3. A measured signal waveform Amplitude A vs. time t gathered by the GPR, emphasizing the early-time direct wave and the first reflected wave (due to the presence of a bottom metal sheet in the configuration).

Figure 4.4. Results of early-time traces derived by the simulation setup. (a) A received waveform (signal amplitude A vs. time t), represented by a Ricker pulse (to be compared with the first part of the measured trace from the experimental setup of Figure 4.1 in the analogous operative conditions). (b) The relevant frequency spectrum of the signal amplitude (Fourier-transformed amplitude vs. f).

Figure 4.5. Simulated results of ETS characteristics for a ground-coupled radar system with interfacial Tx/Rx dipoles using an input Ricker pulse. The envelope amplitudes of the output ETS signal A (V) vs. time t (ns) are displayed for different relative permittivities ε_r of a non-magnetic and non-lossy ground medium (see labels with associated colours). The relevant ETS 'onset' attribute is also identifiable. The antenna elevation above interface is fixed (h = 1 cm), but different mutual offset distance are chosen: d = 4 cm (upper plot) and d = 8 cm (lower plot).

Figure 4.6. The experimental setup for the analysis of early-time signal features. (a) An air/dielectric (glass beads) environment is investigated by means of a simple commercial GPR system with fixed interfacial antennas. The ground dielectric constant and conductivity can be changed in controllable ways. (b) The TDR-derived electrical conductivity as function of salt (KCl)

concentrations in a porous sandy soil, for all the measurements.

Figure 4.7. Representative GPR acquired trace (solid line) and related Envelope Amplitude (dashed line). The first half-cycle bolded and the reflection from the investigated media bottom is highlighted by the red dashed line.

Figure 4.8. a) GPR averaged early-time first half cycle (on the left) and the related envelope (on the right) for different KCl concentrations (e.g., conductivities), acquired by measurements from the experimental setup; b) same quantities obtained by ad-hoc numerical simulations. Note that in the legend the term "sat" refers to deionised water and KCl1 and KCl7 refer to the lowest and the highest potassium chloride concentration, respectively.

Figure 4.9. Envelope maximum of the reflected wave as a function of the corresponding conductivity values derived from the TDR measurements. The curve is the exponential data fitting.

Figure 5.1. An illustration of the various wavefronts for a small electric dipole on the surface of a dielectric (Annan, 2002).

Figure 5.2. Schematic diagram showing the possible raypaths of GPR emitted signals and (b) a representative CMP soundings; direct air wave and DGW, critically refracted air and ground waves, and reflected ground waves are indicated (Steelman and Endres, 2010).

Figure 5.3. GPR waveform (a) and its related Envelope Amplitude (b). The first half-cycle duration is indicated in the panels using bold lines. The circle in (b) indicates the maximum amplitude value.

Figure 5.4. Representative early-time GPR signals for a range of soil dielectric permittivity values at the sand site. The permittivity values were obtained from the corresponding DGW velocity measurements. The first half-cycle is indicated with bold lines.

Figure 5.5. The complex trace amplitude envelopes for the GPR signals shown in Figure 2. The first half-cycle is highlighted with bold lines and the maximum amplitude values with circles.

Figure 5.6. Histograms of the early-time envelope maximum values obtained along the survey line at the sand site for two dates (9 July 2008 and 16 May 2007, respectively) corresponding to low and high permittivity values based on the DGW velocity measurements.

Figure 5.7. The standard deviation of the early-time envelope maximum measurements for each survey date as a function of the permittivity derived from the corresponding DGW velocity measurements for all the three sites.

Figure 5.8. Correlation coefficient for the inverse relationship between the average envelope maximum in the first half-cycle and the CMP derived averaged permittivities as a function averaging window width.

Figure 5.9. Temporal variation in the early-time envelope maximum and the corresponding $\frac{1}{\varepsilon_r}$ values derived from the DGW velocity measurements for (a) sand, (b) sandy loam and (c) silt loam sites. The error bars for the envelope maximum values are based on the standard deviation of the mean value for each date and are very small and not shown. Error bars for $\frac{1}{\varepsilon_r}$ values are very small (see Steelman and Endres, 2010 for further details) and not shown.

Figure 5.10. Early-time envelope maximum as a function of the corresponding ε_r values derived from the DGW velocity measurements for all three sites. Curve is the best fitting version of the relationship based on previous theoretical work (Di Matteo et al., 2013). Error bars for the envelope amplitude values are very small and not shown.

Figure 5.11. Comparison between the predicted volumetric water content from the early-time amplitude measurements and the volumetric water content derived from soil sampling for cumulative depth intervals to 0.50 meters. The black dashed line indicates $\theta_w^{predicted} = \theta_w^{measured}$ data. The error bars for the early-time predicted water content values are very small and not shown.

Figure 5.12. Penetration depth of the GPR signal according to different models: Full wavelength approximation, Half wavelength approximation, Van Overmeeren's (or seismic) approximation, Sperl's approximation, Galagedara's approximation.

List of Tables

Chapter 1

Introduction

1.1 Background

Over the past few decades, technological advances have resulted in the development of geophysical methods to investigate and characterize the shallow subsurface (Annan and Davis, 1989; Olhoeft, 1992; Peters et al., 1994; Daniels et al., 1998). These geophysical techniques have been increasingly used as an effective medium characterization tool offering a range of non-invasive to minimally invasive sensors with the capacity to provide detailed soil electromagnetic (EM) parameter information at different depths. In particular, one of the best options in terms of spatial resolution, fast acquisition time, extension of the investigated area, and repeatability of the measurements is the Ground Penetrating Radar (GPR) (Annan, 2004; Daniels, 2004; Jol, 2009).

This system employs high-frequency electromagnetic waves that, in low-loss and non-magnetic soils, respond primarily to the bulk dielectric permittivity of the medium. As the permittivity of liquid water is much larger than other geologic constituents, the device is highly suited for measuring volumetric water content.

Nowadays, GPR instrumentation is becoming stable, reliable and reproducible. As instruments evolve and designs get better, even the amplitude information of the data is becoming more controllable. Historically, the travel time was the most useful part of the GPR record. Relative amplitudes were good indicators but absolute amplitude information was unattainable. As GPR becomes more sophisticated and stable, reliable quantitative amplitude information will spawn another generation of data analysis and interpretation tools based on inversion to image material properties (Annan, 2004).

Ground penetrating radar measurements fall into two categories, reflection and transillumination, as depicted in Figure 1.1. In the first, reflected or scattered energy is detected. In the second, effects on energy transmitted through the material are observed (Jol, 2009). Reflection surveys are the most common and they can be conducted with air-launched antennas (operating at some distance above the ground surface) or surface-based systems. In particular, ground-based GPR systems are suitable for subsurface studies because of their ability to indicate anomalous target location and also to

extract quantifiable wave property variables such as velocity, attenuation, or impedance and then translate the wave properties into application-specific quantities (e.g. Annan, 2004; Jol, 2009).

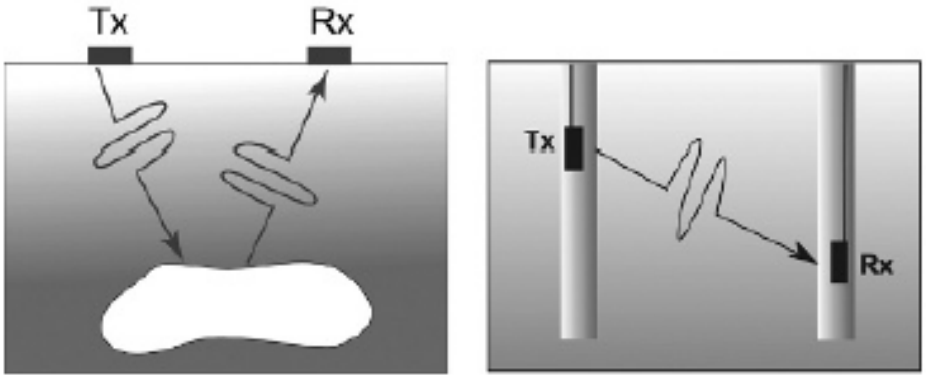

Figure 1.1. Ground penetrating radar (GPR) uses radio waves to probe the subsurface of lossy dielectric materials. Two modes of measurement are common. In the first, reflected or scattered energy is detected. In the second, effects on energy transmitted through the material are observed (Jol, 2009).

1.2 Objectives

The quantitative evaluation of the electromagnetic properties of a material is an important goal for multiple purposes in many fields of application.

The main objective of this thesis is to examine the capacity of surface GPR for the estimation of the physical soil properties in a fast and non-invasive way developing novel processing strategies and providing valuable information about the investigated material. In particular, an alternative surface GPR method for monitoring EM parameters directly below the air-soil interface has been introduced in two previous works (Pettinelli et al., 2007; Di Matteo et al., 2008), but it is studied in-depth in this work.

This new approach analyses the amplitude attributes information over the early-time portion of a GPR pulse obtained from conventional single-offset surface-coupled profiling. To achieve the objective of this study, the early-time technique was examined in different experimental test settings and in modelling and theoretical studies, showing that amplitude-attributes of the first positive half-cycle of the early-time signal reveal a strong correlation with measured soil dielectric parameters.

The specific goals of this thesis are due to the electromagnetic parameters information obtained from early-time GPR signal analysis:

- test the early-time technique in a controlled laboratory setting (Ferrara et al., 2011 and 2013a), where this signal processing analysis was used to map the near surface lateral distribution of

the dielectric permittivity;

- examine the early-time method via numerical simulations, to establish what are the more revealing signal attributes that allow for predictable correlation to the ground dielectric properties (Ferrara et al, 2013b and Comite et al., 2014);
- evaluate the early-time approach in a controlled laboratory setting, with the aim of detecting the variations of electric conductivity in a porous material having a uniform permittivity (Ferrara et al., 2013b) ;
- assess the capacity of the early-time to monitory highly dynamic vadose zone processes in a natural field condition over a complete annual cycle of soil conditions (i.e., natural wetting/drying and freeze/thaw cycles), where surface roughness, lithology, lateral heterogeneities, vegetation and water content dynamics are allowed to change with the natural environment (Ferrara et al., 2013c);
- address the ability of the early-time GPR technique for accurate predictions of shallow soil water content, as a potentially valuable method for quantitatively monitoring near-surface moisture under natural field conditions (Ferrara et al., 2013c).

1.3 Thesis Organization

This thesis is organized in 6 chapters, including 2 introductory chapters (chapters 1 and 2), and 3 core chapters (chapters 3–5) written as independent research papers. Each core chapter includes the necessary background information so that they can be read independently of the thesis document. Finally, the main contributions of this thesis and recommendations for future works are summarized in Chapter 6.

GPR is an effective non-invasive soil moisture tool capable of providing physical information from the subsurface, and the majority of this research is focused on the early-time GPR method as electromagnetic technique to estimate material parameters. To address this, Chapter 2 presents at the beginning the GPR fundamentals and then the early-time methodology; in particular, the aim of this chapter is to introduce and explain this new radar approach at the determination of EM material properties.

Chapter 3 examines the application of the early-time signal processing analysis tested in a controlled laboratory setting, where this signal analysis was used to map the near surface lateral distribution of the dielectric parameters, induced by changing the shallow water content on a concrete slab. This controlled experiment was specifically designed to study the effect of the water content variations on the antenna-material coupling, minimizing the influence of both surface

roughness and heterogeneity. The quantitative control of the water in the shallow portion of the slab was performed by using a portable unilateral Nuclear Magnetic Resonance (NMR) sensor, which is able to determine the water content in the material on the basis of the measured proton density.
This first study has focused the attention just on the spatial permittivity distribution in the subsurface, overlooking the capacity of the early-time approach to monitor the electrical conductivity changes. To address this, Chapter 4 examines the application of GPR soundings for examining the variations of electric conductivity in a porous material having a uniform permittivity. A specific laboratory setup has been realised to evaluate the sensitivity of the early-time amplitudes to the variations of the subsurface salt concentration (i.e., conductivity). This chapter, also, presents the numerical evaluation of the early-time approach and, more specifically, of the experimental setup measurements; the acquired radar signal has also been simulated by means of a suitable implementation of a CAD electromagnetic tool, *CST Microwave Studio*.
Those initial experiments do not consider highly dynamic shallow moisture responses that would be encountered under natural field conditions (e.g., different soil textures, significant permittivity and conductivity variations, and relevant water content changes). For these reasons, Chapter 5 examines the use of this method in 'real-life' applications, evaluating the early-time GPR technique under natural field conditions where surface roughness, lithology, lateral heterogeneities, vegetation, and water content dynamics are not controlled. The capacity of the early-time amplitude method is tested over a complete annual cycle of soil moisture conditions at three textural sites.
Finally, the main findings of this thesis and conclusions are remarked in Chapter 6.

1.4 Electromagnetic Theory

1.4.1 Basic Principles

The foundations of GPR lie in EM theory. Maxwell's equations mathematically describe the physics of EM fields, while constitutive relationships quantify material properties. Combining the two provides the foundations for quantitatively describing GPR signals (Annan, 2005).
The electrical properties (dielectric permittivity ε, electric conductivity σ, magnetic permeability μ, magnetic susceptibility χ) of materials are a wide-ranging topic. The general theory of EM phenomena is based on Maxwell's equations, which constitute a set of four coupled first-order vector partial-differential equations relating the space and time changes of electric and magnetic fields to their scalar source densities (divergence) and vector source densities (curl). In mathematical terms, electromagnetic fields and related properties are expressed as the Maxwell's equations:

$$\overline{\nabla} \times \overline{E} = -\frac{\partial \overline{B}}{\partial t} \quad (1.1)$$

$$\overline{\nabla} \times \overline{H} = \overline{J} + \frac{\partial \overline{D}}{\partial t} \quad (1.2)$$

$$\overline{\nabla} \bullet \overline{D} = \rho \quad (1.3)$$

$$\overline{\nabla} \bullet \overline{B} = 0 \quad (1.4)$$

where $\overline{E}$ and $\overline{H}$ are the electric and magnetic fields intensity, $\overline{B}$ is the magnetic flux density vector, $\overline{D}$ is the electric displacement vector, $\overline{J}$ is the electric current density vector, ρ is the electric charge density, and t is the time.

These fields interact with the surrounding media, where this interaction is macroscopically described by the constitutive equations:

$$\overline{J} = \sigma \overline{E} \quad (1.5)$$

$$\overline{D} = \varepsilon \overline{E} \quad (1.6)$$

$$\overline{B} = \mu \overline{H} \quad (1.7)$$

$$\overline{M} = \chi \overline{H} \quad (1.8)$$

where $\overline{M}$ is the magnetic polarization vector. In general, equations (1.5-8) describe the response of a medium to a variety of electromagnetic input. Two of them describe the relationship between the electric field $\overline{E}$ and the conductive current $\overline{J}$, and the electric displacement $\overline{D}$, and the other two describe the relationship between the magnetic field $\overline{H}$ and the magnetic induction $\overline{B}$, and the magnetic polarization $\overline{M}$. The dielectric permittivity ε, the electric conductivity σ, the magnetic permeability μ, and the magnetic susceptibility χ are the four constitutive parameters that exclusively describe the electromagnetic properties of a material. It is necessary to point out that some of them are inter-related.

1.4.2 Material Properties

The manner in which the electromagnetic fields interact with natural materials controls how electromagnetic fields spread into the medium and are attenuated in the medium. In addition, the variation in physical properties gives rise to the observed subsurface reflections of the EM waves (Annan, 2004).

From these relationships, all classic EMs (induction, radio waves, resistivity, circuit theory, etc.) can be derived when combined with formalism to characterize material electrical properties. The radio waves propagation properties depend on the electromagnetic constitutive parameters of the material, i.e. the relative complex dielectric permittivity:

$$\varepsilon = \varepsilon^{'} - i\varepsilon^{''} \tag{1.9}$$

The relative complex magnetic permeability:

$$\mu = \mu^{'} - i\mu^{''} \tag{1.10}$$

And the relative complex conductivity:

$$\sigma = \sigma^{'} + i\sigma^{''} \tag{1.11}$$

In equation (1.9) the real part of permittivity $\varepsilon^{'}$ is associated with the polarizability of the material, whereas the imaginary part $\varepsilon^{''}$ represents the effects of the DC (Direct Current) conductivity and the dissipation associated to the polarization process (Chelidze and Gueguen, 1999; Chelidze et al. 1999).

In equation (1.10) $\mu^{'}$ is the real part associated with the magnetization of the material and the imaginary part of permeability $\mu^{''}$ is related to magnetic losses (du Tremolet de Lacheisserie et al., 2005).

For a more convenient mathematical manipulation, the real electric permittivity ε and the real magnetic permeability μ can be written into two parts as, $\varepsilon = \varepsilon_0 \varepsilon_r$ $\mu = \mu_0 \mu_r$ with ε_0 and μ_0 defined as the dielectric permittivity and magnetic permeability in free space; note that the parameters with subscript *r* defined as the relative permeability and relative permittivity. Note that the magnetic susceptibility and the relative magnetic permeability are related, $\mu = 1 + \chi$, and the dissipation caused by rearranging the magnetic domains gives rise to a complex magnetic susceptibility, $\chi = \chi^{'} - i\chi^{''}$. The real part of the susceptibility is proportional to the component of the magnetization that is induced in-phase with the applied modulation while the imaginary part is proportional to the $\pi/2$ out of phase or quadrature component of the magnetization. It is this latter part which is directly proportional to the dissipation in the material. In equation (1.11) the real part of conductivity is the static conductivity, and we can define the imaginary term to be conductivity due to an alternating field.

The key EM wave field properties are phase velocity, v, attenuation, α, and electromagnetic impedance, Z. The velocity of a uniform wave in a homogeneous material can be written as:

$$v = \frac{\sqrt{2}}{\left(\sqrt{\mu^{'2} + \mu^{''2}}\sqrt{\varepsilon^{'2} + \varepsilon^{''2}} + \varepsilon^{'}\mu^{'} - \varepsilon^{''}\mu^{''}\right)^{\frac{1}{2}}} \tag{1.12}$$

In a low-loss medium, equation (1.12) reduces to $v = \frac{c}{\left(\varepsilon' \mu'\right)^{\frac{1}{2}}}$ (where c is the EM velocity in free space). Whereas the attenuation factor is given by:

$$\alpha = \frac{\omega}{\sqrt{2}}\left(\sqrt{\mu'^2 + \mu''^2}\sqrt{\varepsilon'^2 + \varepsilon''^2} - \varepsilon'\mu' + \varepsilon''\mu''\right)^{\frac{1}{2}} \qquad (1.13)$$

In a low-loss medium, equation (1.13) reduces to $\alpha = \frac{\sigma}{2}\sqrt{\frac{\mu}{\varepsilon}}$. The radio waves travel through the material, are scattered and/or reflected by changes in impedance; the magnitude and character of the return signal are controlled by the geometry and the impedance contrast of the object generating the return signal. Each material has an intrinsic impedance $Z = \left(\frac{\mu}{\varepsilon}\right)^{\frac{1}{2}}$, therefore for "normally-incident" plane waves, the reflection coefficient between the target and the background (or between adjacent layers), is described by the well-known equation:

$$R = \frac{Z_2 - Z_1}{Z_2 + Z_1} \qquad (1.14)$$

where R is the reflection coefficient for normal incidence on a planar surface, and Z_2 and Z_1 are the intrinsic impedances of the background and the target respectively.

The magnetic permittivity μ is generally assumed to be approximately equal in value to its value in free space (μ_0 = 4 × 10^{-7} H/m) for most near surface applications due to the negligible amount of magnetic material present. Using this assumption, equation (1.14) can be expressed as:

$$R = \frac{\sqrt{\varepsilon_2} - \sqrt{\varepsilon_1}}{\sqrt{\varepsilon_2} + \sqrt{\varepsilon_1}} \qquad (1.15)$$

From this equation it can be seen that as the difference between values increases for adjoining materials the larger the amount of EM energy will be reflected. For non-normal incidence pulses (i.e., θ_I >0), the value of R is also dependent on the orientations of the electric and magnetic field components of the EM pulse. The following versions of R for differing electric and magnetic field orientation are given by Annan (2005).

The reflection coefficient perpendicular $R^{\perp}$ is given by:

$$R^{\perp} = \frac{\varepsilon_2^{-1/2}\cos\theta_I - \varepsilon_1^{-1/2}\cos\theta_T}{\varepsilon_2^{-1/2}\cos\theta_I + \varepsilon_1^{-1/2}\cos\theta_T} \qquad (1.16)$$

whereas the reflection coefficient parallel $R_{\parallel}$ is defined as:

$$R_{\parallel} = \frac{\varepsilon_2^{-1/2}\cos\theta_T - \varepsilon_1^{-1/2}\cos\theta_I}{\varepsilon_2^{-1/2}\cos\theta_T + \varepsilon_1^{-1/2}\cos\theta_I} \quad (1.17)$$

where θ_I and θ_T are the angle of the incident EM wave and the angle of the transmitted EM wave, respectively. These angles are related by Snell's Law:

$$\frac{sen\theta_I}{v_1} = \frac{sen\theta_T}{v_2} \quad (1.18)$$

where v_1 and v_2 are the EM wave velocities in the first and in the second medium, respectively. The expressions for $R^{\perp}$ and $R_{\parallel}$ are commonly referred to as the Fresnel's equations (McNaughton, 2011).

From the Fresnel's equations (1.16-17), it can be seen that the amplitude of reflected waves are dependent on the incident angle and the contrasts in electrical properties between the two media (Baker 1998).

1.5 Use of GPR to detect subsurface electromagnetic parameters

The idea to use radio waves for subsurface exploration and imaging comes from an accidental observation made in the 1950's in Greenland, where the aircraft altimeters were systematically making an error when attempting to land aircraft on the Greenland ice sheet (Waite and Schmidt, 1961). Then, the radio echo sounding activity continued not only for the ice exploring, but also for the exploration of geologic materials (Cook, 1973; Holser et al., 1972; Unterberger, 1978; and Thierbach, 1973) and for the lunar science mission planning for the Apollo program. Several experiments were developed to examine the lunar subsurface which was believed to have electrical characteristics similar to ice. The work of Annan (1973) reports on some of these developments.

Other GPR applications have involved, with mixed success, road investigations (Ulriksen, 1982), contaminated land exploration (Benson et al., 1984), landmine detection and utility mapping. GPR advances were applied to archaeology (Goodman, 1994), environment (Brewster and Annan, 1994; Redman et al., 1996), geological stratigraphy (Jol, 1996) and many other areas.

After that, the evolution of the computers and technologies drove all of GPR developments. Numerical modelling of full 3D problems became more extensive albeit still with large computers (Holliger & Bergmann, 2000; Lampe & Holliger, 2000).

GPR is now on very solid footing. Research groups with good understanding of the basic physics are developing modelling tools and analysis capabilities although the complexities and interactions in specific instances are still subjects for research (Annan, 2004).

Ground penetrating radar is a non-invasive geophysical technique used to explore the shallow subsurface. GPR uses electromagnetic fields to probe a lossy dielectric medium to detect structures and changes in material properties within the medium (Davis and Annan, 1989).

GPR emits EM pulses from few MHz till few GHz propagating into the subsurface from a transmitting antenna and reflected back to a receiving antenna where the signal is recorded. The propagation of this EM pulse is controlled by electrical properties (i.e., electrical conductivity, dielectric permittivity and magnetic permeability) of the subsurface; in particular, the radar signals interact with underground obstacles and discontinuities to image the permittivity and conductivity distributions. These electromagnetic properties generally reflect the geological properties, such as rock and soil type, as well as rock condition (e.g., fracturing, moisture content, and porosity). It necessary to have a change in the electrical properties from the surrounding host material, and changes in dielectric permittivity and electrical conductivity caused by the scattering of radio waves (electromagnetic energy). By detecting this scattered energy, it is possible to detect and locate the sources of the scattered energy. Figure 1.2 illustrates the general concept of how this detection is carried out.

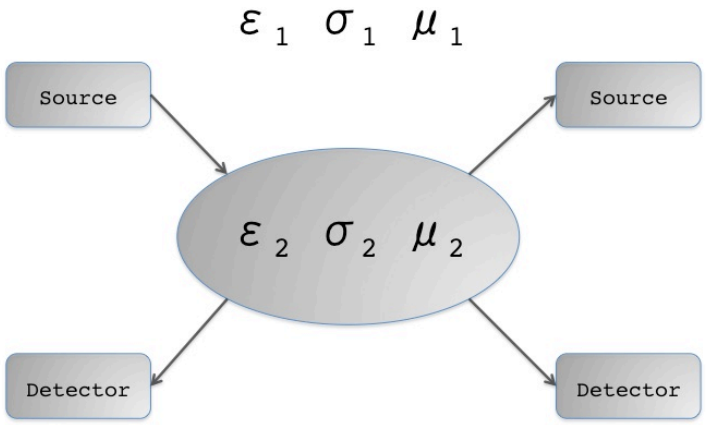

Figure 1.2. Concept of using reflected or scattered signal to detect and define an object. The distance to the object and some information on its composition can be obtained from reflected signal. Implicit in the full three dimensional positioning is the ability to sense or detect the signals in or from specific directions or make measurements in a number of different positions (after Annan, 2004).

In a nutshell, if there is an object with certain electrical properties immersed in a medium, which has a different set of electrical properties, a source of EM energy, which transmits its signals in the form of radio waves, sends out energy towards the target, and scattered signal is detected by a receiver (Annan, 2004).

The electrical properties of near surface materials are dependent on electrical properties of their components (e.g., air, water and solid grains), as well as the relative abundance of these

components in the system (e.g., porosity, degree of water saturation) (Davis and Annan 1989). The permittivity of liquid water (ε_w = 78–88) contrasts strongly with other common components of the soil system (i.e., mineral soil grains ε_s = 4–6 and air ε_a = 1), as well as ice ($\varepsilon_i \simeq 3.2$) (Cassidy, 2009); hence, this provides the basis for estimating volumetric water content using GPR measurements.

Chapter 2

Ground penetrating radar and the early-time technique

2.1 Ground penetrating radar fundamentals

Ground penetrating radar takes advantage of contrasts in EM wave propagation properties of subsurface porous media to produce high-resolution images of the surveyed area. GPR uses radio waves emitted from a source to detect an object at a distance, and to determine the position of the object as well as the distance to the object. In order to detect a target, it must re-emit some of the radio wave energy that impinges on it. This requires a contrast in the electrical properties from the surrounding host material. As discussed previously, changes in dielectric permittivity and electrical conductivity cause scattering of radio waves (EM energy). By detecting this scattered energy, it is possible to detect and position the sources of the scattered energy. The dielectric permittivity ε of a medium describes its ability to polarize in presence of an EM field. In geophysics, for convenience, the dielectric properties of geological materials are commonly expressed in terms of a normalized quantity called relative dielectric permittivity (or dielectric constant) ε_r defined as

$$\varepsilon_r = \frac{\varepsilon}{\varepsilon_0} \qquad (2.1)$$

where ε_0 is the dielectric permittivity of free space (ε_0 = 8.85418 × 10^{-12} F/m). The permittivity of subsurface materials can vary dramatically, especially in presence of free and bound water, and it is usually a complex, frequency-dependent quantity with real (storage) and imaginary (loss) components. The permittivity value of a material is often simplified to its constant, low-frequency (or static) real component with the loss term ignored. This is convenient for the approximate calculation of radar wave velocities and wavelengths, but it is too general for a detailed analysis. Table 2.1 lists the relative permittivity and conductivity of some common subsurface materials at 100 MHz and their typical range under natural conditions. They are 'typical' values derived from experiments and illustrate the influence of free and bound water, i.e., wetter higher, drier lower (Jol, 2009).

Table 2.1. Typical values of relative permittivity (real component) and static conductivity for common subsurface materials at an antenna frequency of 100 MHz (Jol, 2009).

Material	Static conductivity, σ_s (mS/m)	Relative permittivity, ε_{ave}
Air	0	1
Clay – dry	1–100	2–20
Clay – wet	100–1000	15–40
Concrete – dry	1–10	4–10
Concrete – wet	10–100	10–20
Freshwater	0.1–10	78 (25 °C)–88
Freshwater ice	1–0.000001	3
Seawater	4000	81–88
Seawater ice	10–100	4–8
Permafrost	0.1–10	2–8
Granite – dry	0.001–0.00001	5–8
Granite – fractured and wet	1–10	5–15
Limestone – dry	0.001–0.0000001	4–8
Limestone – wet	10–100	6–15
Sandstone – dry	0.001–0.0000001	4–7
Sandstone – wet	0.01–0.001	5–15
Shale – saturated	10–100	6–9
Sand – dry	0.0001–1	3–6
Sand – wet	0.1–10	10–30
Sand – coastal, dry	0.01–1	5–10
Soil – sandy, dry	0.1–100	4–6
Soil – sandy, wet	10–100	15–30
Soil – loamy, dry	0.1–1	4–6
Soil – loamy, wet	10–100	10–20
Soil – clayey, dry	0.1–100	4–6
Soil – clayey, wet	100–1000	10–15
Soil – average	5	16

Because the permittivity of liquid water contrasts strongly with other common components of the soil system (i.e., mineral soil grains and air), as well as ice (Jol, 2009), EM wave velocity in a soil is strongly dependent on its liquid water content.

The propagation of this EM pulse is controlled by electrical properties (i.e., electrical conductivity, dielectric permittivity and magnetic permeability) of the subsurface. These propagation effects are manifested in two ways: (i) the EM wave velocity is a function of the electrical properties, determining the travel time for a pulse to propagate through a material, and (ii) the energy of an incident EM pulse is partitioned into reflected and transmitted pulses when it encounters at interface between materials with differing electrical properties; the magnitude of the electrical property contrast across this boundary controls the partitioning process (McNaughton, 2011).

The fundamental physical behaviour is the propagation delay between the time for the source to emit a signal and the time for the detector to receive any echoes back. As radio waves travel at high speeds (in air 0.3 m/ns), the travel time of a radio wave from instant of transmission through to its

subsequent return to the receiving antenna is in the order of a few tens to several thousand nanoseconds (Reynolds, 1997). This time delay is determined by the distance to and from the target divided by the speed of the wave propagation through the host medium:

$$t = \frac{2d}{v} \tag{2.2}$$

where velocity v of the GPR pulse is given by

$$v = \frac{1}{\sqrt{\varepsilon\mu}} \tag{2.3}$$

The magnetic permittivity μ is generally assumed to be approximately equal in value to its value in free space (μ_0) for most near surface applications due to the negligible amount of magnetic material present. Using this assumption, equation (2.2) can be expressed as

$$v = \frac{c}{\sqrt{\varepsilon_r}} \tag{2.4}$$

The essence of GPR (and all radars) is to measure the time delay (equation 2.2). Basically, larger is the time delay, greater is the distance to the target, assuming uniform velocity conditions (Annan, 2004).

2.1.1 Antennas

GPR antennas create and detect key EM fields. The transmit antenna must translate the excitation voltage into a predictable temporal and spatial distributed field. The receiving antenna must detect the temporal variation of a vector component of the EM field and translate it into a recordable signal.

Short electric dipoles are the most effective antennas for a GPR system. Resistively loaded small dipoles yield a fair degree of faithfulness to desired predictable and invariant behaviour while retaining some efficiency. The ground controls the directional characteristics of a short electric dipole antenna. Although the analysis of this problem is complex, the basic characteristics can be explained. Background for this can be found in Annan (1973), Annan et al. (1975), Engheta et al. (1982), and Smith (1984).

The pattern of a dipole antenna placed on the ground surface is depicted in Figure 2.1. The refractive focusing associated with the air-ground interface causes the change in directivity. This pattern represents the far-field radiated component of the fields. Near the antennas, the fields are more complex and require numerical simulation. For any given propagation direction, two independent fields exist. For planar interfaces, it is tradition to discuss the two waves, one with the

electric field in the interface plane called transverse electric (TE), and one with the magnetic field vector in the interface plane called transverse magnetic (TM).

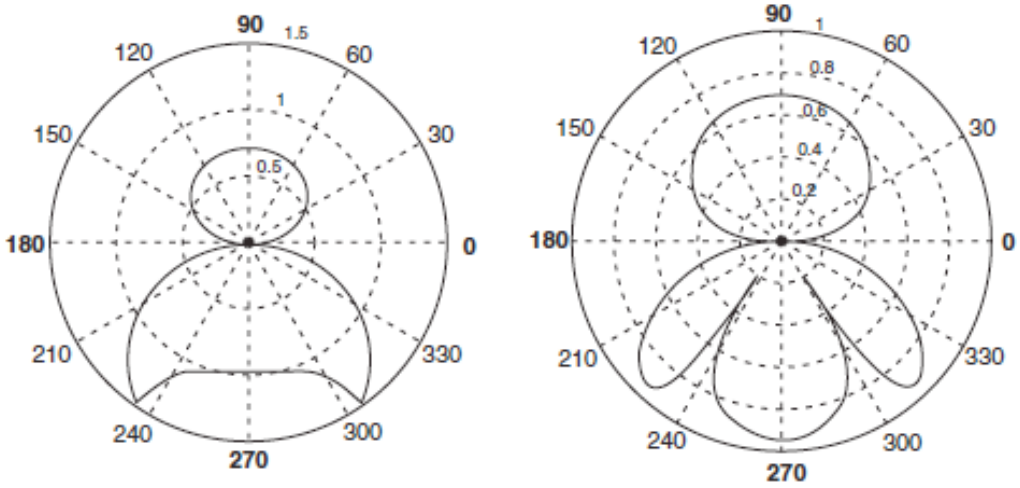

Figure 2.1. When the dipole is on the ground surface, directivity is drastically altered and depends on ground permittivity. The TE and TM (left and right, respectively) patterns shown here are for ground permittivity of 3.2 (Jol, 2009).

Because antenna directivity is ground-dependent, it changes with ground properties variations. Figure 2.2 shows a sequence of patterns as the permittivity is carried from 3.2 to 80.

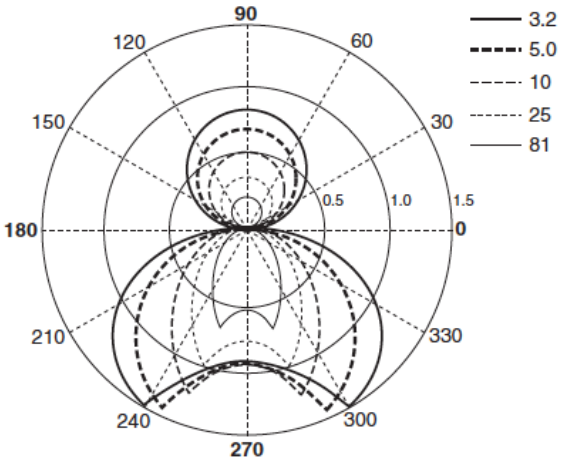

Figure 2.2. When the ground permittivity changes, the patterns change. The transverse electric (TE) pattern is shown for permittivities ranging from ice (low) to water (high). (Jol, 2009).

The effect of antenna elevation off the ground surface is also important. In real-field situations, surface roughness and the need to transport antennas over the surface can limit close ground

contact. Antenna elevation modifies antenna directivity, indeed more signals are transmitted upward into the air and antenna efficiency is reduced (Annan, 2004; Jol, 2009).

2.1.2 Survey Considerations

The three main factors that characterize a GPR survey performance are: the amount of attenuation, the depth of investigation vs. resolution, and the amount of the external noise.

The EM pulse attenuation (Davis and Annan, 1989) is:

$$\alpha = \frac{\sigma}{2}\sqrt{\frac{\mu}{\varepsilon_r}} \qquad (2.5)$$

where α is the attenuation constant in dB/m and σ is the conductivity of the medium in mS/m. The value of α describes the ability of a medium to transmit an EM pulse (McNaughton, 2011). The attenuation is proportional to the electrical conductivity, which leads to high attenuation in materials with high electrical conductivity. The electrical conductivity normally increases with the presence of water, soluble salt, and/or clay contents (McNeill, 1980). In soils, the most significant conduction-based energy losses are due to ionic charge transport in the soil solution and electrochemical processes associated with cations on clay minerals (Neal, 2004). These losses can seriously impact the performance of GPR (Campbell, 1990; Olhoeft, 1998).

Secondarily, is necessary to consider the depth of investigation vs. resolution. Resolution is the ability to distinguish between two closely spaced features (signals) from each other. Increasing the resolution of a GPR survey allows smaller object or thinner layers to be detected.

Ground penetrating radar resolution consists of two components, namely the longitudinal (range or depth) resolution length and the lateral (angular or sideways displacement) resolution length (Figure 2.3).

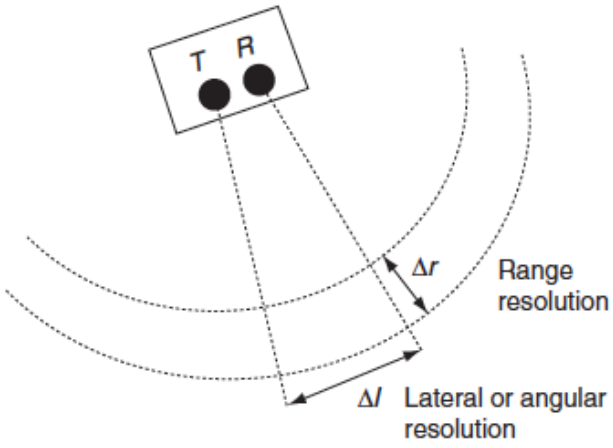

Figure 2.3. Resolution for GPR divides into two parts, namely range resolution and lateral (or angular) resolution (Jol, 2009).

The longitudinal resolution depends primarily of the wavelength, λ, of the propagating electromagnetic wave, which is determined by the GPR frequency, f, and velocity, v, of the ground material, as λ=v/f. An increase in f (decrease in λ) enhances the resolution, but decreases the investigation depth. For the longitudinal resolution, theoretically, the distance between two reflectors should be ¼ of the size of a wavelet (Sheriff and Geldart, 1982). The size of the wavelet that are recorded on GPR data is function of the pulse width of the original transmitted pulse:

$$\Delta r \geq \frac{Wv}{4} = \frac{\lambda_s}{4} \qquad (2.6)$$

where Δr is the range resolution length, W is a ¼ of wavelength at half of maximum amplitude, v is the EM wave velocity in the subsurface, and λ_s is the wavelenght into the material. Essentially, at larger distances, pulse dispersion and attenuation will affect radial resolution.

The lateral resolution length is as follows:

$$\Delta l \geq \sqrt{\frac{Wvr}{2}} \qquad (2.7)$$

where *r* is the distance to the target. The lateral resolution depends on the velocity, the pulse width, as well as the distance from the system. The larger the distance, the greater the lateral resolution length (Jol, 2009).

The horizontal resolution is a determined by the area illuminated by a GPR antenna – the antenna footprint – illustrated in Figure 2.4.

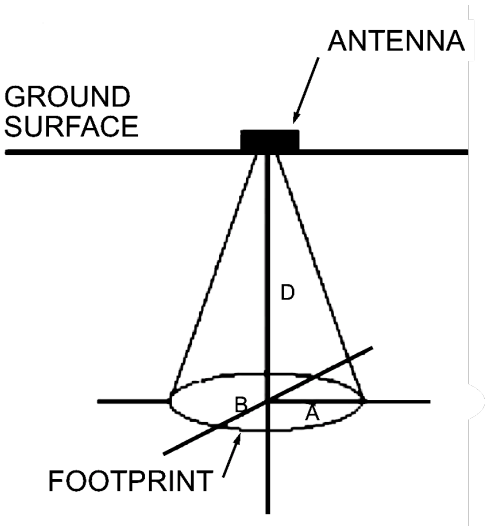

Figure 2.4. Simplified GPR footprint concept where shaded zone depicts area illuminated at depth (after Conyers and Goodman, 1997).

The footprint is elliptical in shape and its size increases with depth. For common dipole antennas, Annan (1992) provides a way to estimate the footprint dimensions using:

$$A = \frac{\lambda}{4} + \frac{D}{\sqrt{\varepsilon_r - 1}}, \quad B = \frac{A}{2}, \tag{2.8}$$

where A is the long axis diameter of the oval footprint, B is the short axis diameter, D is the distance (or depth), and ε_r is the dielectric constant of the medium.

It is clear that for higher λ values correspond bigger footprint dimension and lower resolution and vice versa. Moreover, higher is the dielectric constant, lower is the radar energy velocity and, therefore, the transmission cone.

To increase resolution, it is necessary to increase the frequency at which the EM pulse is generated: higher frequency pulses have shorter wavelengths and can be image smaller subsurface features. However, attenuation mechanisms affect preferentially higher frequency components, causing high frequency EM pulses to be attenuated more rapidly in the near surface. To increase the depth of investigation, longer wavelengths (corresponding to lower frequency EM pulses) are required. But, these longer duration pulses are unable to resolve the finer details of the subsurface.

The third consideration illustrated by Davis and Annan (1989) is the amount of noise generated by electrical transmission wires and other anthropogenic sources. The GPR system normally has shielded antennas, which eliminates or reduces potential noise and cluttering, minimizing coupling with signals in the air, and maximizing coupling with signals in the ground (McNaughton, 2011).

To conduct high quality GPR surveys, these factors should be considered. The more planning that goes into a survey, the higher the likelihood of success and the easier the interpretation of the results (Annan, 2004).

2.1.3 Common-offset reflection survey

GPR surveys design discussions and information can be found in excellent literature (e.g., Annan and Cosway 1992-1994; Neal, 2004; Annan, 2005; Jol, 2009). Surface GPR techniques use transmitting and receiving antennas positioned along the surface (i.e., the air-ground interface). The most common mode of GPR surveying is the common-offset reflection profiling, as illustrated in Figure 2.5.

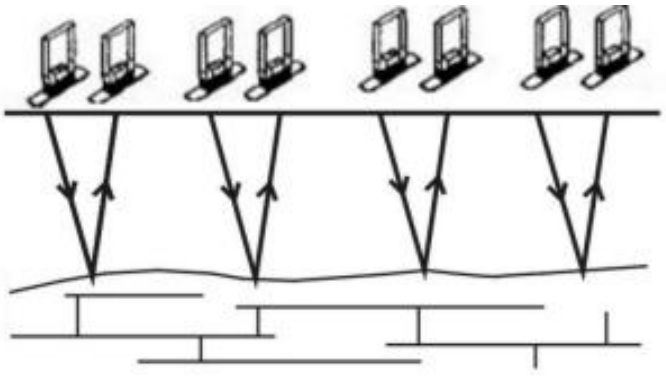

Figure 2.5. Schematic diagram illustrating the reflection profiling sounding technique (Annan, 2004).

In such a reflection survey, a system with the transmitting antenna (Tx) and the receiving antenna (Rx) fixed at a constant offset (or separation) distance is transported along a survey line to map reflections vs. position. This transmitter-receiver array is transported along the profile line at a uniform step size between sounding locations. Each sounding is repeated multiple times and stacked in time in order to suppress random noise; this procedure produces a single composite trace for each sounding location (McNaughton, 2011). A typical radar record is a reflection section, which displays position, horizontally, and travel time, vertically. The reflection events are originated from a contrast in the EM properties of different medium; the time between the EM wave transmission, reflection and reception is a two-way traveltime (TWT) and it is measured in nanoseconds (ns). The TWTs for reflections in each sampling points from these interfaces create the radargram (Steelman, 2012).

2.1.4 Common Mid-Point (CMP) Sounding

The common mid-point survey (CMP) uses a different method to collect reflection data where the transmitter and the receiver are moved apart about a fixed location sequentially at a specified increment, resulting in a separation of coherent events in the wavefield (e.g., direct air wave, direct ground wave, and subsurface reflections). A schematic diagram of this procedure is shown in Figures 2.6 and 2.7.

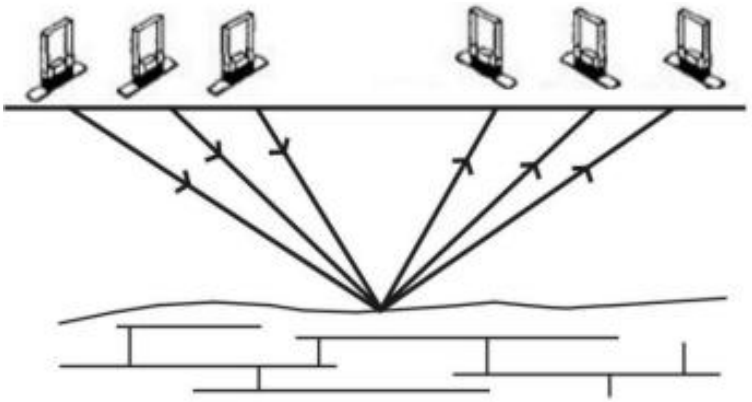

Figure 2.6. Schematic diagram illustrating the common-midpoint (CMP) sounding technique (Annan, 2004).

CMP soundings are primarily used to obtain an estimate of the radar signal velocity vs. depth in the ground by varying the antenna spacing at a fixed location and measuring the change of the TWT to the reflections. Therefore, by increasing the horizontal distance at a constant rate, the increasing TWT can be used to calculate EM wave velocities, as well as the depth to a reflector (Annan, 2004).

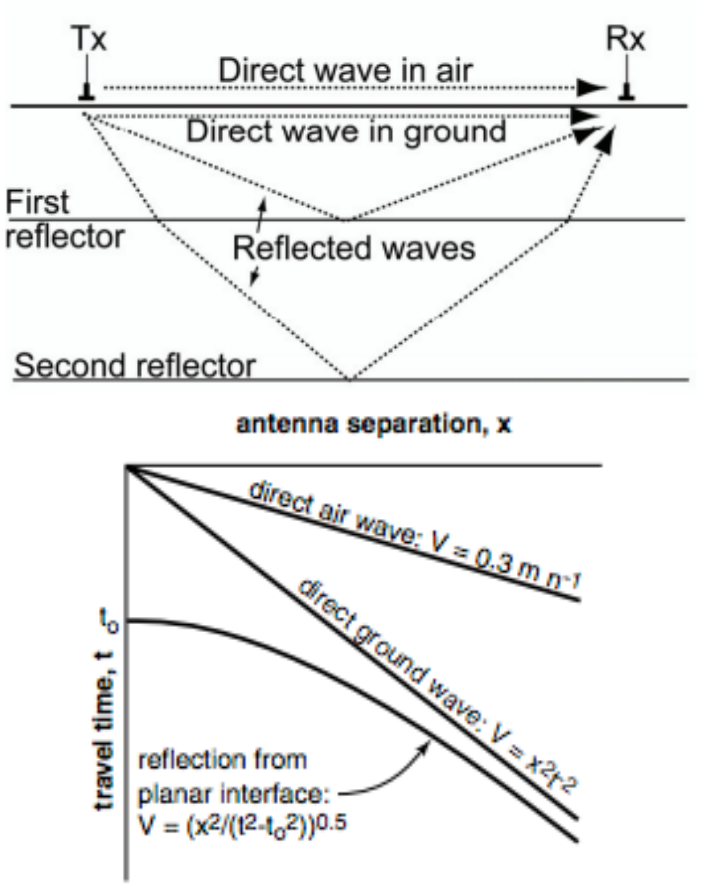

Figure 2.7. Principles of GPR in CMP mode. On the top, sketch of the path of the most common waves that is present in a CMP; on the bottom, a separation vs. travel time plot provides a means of determining ground velocity structure (after Annan, 2004).

2.2 Early-time technique fundamentals

In order to assess the ability of GPR to estimate the water content in a material, several radar methodologies like Single-offset, Multi-offset and Surface Reflection techniques have been widely tested (Dane and Topp, 2002; Huisman et al., 2003a), and their accuracy, in estimating the volumetric water content, has been evaluated by comparing the relevant results with other traditional techniques, like Time Domain Reflectometry (TDR) (Topp et al., 1980) and gravimetric measurements.

More recently, a new radar approach called early-time technique has also been proposed by Pettinelli et al. (2007). It is based on the amplitude analysis of the early-time portion of the GPR waveform using a fixed-offset ground-coupled antenna configuration where the separation between the transmitting and receiving antenna is on the order of the dominant pulse-wavelength. Under these conditions, the early-time signal is a complex superposition of the air and ground waves, whereby the ground wave velocity cannot be measured using simple travel time techniques. However, other measurable attributes of the transmitted signal, such as the wavelet amplitude, duration and shape, contain information about the physical properties of the near-surface material.

Previous experimental (e.g., Pettinelli et al., 2007) and modelling (Di Matteo et al., 2008) studies showed how amplitude-attributes of the first part of the early-time signal exhibit a strong correlation with measured soil dielectric permittivity.

2.2.1 Early-time background

In a bistatic radar configuration, the signal emitted by the Tx antenna, which travels along the air/material interface, is composed by two waves the direct air wave and the direct ground wave (Annan, 1973). In a Single-offset configuration, these two waves arrive totally separated at the receiving antenna (Rx) (i.e., they do not interfere) only if the permittivity of the material is relatively large (>20) (Di Matteo et al., 2013). In this condition the ground wave can be used to estimate the signal velocity in the material, extracting the permittivity value and, therefore, the water content (Huisman et al., 2003a).

When the permittivity is lower, the first signal arriving at the Rx is the combination of the two direct waves; however, the amplitude of the early portion of the signal can be correlated to the dielectric properties of the material under the antennas (Pettinelli et al., 2007). Therefore, when the radar data are acquired on a material where the dielectric properties change laterally, the early-time signals, due to its connection with the antenna-material coupling effects, exhibit different amplitude and time-stretching: higher amplitudes and shorter lengths are associated with lower permittivities

(Di Matteo et al., 2008).

The theoretical basis of the early-time amplitude technique was recently examined by Di Matteo et al. (2013). Their study has asserted that the amplitude of the direct air ($A_{air-wave}$) and ground waves ($A_{ground-wave}$) are related to the relative soil dielectric permittivity ε_r (i.e., $\varepsilon_r = \frac{\varepsilon}{\varepsilon_0}$ where ε_0 is the dielectric permittivity of a vacuum) by

$$A_{air-wave} = \frac{\sqrt{\varepsilon_0 \mu_0}}{2\pi\varepsilon_0\left(\varepsilon_r - 1\right)S^2} \tag{2.8}$$

and

$$A_{ground-wave} = -A^0_{ground-wave} \cdot e^{\left[-\frac{1}{2}\frac{\sqrt{\mu_0}}{\sqrt{\varepsilon_0\varepsilon_r}}\sigma S\right]}, \tag{2.9},$$

where

$$A^0_{ground-wave} = \frac{\sqrt{\mu_0\varepsilon_0\varepsilon_r}}{2\pi\varepsilon_0\left(\varepsilon_r - 1\right)S^2}, \tag{2.10}$$

μ_0 is the magnetic permeability and dielectric permittivity in a vacuum, σ is the soil electrical conductivity and S the antenna separation. The exponential term in Equation (2.9) expresses the evanescent nature of the ground wave. Equations (2.8) and (2.10) indicate an inverse relationship between the early-time amplitude and the soil dielectric permittivity, ε_r, for both the air and ground wavelets.

The study of Di Matteo et al. (2013) also has verified how first positive half cycle of the early-time radar signal is the best choice for signal amplitude evaluation since the first arrival of the GPR signals strongly dependent on shallow subsurface permittivity variations. Note that, the first half-cycle is the positive part of the recorded radar signal included between the first two zero-crossing and it is assumed to be function of the energy of the direct signal, that propagates between the transmitting and receiving antennas. This choice also maximizes the signal to noise ratio by minimizing the interference from reflections caused by shallow interfaces (Ferrara et al., 2013a; Ferrara et al., 2013b).

2.2.2 Complex trace analysis

Amplitude information can be extracted from the early-time signal through complex trace analysis; this technique was originally developed for seismic reflection profiling and seismic processing (e.g.,

Taner et al., 1979; White, 1991) and subsequently has been applied to GPR profiling (e.g., Hwang et al., 2008).

Complex trace analysis is applied by computing the average of the instantaneous-amplitude over a selected time-duration of the early-time signal.

With the early-time technique, the acquired GPR signals are considered to represent the real part of a complex trace; the imaginary part is given by the quadrature component obtained through a Hilbert transform of the real part (Figure 2.8).

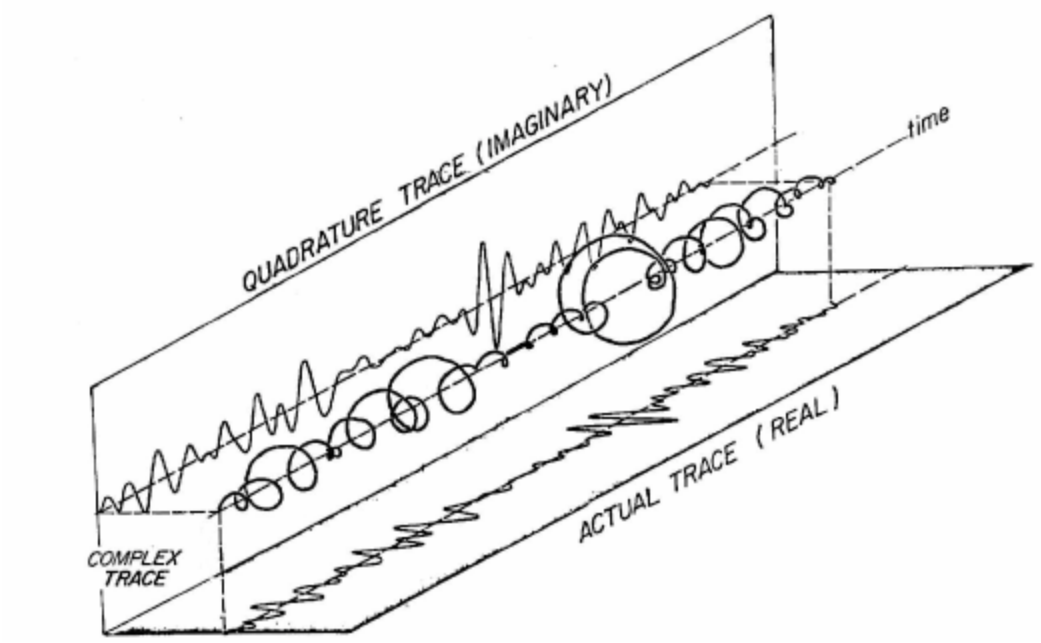

Figure 2.8. Basic scheme of a complex trace rotating in time. The projections on the real and the imaginary planes sinusoidal are the acquired and the associated quadrature components.

The envelope amplitude is given by the absolute value known as the instantaneous amplitude. Let $f(t)$ be an acquired radar trace and let $h(t)$ be its Hilbert transform, or the imaginary trace. An analytic trace $c(t)$ is defined as

$$c(t) = f(t) + ih(t) \tag{2.11}$$

One can also represent the complex trace in terms of the instantaneous amplitude (trace envelope) $A(t)$ and the instantaneous phase, $\varphi(t)$ as follows:

$$c(t) = A(t)e^{i\varphi(t)}, \tag{2.12}$$

Then the envelope is the modulus of the complex function, and varies approximately between zero and the maximum amplitude of the trace:

$$A(t) = \left(c(t) \times c^*(t)\right)^{\frac{1}{2}} = \left|c(t)\right| \tag{2.13}$$

Let $C(f)$ be the Fourier transform of $c(t)$:

$$C(f) = \int_{-\infty}^{+\infty} c(t) e^{-i2\pi ft}\, dt \tag{2.14}$$

We can now rewrite the amplitude as:

$$A(t) = \int_{-\infty}^{+\infty} C(f) e^{i2\pi ft}\, df \tag{2.15}$$

The envelope attribute is a smoothly varying function reflecting the true resolution of the data. For this reason, the envelope is often used to represent reflectivity when generating time/depth slices or creating volume views (Annan, 2005).

2.2.3 Antenna-Material Coupling Theoretical Recall

An antenna is a device for coupling energy from a source of radio frequency energy into a transmitting medium, which is normally air. As briefly mentioned above, for GPR, the radiation from the antenna is normally coupled into the ground, and this affects the radiation characteristics of the antenna to a considerable extent, if the latter is electrically close to the ground. An antenna can be used to transmit energy, receive energy, or both.

The proximity of the antenna to the ground means that it is necessary to consider the coefficients of reflection and transmission as the wave which passes through the dielectric to the target. Snell's laws describe the associated angles of incidence, reflection, transmission and refraction. For proximal operation, the efficiency of the coupling process is generally high, hence to maximise the operating range, the radar should be mounted as high off the ground as possible.

It is important to appreciate the effect of the material in close proximity to the antenna. In general, this material, which in most cases will be soil or rocks or indeed ice, can be considered as a lossy dielectric, and, by its consequent loading effect, it can play a significant role determining the low-frequency performance of the antenna and hence surface-penetrating radar.

The interaction between the antenna and the lossy dielectric half space is also significant as this may cause modification of the antenna radiation characteristics both spatially and temporally, and it should also be taken into account in the system design.

In the case of an antenna placed on an interface, the two most important factors are the current distribution and the radiation pattern. At the interface, currents in the antenna propagate at a certain velocity, which is in-between the one in free space, and the other in the dielectric. In general, the velocity is retarded by the factor $\sqrt{\varepsilon_r}$ (Jol, 2009).

The net result is that evanescent waves are excited in air, whereas in the dielectric, the energy is concentrated and preferentially induced. Therefore, the behaviour of the antenna is intimately linked with the material, and, when there are small antenna offsets, the direct signal (i.e., the early-time signal) is a complex combination of the air and ground waves and carries information on the physical properties of the surrounding material.

Amplitude, shape, and duration of this signal, which change as a function of the EM properties of the material, cannot be analytically derived and thus the only practical approach is represented by numerical simulations (Klysz et al., 2006; Oden et al., 2008; Di Matteo et al., 2013; Ferrara et al, 2013b; Comite et al., 2014).

Chapter 3

An Examination of Early-Time Technique Electromagnetic Parameter Monitoring on a Laboratory Scale Experiment: First Step

3.1 Executive Summary

Several factors affect the antenna-soil coupling in a Ground Penetrating Radar survey, like surface roughness, lithology, lateral heterogeneities, vegetation, antenna height from the surface, and water content. Among them, lithology and water content have a direct effect on the bulk electromagnetic properties of the material under investigation. It has been recently pointed out that the wavelet of the early-time portion of the radar signal is correlated to the shallow subsurface dielectric properties of a material. This result indicates that some information on such properties can be directly extracted from the analysis of the GPR early-time traces.

In the present work, we used the early-time GPR signal, in terms of average envelope amplitude computed on the first half-cycle, to map the near surface (few centimetres) lateral distribution of the dielectric parameters, induced by changing the shallow water content on a concrete slab. This controlled experiment was specifically designed to study the effect of the water content variations on the antenna-material coupling, minimizing the influence of both surface roughness and heterogeneity. Using a portable unilateral Nuclear Magnetic Resonance sensor, which is able to determine the water content in the material on the basis of the measured proton density, was performed the quantitative control of the water in the shallow portion of the slab. The results show a matching pattern of the physical parameters measured with the two different techniques, and a very high degree of linear correlation (r=0.97) between the radar early-time signal average amplitude and the intensity of the Nuclear Magnetic Resonance signal which is proportional to the proton density, i.e. to the water content.

This experiment suggests that the early-time approach could be used as a fast and high spatial resolution tool for qualitatively mapping water content lateral variations in a porous material at shallow depth, using a ground-coupled single-offset antenna configuration, and that a quantitative evaluation of the moisture content would require a calibration procedure.

3.2 Introduction

Assessing water content in porous materials by means of non-destructive methods is of great importance for many applied sciences like hydrology, environmental physics, civil engineering, agriculture, and cultural heritage protection. Several geophysical techniques, particularly those based on the interaction between electromagnetic (EM) fields and matter, can be successfully applied to indirectly estimate water content in a material (Rubin and Hubbard, 2005). The choice of a specific method depends on the goal of the research and the characteristics of the site (or of the material under investigation).

In a survey design several factors should be taken into consideration, like the investigation depth, the spatial resolution, the characteristics of the medium (e.g. granular or solid), the physical properties of the material, the site conditions, and the reliability of the retrieved physical parameter in terms of water content estimator. If the required investigation depth is limited to a few meters, Ground Penetrating Radar (GPR) represents one of the best options in terms of spatial resolution, fast acquisition time, extension of the investigated area, and repeatability of the measurements (Annan, 2004; Barone et al., 2010; Daniels, 2004; Jol, 2009). Such a technique is based on radio waves propagating through the medium, and the water content value can be indirectly retrieved from the measurement of the signal velocity. In particular, several radar methodologies like Single-offset, Multi-offset and Surface Reflection techniques have been widely tested with the aim of assessing the ability of GPR to estimate the water content in a material (Dane and Topp, 2002; Huisman et al., 2003a). Their accuracy has been evaluated by comparing the relevant results with other traditional techniques, like Time Domain Reflectometry (TDR) (Topp et al., 1980) and gravimetric measurements. More recently, a new radar approach called early-time technique has also been proposed (Pettinelli et al., 2007), with the attempt to correlate the radar signal amplitude with the shallow soil dielectric properties. In that study, the permittivity and conductivity measured by TDR, showed a high degree of correlation with the average envelope amplitude of the early portion of the radar signal. Note that, adopting a single-offset configuration, such a portion of the signal contains both the air and the ground waves (Huisman et al., 2003a).

On the other hand, if the required investigation depth is of the order of tens to hundreds of meters, Surface Nuclear Magnetic Resonance (SNMR) can be successfully applied to estimate the water content, as the measurement is directly sensitive to the proton density. SNMR is based on the Free Induction Decay (FID) produced by a radiofrequency excitation pulse applied to an object immersed in the Earth's magnetic field (primary magnetic field). The relaxation signal is probed by using large surface coils (tens of meters in dimension) capable of detecting signals from depths up

to hundreds of meters. In the SNMR configuration, the object under investigation is outside the coil, therefore the excitation field is more inhomogeneous than in the case of the sample inside the coil. As a consequence, the long dead time between the shutdown of the excitation field and the signal recording, makes SNMR able to detect only signals with sufficiently long relaxation time and usually prevents the detection of clay-bound water or ice (Müller-Petke et al., 2011). In contrast to GPR, SNMR has a low spatial resolution and the investigated volume for each measurement is quite large (Legchenko and Valla, 2002). Due to such differences, GPR and SNMR techniques can rarely be combined or compared in common applications, and to our knowledge, only few papers on complementary measurements are present in the literature (Yaramanci et al., 2002; Yaramanci, 2004; Muller-Petke et al., 2011). It should be pointed out however, that a much higher spatial resolution and a much smaller volume investigation can be achieved using borehole NMR and/or unilateral NMR, which are able to provide information on several parameters like water content, pore scale properties and hydraulic permeability (Walsh et al., 2010; Sharma et al., 2003; Blümich et al., 1998; Blümich et al., 2003; Blümich et al., 2011). Joint dielectric permittivity and NMR measurements, performed on soil and rock samples, can be found in the relevant literature. In particular, Yoshikawa and Overduin (2005), and Watanabe and Wake (2009) studied the freezing characteristics in various saturated and unsaturated soils above and below 0° C, measuring the liquid water content and relative permittivity with NMR and TDR techniques. Zhang et al. (2010) and Clennel et al. (2007) found that the liquid water content estimated using the expanded mixing model is in agreement with the values measured by NMR for different soil type, water and ice content, and temperature.

In this work, we compare GPR and unilateral NMR data collected on a concrete slab in which the water content was changed. In particular, we used NMR as a control technique to verify the ability of the GPR early-time signal method to detect the lateral variations of the dielectric properties produced changing the water content in the shallow portion of the slab. The direct comparison was possible thanks to the use of unilateral NMR which probes the sample up to a depth of 1-2cm by exposing the object to the coil stray field in a configuration similar to the one used to radiate the EM field from GPR antennas.

3.3 Elements of GPR Early-Time Technique

In a bistatic radar configuration, the signal emitted by the transmitting antenna (Tx), which travels along the air/material interface, is composed by two waves the direct air wave and the direct ground wave (Annan, 1973). These two waves arrive totally separated at the receiving antenna (Rx) (i.e.

they do not interfere), if the wavelength is smaller than the Tx-Rx offset particularly when the permittivity of the material is sufficiently high. Then, the ground wave arrival time can be used to estimate the permittivity of the material (through the measurement of the wave velocity), and therefore, its water content (Huisman et al., 2003a).

On the other hand, for low material permittivities, the first signal arriving at the Rx is the superposition of the two direct waves, and the ground wave velocity cannot be measured. However other antenna parameters, like the signal amplitude of the wavelet, could be used to evaluate the EM properties of the material in the region, close to the antennas, where the signal propagates through a surface material (Turner, 1993; Sbartai et al., 2007). Indeed, the potential of estimating the soil dielectric parameters using the wavelet amplitude of the radar early-time signal has been experimentally demonstrated (Pettinelli et al., 2007), and also validated by numerical simulations (Di Matteo et al., 2008; Di Matteo et al., 2013). In particular, the dielectric permittivity affects both amplitude and time length of the GPR signal, so that higher amplitudes and shorter wavelets are associated to lower permittivities.

A robust approach to estimate the instantaneous amplitude of the early-time signal is given by the complex trace analysis, introduced in seismic data processing (Taner et al., 1979). According to this method, the average of the instantaneous amplitude in the early portion of the radar signal is calculated for each GPR waveform. Applying such processing, we verify the possible correlation between the average amplitude of the early portion of the radar signal and the NMR signal intensity, i.e. the material water content.

3.4 Unilateral Nuclear Magnetic Resonance (NMR) Methodology

Unilateral NMR is a portable technique, recently developed on the basis of the measurement principle used in well-logging (Blümich et al., 2011), which provides in situ water content measurements in a completely non-invasive way (Di Tullio et al., 2010; Capitani et al., 2009), and it is particularly suitable to investigate flat solid surfaces or granular materials (Blümich et al., 2003). The unilateral NMR is made of a U-shaped open permanent magnet with the radiofrequency coil centered within the magnet air gap (Figure 3.1).

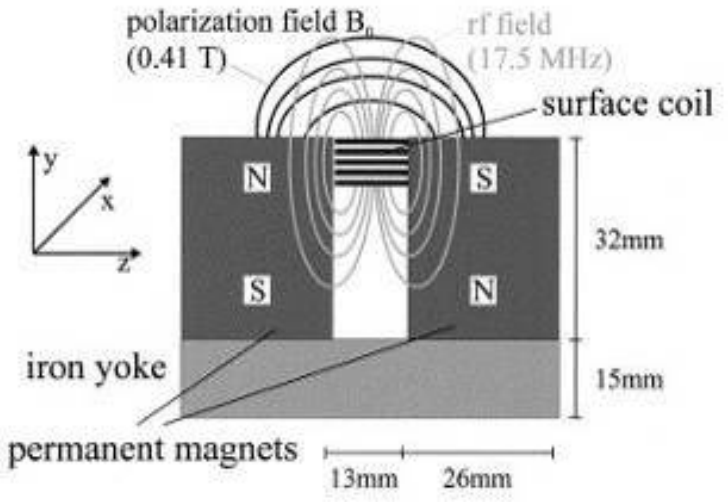

Figure 3.1. Schematic of a unilateral NMR sensor, with two permanent magnets with antiparallel magnetization that generate an inhomogeneous B_0 static field. A radiofrequency (rf) coil situated in the gap between the magnets produces a rf field.

The magnet exposes one side of the object under investigation to its stray field, and the NMR signal is acquired from a defined "sensitive" volume of the object. As the magnetic field generated by the sensor is inhomogeneous, the signal decays much faster than in a homogeneous field, and it must be recovered as the echo of the response to the applied pulse, using NMR echo methods (Blümich et al., 2011). As a consequence, the signal intensity in the sampled volume, which is proportional to the number of water molecules (i.e. the proton density), is measured after applying a Hahn echo sequence which consists of a 90°--180° pulse sequence and detecting the signal echo at the refocusing time 2τ. The dead time of the instrument, namely the time between the end of the pulse and the beginning of the data acquisition, is short enough to allow the measurement of water confined in a porous matrix even with short relaxation times. Note that in this experimental setup, the hydrogen atoms, constituting the solid concrete matrix, do not contribute to the recorded signal.

3.5 Experimental Description

3.5.1 Laboratory Setup

In order to perform a direct comparison between GPR and NMR measurements, some care in the design of the experiment is required. Since the antenna-material coupling can be affected by several factors, e.g. the large scale roughness of the surface, the lateral inhomogeneities in the solid matrix, the lateral salinity variation of the fluid, etc. (Lampe and Holliger, 2003), we performed the measurements on a solid, flat, uniform and porous material; so that the antenna-coupling was

affected only by the surface permittivity variations due to the change in water content. Another relevant point to consider is that, since the two techniques are characterized by very different data acquisition times, the water content in the material could change during the two sets of measurements. In principle, the experiment could be performed on any porous material with a low content of magnetic impurities, however in this case loose materials like sand are not recommended due to fast water drainage; therefore to minimize the amount of water lost in percolation, we used Portland cement and we built a 1.20m x 0.80m x 0.15m concrete slab as a test material. Table 3.1 summarizes the characteristic of the slab. Note that no reinforcing bars were buried in the cement.

Table 3.1. Concrete specifications according to the manufacturer.

TYPE OF CONCRETE	PORTLAND ROCK 30 N/MM^2
Dry Mass of Cement	50kg
Mixing Water added to the cement	25l
Sand (fine aggregate)	0.06m^3 – Ø 0.0-0.05mm
Gravel (coarse aggregate)	0.13m^3 – Ø 0.10-0.25mm
Bulk Density	2200kg/m3
Age	28 days
Porosity	~19%

The effective porosity φ of the concrete was estimated using standard gravimetric method separately applied to four specimens with dimension 0.05m x 0.05m x 0.01m made of the same material of the slab. To estimate the porosity, the specimens were first oven dried and weighed, then saturated by total immersion with water and weighed again (Dane and Topp, 2002). Assuming that at saturation all pores are filled with water, we estimated a water content value in weight θ_{mSAT} of (9.30±0.01)% (averaged on four specimens) that corresponds to an average effective porosity φ of (19 ± 1)%, where the uncertainty was calculated as the half- dispersion (where and are the highest and lowest values of the data set). Note that this value is in agreement with the porosity given by the manufacturer (see Table 3.1).

3.5.2 Measurement procedures

A first set of measurements was conducted with both GPR and NMR on the dry slab. In particular, 23 NMR measurements were collected at the positions shown in Figure 1, whereas the GPR data were acquired along parallel lines crossing the points investigated with NMR (see Figure 1). Subsequently, three other sets of measurements were performed after wetting a portion of the dry slab with deionised water. In particular, before each set of measurements one litre of water was nebulised on the portion of the slab that included 12 out of the 23 points previously measured by NMR in dry conditions (see Figure 3.2). Furthermore, in order to wet precisely the same portion of the slab, a plastic dam was built on the concrete to contain the nebulised water, thus avoiding to wet other points on the slab.

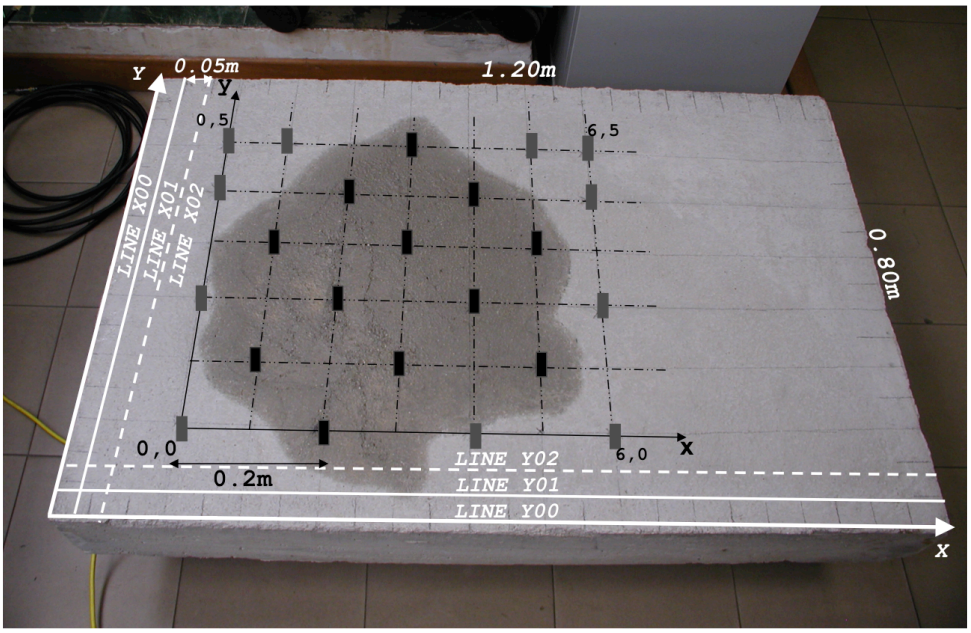

Figure 3.2. Test material made of a concrete slab. The 23 rectangles represent the areas measured by NMR, whereas the lines indicate the directions of GPR data acquisition. Note that the 12 NMR measurements in wet conditions are in black, whereas the dry NMR points are in grey.

During the experiment, the water never percolated through the concrete, as the slab bottom remained dry for all measurement conditions. We followed a procedure for which the measurement session always started with a GPR multi-profile acquisition, in both X and Y directions (XY grid) (Jol, 2009). After that, three NMR measurements were collected, and each of them lasted approximately 20 minutes. Then a second XY GPR grid was collected, followed by another three NMR measurements and so on, until all 12 NMR wet points were collected. Note that each radar grid was performed in about 10 minutes, therefore every complete measurement session lasted

about five hours. This procedure, although producing a very large quantity of GPR data with respect to the NMR ones, allowed us to minimize the effect of the consistent delays among the GPR and NMR acquisitions. Indeed the quite different acquisition time (less than one second for each GPR trace in contrast to the twenty minutes needed for each NMR acquisition), could have produced significant degradation of the possible correlation between the NMR and GPR data collected on the same points, if the water content in the concrete matrix were varying vs. time. Note also that in order to reduce the evaporation during the measurements we covered the wet area with a thin protective film. Furthermore, to check the stability of the room microclimate, we monitored both the temperature and the humidity of the laboratory every hour, finding stable values of 22±1°C and 33±3%, respectively.

3.5.3 GPR and NMR Data Acquisition

GPR data were collected using a bistatic TR1000 radar unit (Sensors & Software, Inc) equipped with 1000 MHz shielded antennas, with 7 cm Tx-Rx separation. The GPR XY grids were performed acquiring a total of 17 Y lines and 25 X lines on the test area (see Figure 3.1), with a line spacing of 0.05 m, a 0.005 m step-size, a time window of 10 ns, a time sampling rate of 0.1 ns and a stacking of 4.

NMR measurements were carried out with a unilateral NMR instrument from Bruker Biospin using a probe head operating at 16.3 MHz, which allowed us to reach an investigation depth of about 0.5 cm, with a maximum sensitivity between 0.45 and 0.55 cm. Each experimental ‘‘point’’ accounts for a volume of 2cm x 5cm x 0.1cm. The moisture content was evaluated from the Hahn echo intensity. The Hahn echo pulse sequence was used with a $\pi/2$ pulse width of 4μs, the recycle delay was 0.6 s, and 4096 scans were collected for each measurement. Note that the recycle delay was optimized according to the measured T1 relaxation time.

Spin–spin relaxation times T2 were measured with the CPMG sequence (Farrar and Becker, 1971) and 2048 echoes were recorded with an echo time 2τ of 50 μs. This pulse sequence used with an echo time as short as possible is useful to minimize the diffusion effects which affect T2 measurements. However, because the magnetic field of portable NMR is rather inhomogeneous, the values of longest T2 relaxation times are usually found to be shorter than values measured in a homogeneous magnetic field.

The CPMG pulse sequence was also applied to scale the value of the effective porosity of the concrete with respect to that of bulk water.

3.5.4 GPR and NMR Data Processing

To extract the early-time information from each radar trace, we analysed the first half-cycle of the antenna-material coupling signal, i.e. the positive part of the recorded signal included between the first two zero-crossing (see the bold portion in Figure 3.3a).

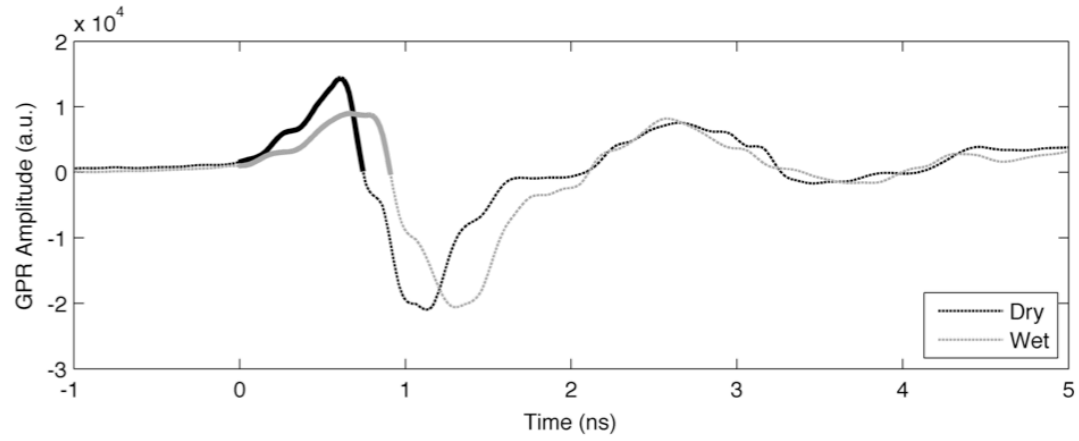

(a)

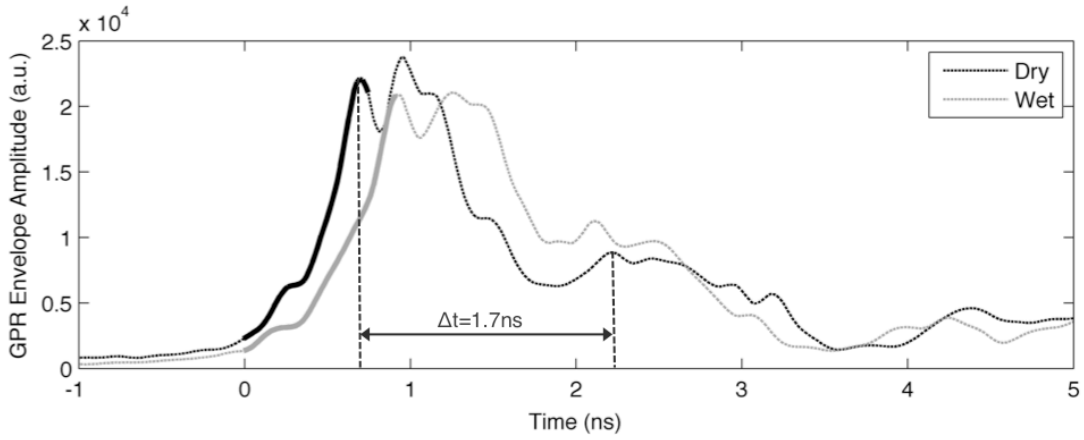

(b)

Figure 3.3. GPR real signals and relevant envelopes collected on dry (solid line) and wet (dashed line) portion of the slab. The signals correspond to the traces acquired at X=0.3m and Y=1.0 m in dry condition, and X=0.3m and Y=0.2 m in wet condition. The first half-cycle is highlighted in bold line. The real signals and the envelopes are expressed in arbitrary units (a.u.). Moreover, figure 3.2b shows the time delay Δt, between the direct and reflected envelope maxima.

This portion of the radar trace is assumed to be the direct signal that propagates between the transmitting and receiving antennas, where the air and ground waves interfere. Note that the collected data were generally of good quality, and did not require any particular pre-processing. In practice, we first created an analytic signal, $c(t)$, from the real acquired signal, $f(t)$:

$$c(t) = f(t) + ih(t) \qquad (3.1)$$

where $h(t)$ is the Hilbert transform of the real signal (Rabiner and Gold, 1975; Yilmatz 2001), that is a Cauchy principle-valued function (P.V.), expressed on the form:

$$h(t) = \frac{1}{\pi} P.V. \int_{-\infty}^{\infty} \frac{f(\tau)}{t-\tau} d\tau \qquad (3.2)$$

Knowing the analytic signal, we calculated its envelope $A(t)$, which represents the instantaneous amplitude of the complex signal (Figure 3.3b), as follows:

$$A(t) = \left| f(t) + ih(t) \right| \qquad (3.3)$$

and then we averaged the envelope in the first half-cycle. It is important to note that the enhancement of the instantaneous amplitude observed for both dry and wet traces at about 2.0 ns (Figure 3.2), indicates the arrival of the reflected signals from the concrete slab bottom.

To determine the uncertainty associated with the GPR envelope amplitudes of the first half-cycle calculated above, we chose three different points of the slab (in wet conditions) and we acquired a total of 1000 traces in each selected point. The data analysis showed that the envelope amplitudes follow a Gaussian distribution, with an associated relative uncertainty of 3%.

The early-time effect on the GPR data collected in the three different water conditions was clearly recognizable. In fact, the radar signals, collected in dry and wet portion of the slab, have a variation in amplitude and the time-stretching due to the lateral variation in permittivity. Figures 3.4a and 3.4b show the radar sections in dry and wet configuration respectively; in figure 3.4b a step is evident caused by the presence of water, which produces a time stretching of the early signal.

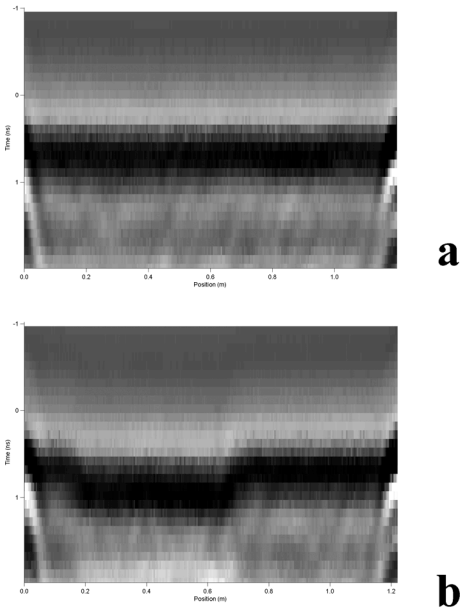

Figure 3.4. Figure 3.4a shows an example of the radargram in dry condition; whilst figure 3.4b illustrates the radargram in wet condition. Here it is well visible the step due to the presence of the water effects and the signal time-stretching.

For each data point collected on the slab, the intensity of NMR signal was measured and 113 Hahn echo measurements were carried out on a water-saturated specimen (made of the same material of the slab) to determine the uncertainty associated with the NMR data. The intensity of the NMR signal was found to be normally distributed, and a relative uncertainty of 3% was calculated.

Then, we converted the NMR signal intensity into NMR-estimated water content by using a calibration procedure described in a previous paper (Capitani et al., 2009). Briefly, specimens were dried until reaching a constant weight $\overline{P}_{DRY}$ and the intensity of the signal $\overline{A}_{DRY}$ was measured. Then the specimens were fully saturated with water up to a constant weight $\overline{P}_{SAT}$, and the intensity of the signal $\overline{A}_{SAT}$ was measured. The procedure was repeated four times and the average values $\overline{P}_{SAT}$ and $\overline{P}_{DRY}$ were used to calculate the water content in weight, previously mentioned, using the equation $\theta_{mSAT} = \frac{\overline{P}_{SAT} - \overline{P}_{DRY}}{\overline{P}_{DRY}} * 100$. Then we calculated the NMR-estimated water content θ_{m_i} for each measured point on the slab using the following equation:

$$\theta_{m_i} = \left(A_i - A_{\min}\right)\left(\frac{\theta_{mSAT}}{\overline{A}_{SAT} - \overline{A}_{DRY}}\right) \qquad (3.4)$$

where A_i is the intensity of the NMR signal at the i-th point, and A_{min} is the lowest value of the NMR signal intensity measured on the slab. The uncertainty associated to θ_{m_i} was evaluated applying the linear propagation error formula to equation (4.4) (Taylor, 1997).

The effective porosity of the concrete was evaluated from the CPMG decays which allows to obtain the value of the echo at t=0 fitting the experimental decay. In particular, the effective porosity was calculated normalizing the CPMG pulse sequence with respect to the value obtained for bulk water (i.e. 100% of porosity). Note that the use of the CPMG pulse sequence with a short echo time minimizes the effect of diffusion, which is more effective in bulk water than in water confined into the concrete. The obtained experimental data were fit to the equation:

$$Y = C_0 + \sum_{i=1}^{n} W_i e^{\frac{-2\tau}{T_{2i}}} \qquad (3.5)$$

where n is the number of components of the CPMG decay of the magnetization, W_i and T_{2i} are the weight and the spin-spin relaxation time of the i-th component, respectively, and C_0 is the offset value, which accounts for the noise of the measurement. Figure 3.5a shows the CPMG decays measured for bulk water (circles) and for water-saturated concrete specimen (squares), along with the relevant best fit (solid line).

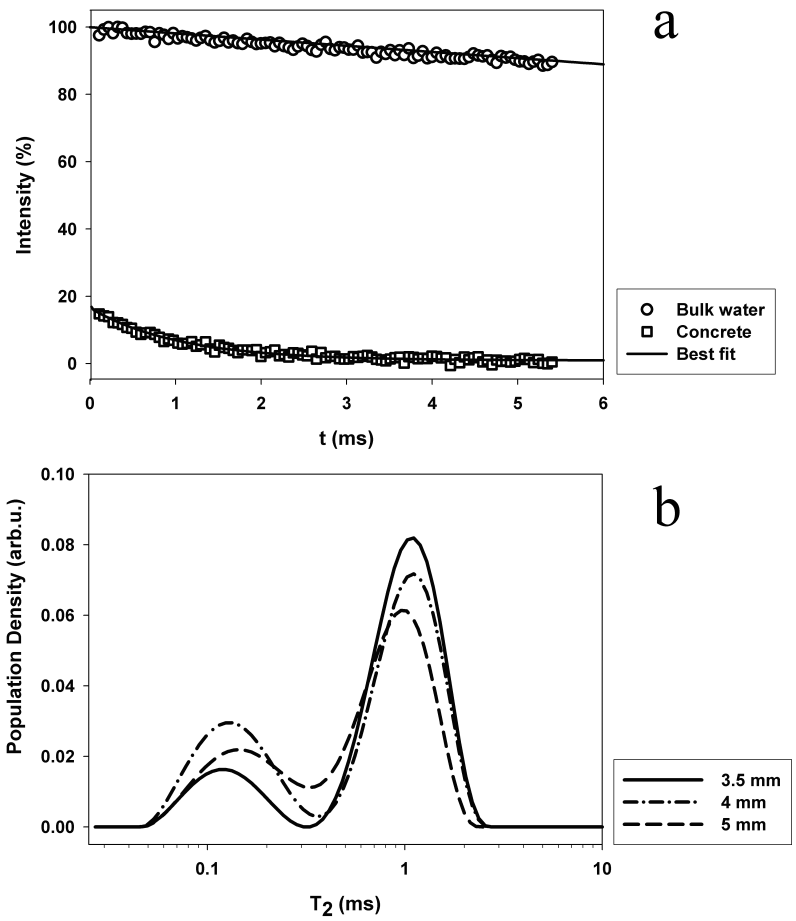

Figure 3.5. (a) Echo envelopes obtained by applying the CPMG pulse sequence to bulk water (circles) and to water saturated specimen (squares). (b) Transverse relaxation time distributions measured in a water saturated concrete specimen at 3.5 mm, 4 mm, and 5 mm depths.

In order to estimate the concrete effective porosity on the four water-saturated specimens, we averaged the CPMG signal amplitude, extrapolated at zero echo time M_{0s}^{i} and we normalized this value ($\overline{M}_{0s}$) to the amplitude measured on bulk water M_{0b} (which is equivalent to an effective porosity of 100%):

$$\phi_{NMR} = \frac{\overline{M}_{0s}}{M_{0b}} \cdot 100 \qquad (3.6)$$

Equation (3.6) gives a value of (17.6±0.5)%, which is comparable with the effective porosity of (19±1)% evaluated by gravimetric method considering the uncertainty of both methods. It is worth to note that the calculation of the effective porosity based on NMR data, was a further test to evaluate the reliability of our measurements in this specific material.

To obtain the distribution of T_2 relaxation times, we applied the inverse Laplace transform to the CPMG decay, and we computed such distribution for different depths (Watson and Chang, 1997).

As an example the T_2 distributions obtained at depths of 3.5, 4, and 5mm are reported in Figure 3.5b, which shows a bimodal trend, with peaks centered at about 1ms and 0.2ms. Note that the peaks represent the most probable T_2 values, whereas the peak areas correspond to the number of spin of each decay component. The presence of two peaks at different T_2, indicates that the water is confined in pores having different sizes (i.e. the longer the T_2 value the greatest the pore size).

3.6 Results and Discussion

3.6.1 Comparison between GPR and NMR Data

The analysis of the radar traces shows the effect of the water on the early-time signals, as illustrated in Figure 3.3, for the three wet measurements sessions, real radar traces collected in dry and wet conditions (a) and the relevant envelopes (b). Note that, the presence of water clearly affects the amplitude and the time length of the signals. In particular, the amplitude effect is systematically present in all GPR data, and it is quite evident on an XY average envelope amplitude map (Figure 3.6).

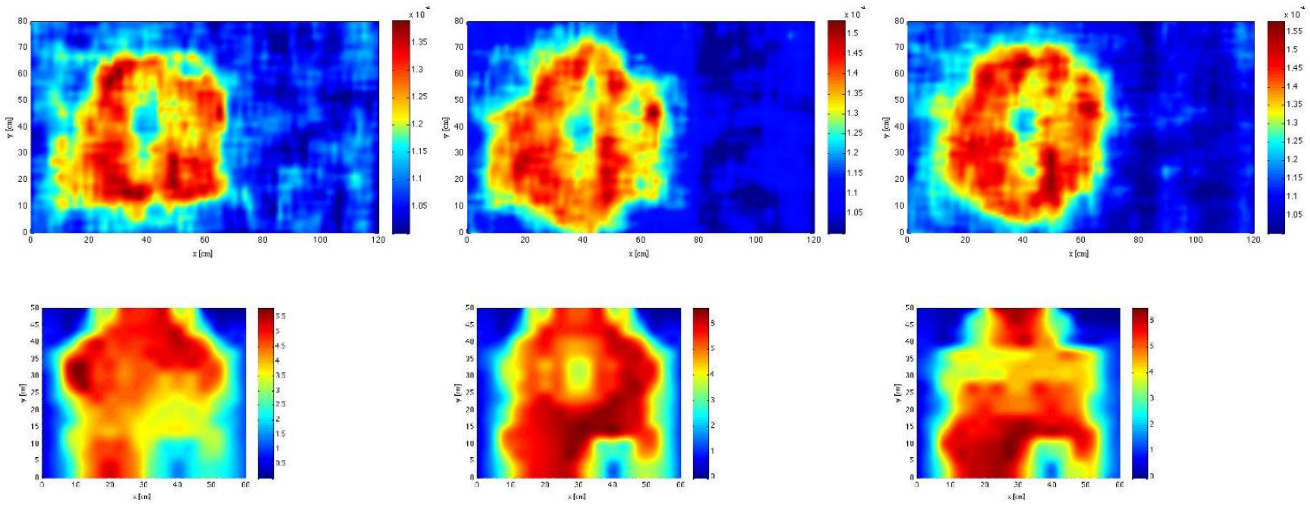

Figure 3.6. Water content distribution measured with GPR (on the top) and NMR (on the bottom). The GPR data are expressed in arbitrary units (a.u.) and the NMR-estimated water contents are expressed in weight percentage. Note that both the GPR and NMR maps have the same origin which correspond to 0,0 in Figure 3.1.

Figures 3.6a and 3.6b depict, as an example, the 2-D maps of the processed data collected with GPR and NMR, after the three water nebulisation. The GPR image was built using the average envelope amplitude of the first half-cycle, whereas the NMR map was obtained producing a colour-scale map, where x and y are the coordinates of the 23 points measured on the test area, and the colour

code represents the NMR-estimated water content calculated from equation (3.4). Figures 3.6a and 3.6b clearly show the distribution of the water in the shallow portion of the slab, even though the spatial resolution of the GPR image is much higher than the one of the NMR. Indeed, each radar map is built interpolating 38400 points, which correspond to all traces collected in the XY grid. Note that Figure 3.6b illustrates that the water content in weight computed using equation (3.4) and relevant to the shallow part of the slab, ranges from about 0% to 6%, never reaching the saturation (9.3%).

The comparison between GPR and NMR maps allows only a qualitative evaluation of the agreement between the two different techniques. However, a quantitative estimation of the correlation between the radar average envelope amplitude of the first half-cycle and the intensity of the NMR signal (i.e. the proton density) can be calculated using the correlation coefficient *r*. To this aim, we used the GPR and NMR data collected on the 12 points located inside the wet area (for a total of 36 pairs of values pertinent to the three different water content conditions). Figure 3.7 shows the GPR average envelope amplitude plotted vs. the NMR signal intensity with the relevant uncertainties, which gives a linear correlation coefficient $r = 0.97$.

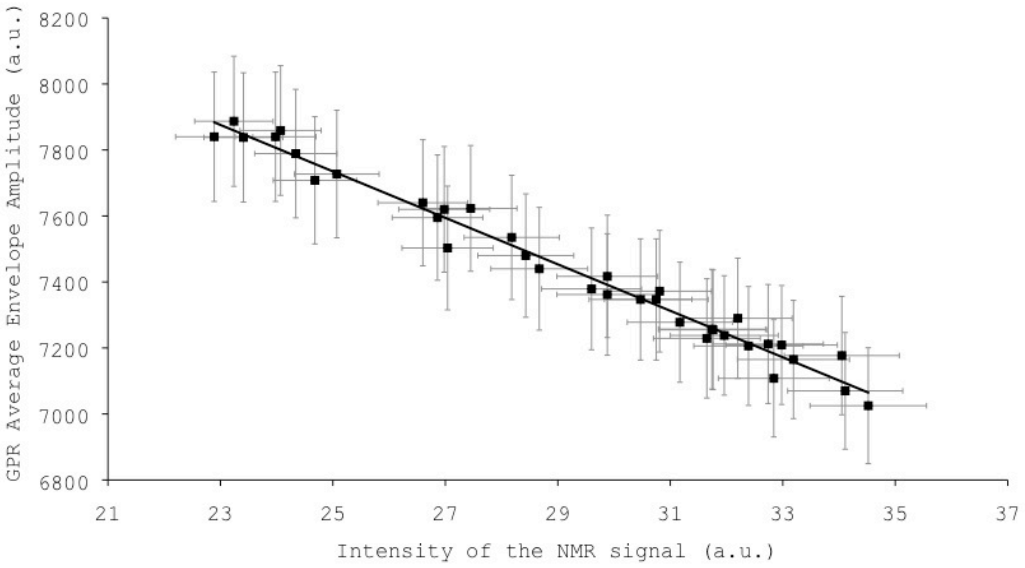

Figure 3.7. XY scatter plot of GPR average envelope amplitude vs. NMR signal intensity with the experimental uncertainties. The trend is clearly linear and the coefficient r=0.97 indicates a high degree of correlation. The GPR and NMR data are expressed in arbitrary units (a.u.).

To provide significant information about the degree of correlation the coefficient *r* has to be associated to the distribution $P_c(r, N)$ which expresses the probability that the observed data could have come, by chance, from an uncorrelated population (Bevington, 1969). In our data, the probability corresponding to $P_c(0.97,36)$ is less than 0.05% implying that the observed variables are very likely correlated.

It is worth to highlight that the GPR signals collected on the 12 points mentioned above, did not exhibit appreciably changes during each measurement session. This internal GPR consistency is evident from the analysis of the data reported in Table 3.2, where the average envelope amplitude values calculated for each measurement section are presented.

Table 3.2. Average envelope amplitude (AEA) values calculated for each measurements session and relative coordinates (x,y). Note that the percentage error among the three AEA values are less than 0.64%, 0.43% and 1% for the first, the second and the third GPR measurement session respectively. The bold AEA values are used for the correlation analysis.

	Dry measurement session	**First wet measurement session**			**Second wet measurement session**			**Third wet measurement session**		
Slab coordinates (x,y)	**GPR AEA (a.u.)**	**First GPR AEA (a.u.)**	**Second GPR AEA (a.u.)**	**Third GPR AEA (a.u.)**	**First GPR AEA (a.u.)**	**Second GPR AEA (a.u.)**	**Third GPR AEA (a.u.)**	**First GPR AEA (a.u.)**	**Second GPR AEA (a.u.)**	**Third GPR AEA (a.u.)**
3,5	10302	**7440**	7449	7461	**7379**	7386	7361	**7170**	7134	7168
2,0	10023	**7417**	7445	7437	**7209**	7211	7215	**7508**	7532	7521
4,4	10285	**7347**	7344	7341	**7257**	7253	7245	**7713**	7734	7701
2,4	10301	**7480**	7501	7469	**7206**	7214	7221	**7645**	7699	7683
5,3	10297	7504	**7535**	7504	7875	**7859**	7855	7601	**7600**	7598
3,3	10311	7591	**7623**	7595	7728	**7727**	7729	7772	**7794**	7783
1,3	10294	7295	**7255**	7250	7218	**7212**	7156	7328	**7377**	7350
2,2	10312	7612	**7620**	7628	7170	**7177**	7122	7286	**7283**	7285
4,2	10403	7837	7826	**7838**	7343	7352	**7362**	7230	7224	**7234**
1,1	9945	7865	7909	**7887**	7077	7028	**7025**	7081	7085	**7075**
3,1	9917	7767	7775	**7840**	7352	7386	**7347**	7231	7223	**7243**
5,1	10297	7940	7913	**7841**	7243	7246	**7295**	7198	7246	**7113**

Moreover, in Table 3.2 we have reported the average envelope values collected in dry condition; the range for the radar data is 9917 – 10403 a.u., which corresponds to a NMR intensity range of 16.56 - 12.97 a.u.

3.6.2 Ground Wave Maximum Penetration Depth

The similarity of GPR and NMR maps with the actual distribution of the water on the surface of the concrete slab, which is well visible, comparing Figure 3.5 with Figure 3.1, points out the ability of both techniques to detect the spatial water distribution in the shallow portion of the slab. Moreover, the high correlation coefficient $r = 0.97$ obtained in this experiment (Figure 3.6), indicates that the two different physical parameters, i.e. the GPR average envelope amplitude and the NMR signal intensity, are affected in the same way by the water content of the concrete.

As mentioned above, however, the volume investigated by NMR is about 2cm x 5cm x 0.1cm and is located about 0.5 cm below surface whereas nothing was said, so far, about the investigation depth of GPR early-time signal. In order to estimate the latter parameter, we can use several equations proposed for evaluating the ground wave maximum penetration depth (Du, 1996; Sperl, 1999; Van Overmeeren et al., 1997).

To this purpose we first evaluated the effective permittivity of the concrete slab for dry and saturated conditions, and then we calculated the ground wave depth for both cases. In particular, we calculated the effective permittivity ($\varepsilon_{eff_{DRY}}$) at dry condition, using the two-way travel time $\Delta t = R_1 - R_0$ of the radar signal reflected at the bottom of the slab according to the following equation (Annan, 2004):

$$\varepsilon_{eff_{DRY}} = \left(\frac{c\left(R_1 - \left(R_0 - \frac{S}{c}\right)\right)}{\sqrt{4d^2 + S^2}} \right)^2 \qquad (3.7)$$

where c is the speed of light in a vacuum, R_0 and R_1 are the times when the GPR receiving antenna detects the direct air wave and the reflected wave respectively, S is the antenna separation and d is the slab thickness. To determine the two-way travel time, being the wavelet composed by non-single phase signals, we followed the procedure applied in Turin (1960), calculating the cross-correlation function between the two (direct and reflected) wavelet envelopes. We have performed this analysis along a GPR single profile (~200 traces) determining an average value of $\Delta t = (1.7 \pm 0.1) ns$ (see Fig.2b where the time delay Δt, between the direct and reflected envelope maxima, is indicated). Note that we could not apply the same procedure to estimate the effective permittivity in the "wet" condition (not saturated). In fact, in this case the wetted volume is much smaller than the thickness of the slab, producing a change in the two way travel time of the same order of magnitude of the uncertainty.

Equation (3.7) gives a permittivity equal to 3.5±0.3 which, using Complex Refractive Index Model (CRIM) (Wharton et al., 1980) for a two phase material (air and concrete), allows us to estimate the

permittivity (ε_s) of the concrete as follows:

$$\sqrt{\varepsilon_{eff_{DRY}}} = \phi\sqrt{\varepsilon_a} + (1-\phi)\sqrt{\varepsilon_s} \qquad (3.8)$$

where φ is the previously calculated effective porosity (about 19%), and ε_a the permittivity of air. From equation (3.8) we obtained a value of $\varepsilon_s = 4.3 \pm 0.5$, for the relative permittivity of the concrete matrix. Finally, applying again the CRIM and assuming for the permittivity of water the value $\varepsilon_w = 79$ (at temperature 22°±1°C) (VV.AA., 1997), we have calculated the effective permittivity of the material for the saturated case:

$$\sqrt{\varepsilon_{eff_{SAT}}} = \phi\sqrt{\varepsilon_w} + (1-\phi)\sqrt{\varepsilon_s} \qquad (3.9)$$

From equation (3.9) we obtained $\varepsilon_{eff_{SAT}} = 11 \pm 1$, where the uncertainties were estimated using the linear propagation formula (Taylor, 1997).

Table 3.3 shows the depths calculated using dry and saturated effective permittivities ($\varepsilon_{eff_{DRY}}$ and $\varepsilon_{eff_{SAT}}$), applying the equations 3.10-14 proposed by Du (1996), Van Overmeeren et al. (1997), Sperl (1999), Galagedara et al. (2005), and Grote et al. (2010):

$$z = \frac{c}{f\sqrt{\varepsilon_{eff}}} \qquad (3.10)$$

$$z = \frac{1}{2}\frac{c}{f\sqrt{\varepsilon_{eff}}} \qquad (3.11)$$

$$z = \frac{1}{2}\sqrt{\frac{c}{f\sqrt{\varepsilon_{eff}}}S} \qquad (3.12)$$

$$z = 0.145\sqrt{\frac{c}{f\sqrt{\varepsilon_{eff}}}} \qquad (3.13)$$

$$z = 0.6015\frac{c}{f\sqrt{\varepsilon_{eff}}} + 0.0468 \qquad (3.14)$$

Note that f is the nominal central frequency of the antennas (1000MHz) and S is the antenna separation.

Table 3.3. Maximum (dry) and minimum (saturated) penetration depth of the radar ground wave according to different models: (a) Full wavelength approximation, (b) Half wavelength approximation, (c) Van Overmeeren's (or seismic) approximation, (d) Sperl's approximation, (e) Galagedara's approximation.

	(Eq. 3.10)	**(Eq. 3.11)**	**(Eq. 3.12)**	**(Eq. 3.13)**	**(Eq. 3.14)**
Dry	0.16m	0.08m	0.05m	0.06m	0.14 m
Saturated	0.10m	0.05m	0.04m	0.04m	0.10 m

On the basis of these results, it is evident that the sampling depth of the early-time radar signal in the wet condition is about 10 times higher than the NMR depth. Despite that, the behaviour of the two physical measured parameters is very similar to each other. Because the NMR technique with a proper calibration procedure is able to precisely evaluate the water content in a material, the high correlation with the GPR data indicates that also the early-time signal attribute is very sensitive to the water content variation. Note that, in this case study, the GPR was able to distinguish relative variations of the water content of about 3% in weight (in the wet area).

It is worth to note that, besides this difference in penetration depth, each area investigated by NMR is about whereas the GPR one, using the early-time technique, is about $10cm^2$ whereas the GPR one, using the early-time technique, is about $50cm^2$. Therefore, this difference in the investigated volumes prevents the possibility of making a quantitative relationship between GPR early-time data and water content, using the correlation analysis. Nevertheless, the results obtained in this experiment show the capability of the early-time approach to create qualitative detailed maps of the water content distribution in the shallow subsurface.

3.7 Conclusions

In the present work, we combined two different non-destructive techniques to detect the spatial distribution of the water in a solid porous material. The goal of the experiment was to "constrain" the GPR data, using the proton density values measured with the unilateral NMR technique, in order to verify the ability of radar early-time signals to map the water content spatial variation in a concrete slab at shallow depth. The experiment was designed to reduce the effect of surface

roughness, lateral heterogeneities, water salinity variation, etc., and to emphasize the dielectric properties effect on the antenna-material coupling. The results confirmed what was observed in a previous work, i.e. that the early-time signal is strongly sensitive to the permittivity variation of the material, which in this specific case, depends only on the water content distribution in the slab subsurface.

Even though it was not possible to directly associate a water content value to an average amplitude signal, due to the difference in the investigated volume of the two techniques, the results obtained in this work corroborate the possibility of using the early-time radar signal features to detect the lateral variations in the physical properties of both natural and man-made materials, with high sensitivity. Moreover, the use of an independent calibration procedure would allow the conversion of the average envelope amplitudes in permittivity and, therefore, in water content values. For this reason, the proposed early-time method could represent a convenient alternative to more traditional radar approaches, for a fast mapping of the subsurface water content variations at a depth comparable to the wavelength in the material.

Chapter 4

A Numerical and Experimental Investigation of Early-Time GPR Amplitude Technique: Second Step

4.1 Executive Summary

Numerical and experimental investigations are presented and discussed with the aim of analysing the features related to the early-time method. The possibility to evaluate the soil dielectric permittivity and conductivity features from the first-arrival signal attributes in ground-coupled radars is firstly studied here with an accurate and versatile approach based on an efficient electromagnetic Computer-Aided-Design (CAD) tool. A quantification of the various physical parameters affecting the early-time characteristics (type, location, and distance of the GPR antennas, transmitted waveforms, etc.) is thus achieved. Numerical results are analysed in order to clearly establish what are the more revealing signal attributes that allow for predictable correlation to the ground permittivity values and what kind of functional relations can be outlined among the involved parameters. Experimental investigations from *ad-hoc* laboratory scale measurements with commercial GPR systems are also carried out and discussed in connection with what derived theoretically as concerns the effects both on the dielectric constant and on the conductivity of the media. Essential information is hence provided for the reliability of this innovative approach in practical testing cases.

4.2 Introduction

It has been recently demonstrated (Di Matteo et al., 2013; Ferrara et al., 2013a) that the early-time portion of the GPR signal, consisting of complex superposition of the direct air and ground wave events, is dependent on the bulk electromagnetic properties of the shallow subsurface material. The early-time technique (Pettinelli et al., 2007) is a new radar approach, which correlates the radar signal amplitude with shallow-soil dielectric properties.

From numerical simulations we know that the amplitude of the early-time GPR signal is affected mostly by dielectric permittivity changes of the investigated material, but there is also a

contribution due to its conductivity variation, as given in (Di Matteo et al., 2013). In that theoretical study, it has been found that the early-time signals change both in amplitude and time length due to permittivity variations: higher amplitudes and shorter time lengths are associated with the lower permittivities.

So far, however, the early-time technique has been tested on GPR data acquired in a laboratory (Ferrara et al., 2013a) with the aim of evaluating the effect of permittivity, while the influence of conductivity has never been analysed. The possibility of monitoring the soil dielectric constant and conductivity features through the first-arrival signal attributes in ground-coupled radars is then analysed with a numerical and an experimental analysis.

Our realistic simulation of the scenario for the early-time method includes the design of the appropriate GPR antennas, the choice of the transmitted waveforms, and the description of the non-homogeneous environment. In this way, it is possible to predict how the various physical parameters (the chosen input signals, the type, location, and distance of the radiators, etc.) affect the early-time signal characteristics. This efficient analysis also enables for the identification of which are the more revealing signal attributes to give predictable correlation with the ground permittivity values, and what kind of functional relations can be outlined among the involved parameters.

This recent early-time GPR amplitude technique was used, in both numerical and experimental contexts, with the aim of detecting the variations of electric conductivity in a porous material having a uniform permittivity. Therefore, a specific laboratory setup has been realised to evaluate the sensitivity of the early-time amplitudes to the variations of the subsurface salt concentration (i.e., conductivity). To assess the capacity of the early-time amplitude to follow the electrical conductivity changes, we compare the early-time results acquired using the envelope of the first part of GPR signals with the concurrent conductivity measured with TDR (Time Domain Reflectometry). Experimental data are discussed in connection with the numerical analysis that has been derived by suitably implementing a full-wave numerical modelling, able to accurately analyse the features of the waves detected by the GPR with flexible parameterization. Both experimental and numerical data have been analysed through the early-time technique, obtaining a very high correlation (i.e., $r=0.95$ and $r=0.99$, respectively) between the early-wavelet amplitudes and the shallow-soil dielectric conductivity derived from TDR measurements.

Our results indicate that the near-surface electromagnetic properties of the material can be directly extracted from the GPR early-time amplitude technique.

4.3 Time Domain Reflectometry (TDR) Methodology

Time Domain Reflectometry (TDR) is one of the most common methods to determine electromagnetic parameters in porous media. TDR operates by propagating a radar frequency EM pulse down a transmission line while monitoring the reflected signal. As the EM signal propagates along the transmission line, it is subject to impedance by the dielectric properties of the media along the transmission line, reflection at dielectric discontinuities (e.g., air-water or water-sediment interface), and attenuation by electrically conductive materials (e.g., salts and clays).

Substantial advances in the measurement of water content and bulk soil electrical conductivity using Time Domain Reflectometry have been made in the last two decades. The key to TDR's success is its ability to accurately measure the permittivity of a material and the fact that there is a good relationship between the permittivity of a material and its water content. The first application of TDR to soil water measurements was reported by Topp et al. (1980). A further advantage is the ability to estimate water content and measure bulk soil conductivity simultaneously using TDR (Robinson et al., 2003).

From the TDR signal travel time analysis the bulk dielectric permittivity ε_b of the material surrounding the probe is computed; in particular, the permittivity is a function of the propagation velocity ($v = \frac{2L}{t}$) according to

$$\varepsilon_b = \left(\frac{c}{v}\right)^2 = \left(\frac{ct}{2L}\right)^2 \qquad (4.1)$$

where c is the speed of light (velocity of electromagnetic waves) in vacuum, and t is the travel time for the pulse to traverse the length of the embedded waveguide (down and back: $2L$).

One of the great strengths of TDR is that it can be used to measure bulk electrical conductivity (σ_{DC}) in addition to permittivity. Originally proposed by Giese and Tiemann (1975), the thin-section approach has been shown to be a particularly effective means of quantifying electrical conductivity, using TDR. The Giese and Tiemann equation may be written as:

$$\sigma_{DC} = \frac{\varepsilon_0^{\frac{1}{2}} \cdot Z_p}{\mu_0^{\frac{1}{2}} \cdot L \cdot Z_c}\left(\frac{2V_0 - V_F}{V_F}\right) \qquad (4.2)$$

where Z_c is the characteristic impedance of the TDR cable (50 Ω), Z_p is the probe impedance in air, L is the rod length, V_0 is the TDR input step voltage, and V_F is the final asymptotic voltage (ε_0 and μ_0 are the vacuum permittivity and permeability) (Figure 4.1).

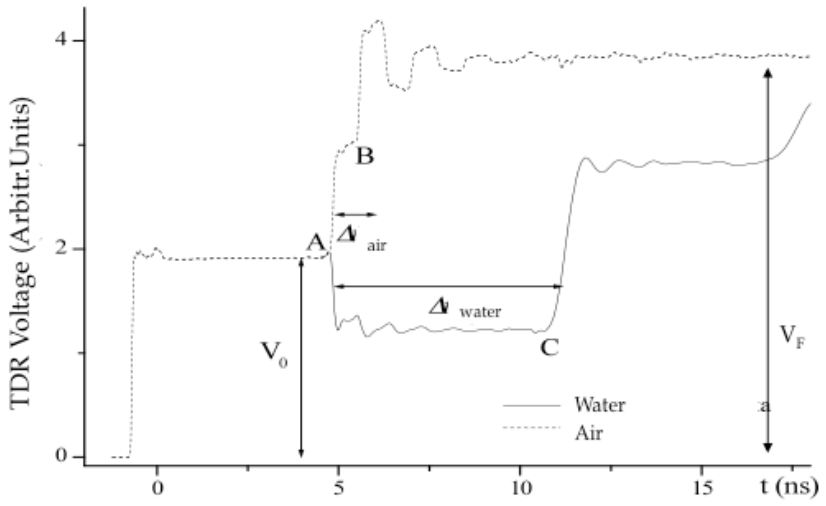

Figure 4.1. Typical TDR waveforms as a function of time (ns), for deionised water, solid line, and air, dotted line. In the figure are indicated the signal travel times in water (AC) and in air (AB) and the initial (V_0) and final (V_F) TDR voltage.

Since its introduction in the early 1980s, the TDR method is one of the most often-applied geophysical measurement techniques. For example, it has been used to determine soil water content, to measure transport properties for ionic solutes under steady and non-steady flow conditions in soils, to monitor water and nitrogen status in the root zone, and to characterize the distribution of water and fertilizers around drippers (Jones et al., 2002).

4.4 Simulation Setup

4.4.1 Early-Time Numerical Investigations

The possibility to evaluate the soil dielectric constant and conductivity features from the first-arrival signal attributes in ground-coupled radars is firstly studied here with the implementation of a numerical setup. In fact, it is seen that, from one side, wide-ranging experimental analyses are rather expensive and time-consuming; from the other side, mere theoretical closed-form modelling, necessarily based on simplifying assumptions and strong approximations for such complex problems, becomes clearly inadequate for accurate understanding of the role played by the various the physical parameters. In this context, it has been settled an efficient and accurate simulation setup for the numerical analysis of the early-time features through a suitable implementation of a CAD simulation tool, which can solve EM problems in the time domain (Valerio et al., 2012). This tool allows us to design a number of different ground-coupled configurations, introducing realistic details of the environment under test in connection with the available computational resources. In

particular, it is possible to freely choose the permittivity parameters of the media (dielectric constant, permeability, and conductivity, also accounting for possible dispersive behaviours), the design of the transmitting and receiving system (antennas, shielding, absorbers, etc.), and the choice of the features of the signals (with time and frequency specifics). Among the various possibilities offered by the numerical implementation, specific attention has been paid to simulate systems as similar as possible to real GPRs. A quantification of the various physical parameters affecting the early-time characteristics (type, location, and distance of the GPR antennas, transmitted waveforms, etc.) is thus achieved. Numerical results are analysed in order to clearly establish what are the more revealing signal attributes that allow for predictable correlation to the ground permittivity values and what kind of functional relations can be outlined among the involved parameters.

To obtain results consistent with a GPR commercial instrument, a 'synthetic' system has been realized. Suitable resistively-loaded half-wavelength folded dipoles have been designed, with specifics (centre frequency, bandwidth, offset distance, etc.) analogous to the real GPR antennas. The basic features of this numerical setup are presented in Figure 4.2. In the GPR configurations of our interest, we basically refer to a two half-space environment (generally air for the upper medium and an unknown dielectric for the lower medium), where fixed ground-coupled Tx/Rx antennas have 'electrically small' mutual separation (in terms of relevant signal wavelengths), so that the interfacial direct wave can account for the presence of the surrounding media (being the 'air' and the 'ground' waves no longer clearly separated) (Comite et al., 2014; Di Matteo et al., 2013; Valerio et al., 2012). In this case, reactive near-field and coupling effects become significant, depending in a complex way on several physical and geometrical system parameters (input signal waveform and frequency spectrum, type and radiation performance of antennas, including location and relevant offset, contrast and dispersive features of the media, etc.). The mutual distance between Tx-Rx antennas can suitably be chosen and fixed as in the related experiments in this case. The bistatic antenna system is placed at the interface between the air and a "soil" layer (made of fiberglass in this test case). In particular, Figure 4.2a displays the synthetic scenario of the ground-coupled system aimed for the analysis of the early-time signal features (with a coordinate frame). Figure 4.2b shows simulated results for the distribution of the radiated EM fields. The plots are displayed in the central *xy* cross plane: in addition to a standard free-space far-field pattern (left picture), a near-field distribution at a fixed distance close to the interfacial antenna is also given (right picture). It should be noted, in fact, that in typical early-time signal operation, the EM near-field behaviours, strongly influenced by reactive and coupling effects, become most significant.

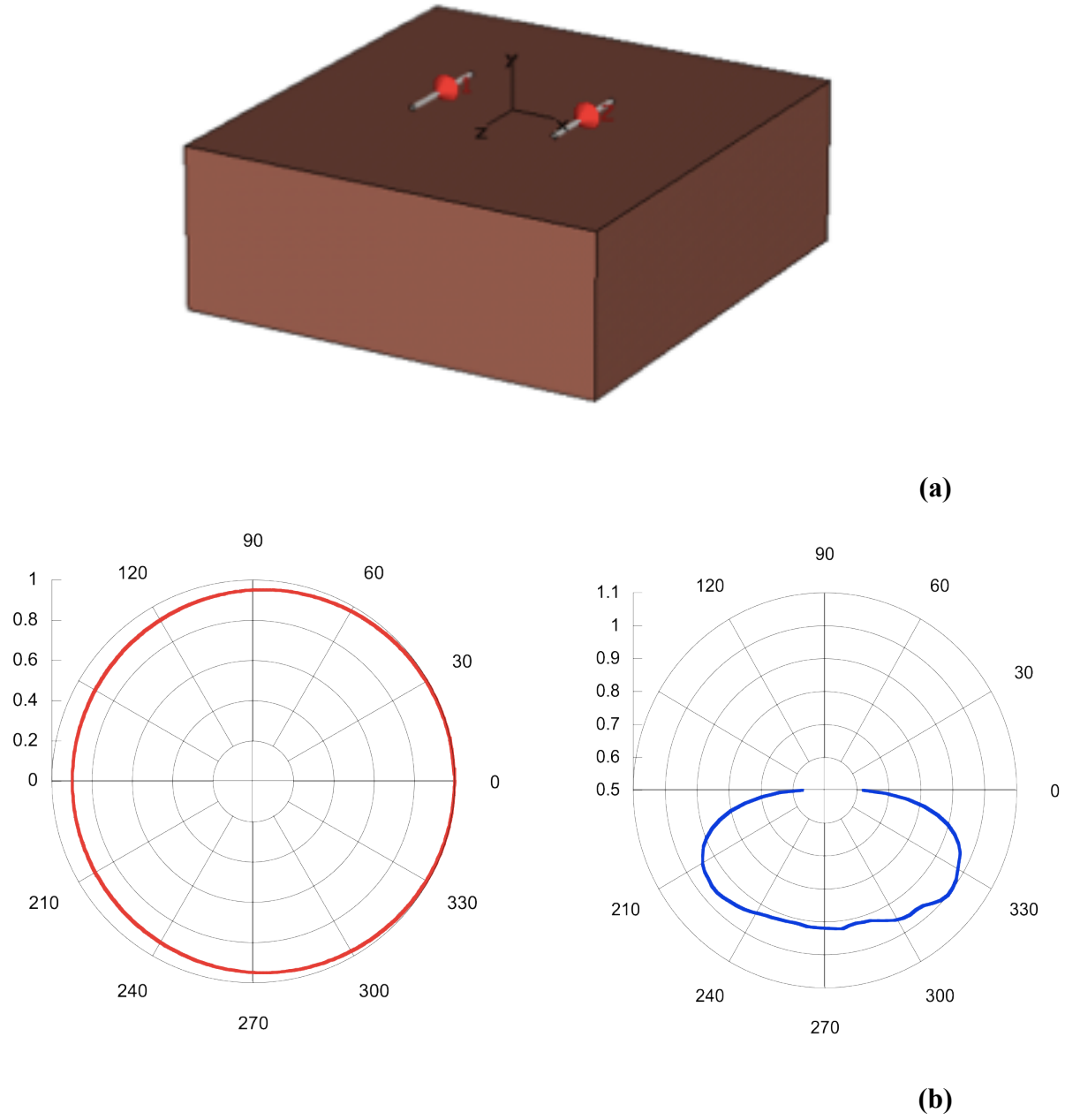

Figure 4.2. GPR numerical setup: half-wavelength dipole antenna in a bistatic configuration. (a) The scenario under analysis (with a coordinate system) consisting of two half-space media (e.g., an air/soil environment, described by the EM parameters ε_r, μ_r, σ) where a fixed bistatic ground-coupled Tx/Rx antenna system is located. Resistively-loaded folded dipoles are chosen in this case. (b) Radiation features of the loaded dipole antenna (in the cross *xy* plane): a far-field pattern in free space (left) and a near-field pattern at close distance (r = 20 cm) from the interfacial ground-coupled dipole (right).

4.4.2 System parameters

For this designed structure, also an input signal similar to what launched in the commercial GPR system has been considered (Figure 4.3), represented by a suitable Ricker pulse.

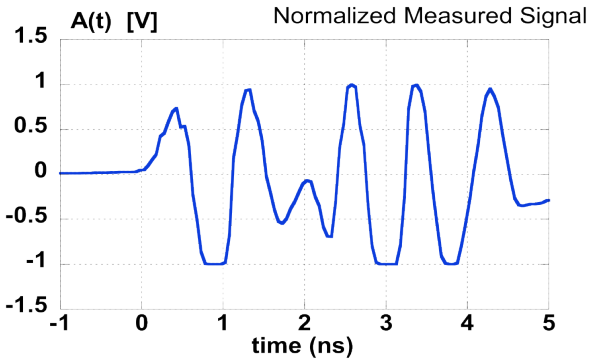

Figure 4.3. A measured signal waveform Amplitude A vs. time t gathered by the GPR, emphasizing the early-time direct wave and the first reflected wave (due to the presence of a bottom metal sheet in the configuration).

In order to test the reliability of the numerical implementation to adequately simulate the commercial GPR system, Figure 4.4a illustrates the time-domain behaviour of a simulated early-time signal waveform picked up by the antenna (to be compared with the initial part of the measured trace of Figure 4.3, for analogous operative conditions). The relevant frequency spectrum of the signal amplitude is given in Figure 4.4b. The excellent agreement that has been found allows us to be fully confident that the simulation setup can provide results that are quite adequate to what revealed experimentally.

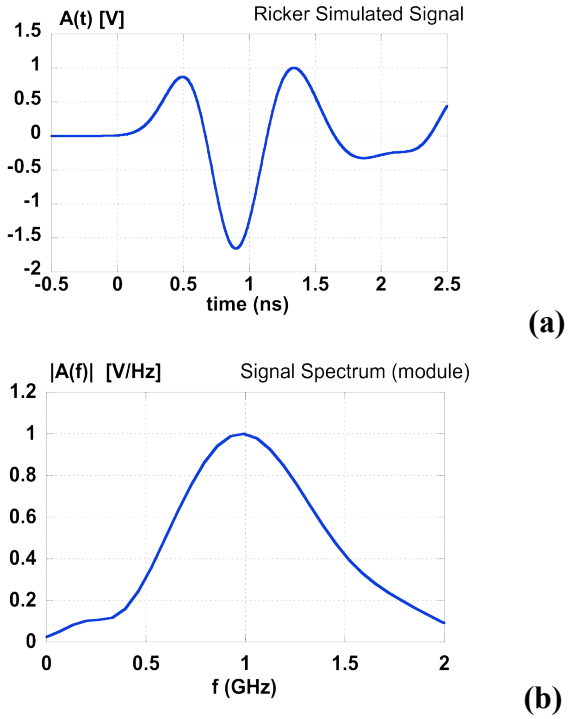

Figure 4.4. Results of early-time traces derived by the simulation setup. (a) A received waveform (signal amplitude A vs. time t), represented by a Ricker pulse (to be compared with the first part of the measured trace from the experimental setup of Figure 4.1 in the analogous operative conditions). (b) The relevant frequency spectrum of the signal amplitude (Fourier-transformed amplitude vs. f).

The availability of efficient setups allows us to perform extensive analysis to quantify accurately the relationships among early-time attributes, the geometry of the setup, and the ground permittivity parameters.

Referring to the scenarios previously introduced, various analyses can be developed from the quantitative outcomes of our implementation. In particular, the received early-time traces vs. time due to a Ricker pulse have been calculated as the ground dielectric constant is varied. From these data, the relevant overall amplitudes of the signal envelope vs. time can also be achieved, using the Hilbert analysis (see Chapter 2, Section 2.2). Examples of the behaviours of the early-time signal envelope amplitudes for a number of different values of ground dielectric constants are presented in Figure 4.5, emphasizing also the fundamental role played by the offset distance d between Tx and Rx interfacial antennas: the upper plot is for $d = 4$ cm, and the lower plot is for $d = 8$ cm (see figure caption and labels for other parameter details).

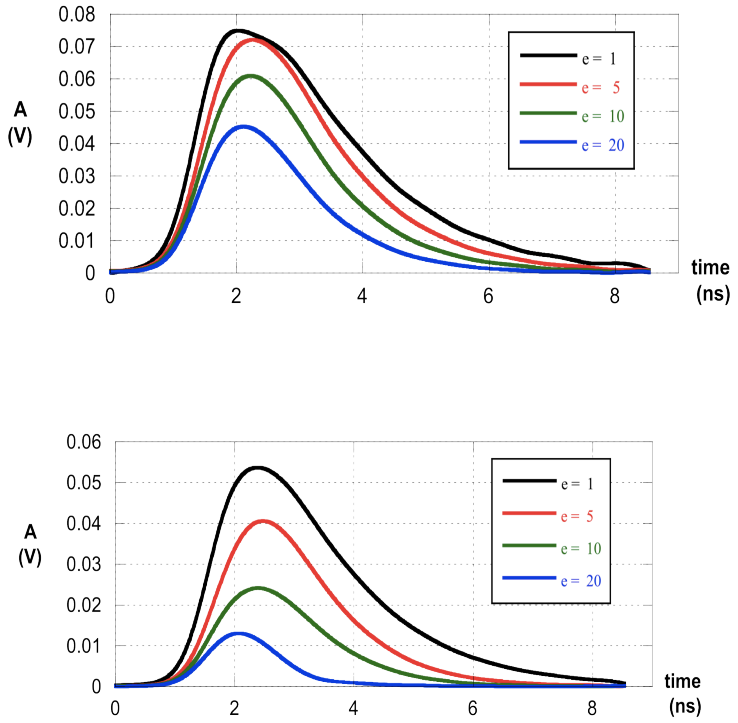

Figure 4.5. Simulated results of ETS characteristics for a ground-coupled radar system with interfacial Tx/Rx dipoles using an input Ricker pulse. The envelope amplitudes of the output ETS signal A (V) vs. time t (ns) are displayed for different relative permittivities ε_r of a non-magnetic and non-lossy ground medium (see labels with associated colours). The relevant ETS 'onset' attribute is also identifiable. The antenna elevation above interface is fixed (h = 1 cm), but different mutual offset distance are chosen: $d = 4$ cm (upper plot) and $d = 8$ cm (lower plot).

Based on this type of outcomes, functional relations between early-time signal amplitudes and permittivity can be derived, by selecting for instance the peak of the early-time first half-cycle as the main observable attribute (Pettinelli et al., 2014; Ferrara et al., 2013b; Di Matteo et al., 2013). By just examining these effects, it is seen that an inverse relationship between the early-time envelope amplitudes and dielectric constant always occurs, but the actual functional dependence between these quantities is not at all related to simple formulas, as supposed so far (Di Matteo et al., 2008; Di Matteo et al., 2013). The functional relationships seem indeed much more complicated and not easily reducible to straightforward closed-form expressions. Nevertheless, by using interpolation procedures on the numerical data, suitable analytical behaviours can be established, depending on the variability ranges of the EM contrast and of offset.

This kind of knowledge is an essential step to point out the practical reliability of the early-time method to predict the EM properties of shallow soils. It also appears very useful to extend this type of study by considering various other parameterizations.

4.5 Experimental Setup

4.5.1 Laboratory Test Site and Measurement Procedures

The early-time approach is based on the amplitude analysis of the first portion of the GPR waveform using a fixed-offset ground-coupled antenna configuration, where the transmitting (Tx) and the receiving (Rx) antennas are separated by a distance comparable with the typical wavelengths of the GPR signal. In particular, the GPR data were collected here using a bistatic TR1000 radar unit (Sensors & Software, Inc) equipped with 1 GHz shielded antennas, having 7 cm Tx-Rx centre-to-centre separation. The GPR measurements were performed in a specifically designed laboratory-scale test site, to remove all the factors that can affect the antenna/material coupling (e.g., large-scale roughness of the surface, lateral inhomogeneities in the solid matrix, lateral permittivity variation), except for the influence of the electric conductivity whose effects are specifically investigated. To this purpose, we performed the measurements on a homogeneous porous material – a 0.35m x 0.35m x 0.17m m box filled with glass beads (∅ 400-800μ) – saturated with deionised water, changing every time the potassium-chloride (KCl) concentration (i.e., the conductivity) and measuring the conductivity variations using TDR, as illustrated in Figure 4.6.

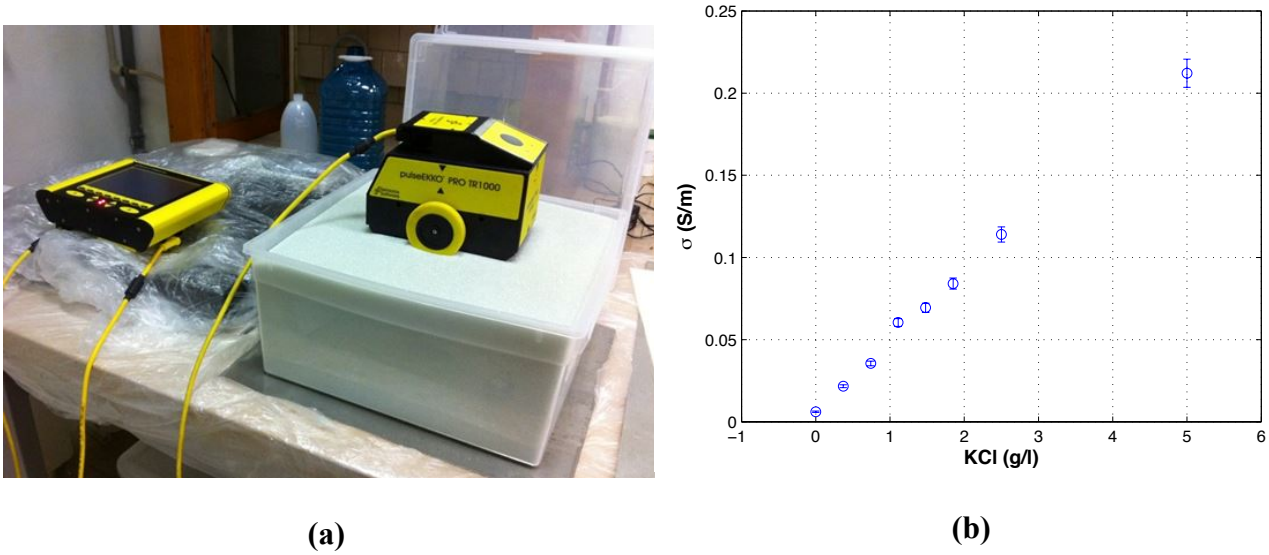

(a) **(b)**

Figure 4.6. The experimental setup for the analysis of early-time signal features. (a) An air/dielectric (glass beads) environment is investigated by means of a simple commercial GPR system with fixed interfacial antennas. The ground dielectric constant and conductivity can be changed in controllable ways. (b) The TDR-derived electrical conductivity as function of salt (KCl) concentrations in a porous sandy soil, for all the measurements.

The TDR data were acquired using a three-pronged probe having a rod length of 15 cm. The probe was connected through a 50-Ω coaxial line to a Tektronix 1502C cable tester (Tektronix, Inc.), which applies a step function wave front and measures the signal reflected by the impedance discontinuities. The TDR data give minimum and maximum conductivities of 0.0061±0.0004 S/m and 0.21±0.01 S/m, respectively.

Through the use of the TDR, we have also verified that the relative permittivity values, for each measurement set, did not significantly change, i.e., ε_{r_TDR}=28.9±0.3. The TDR-derived average permittivity was also compared with the GPR-derived average permittivity, which was determined from the two-way travel (TWT) time according to standard procedures. At the bottom of the test site, we placed a metal sheet to precisely detect the arrival of the GPR reflected signals. Therefore, to extract the permittivity information from the GPR data, we have calculated the cross-correlation function between the direct and reflected wavelet envelopes (Ferrara et al., 2013a; Turin, 1960), determining a permittivity average value of ε_{r_GPR}=29±2.

4.5.2 GPR and TDR Data Analysis

A robust method for extracting the early-time amplitude information is through the use of the complex trace analysis. This technique was originally developed for seismic reflection profiling

(Taner et al., 1979) but can also be applied to GPR (Hwang et al., 2008). In particular, applying the Hilbert transform to the acquired traces (in phase component), the quadrature component can be obtained allowing the calculation of the instantaneous amplitude as shown in Figure 4.6 (de Coulon, 1986).

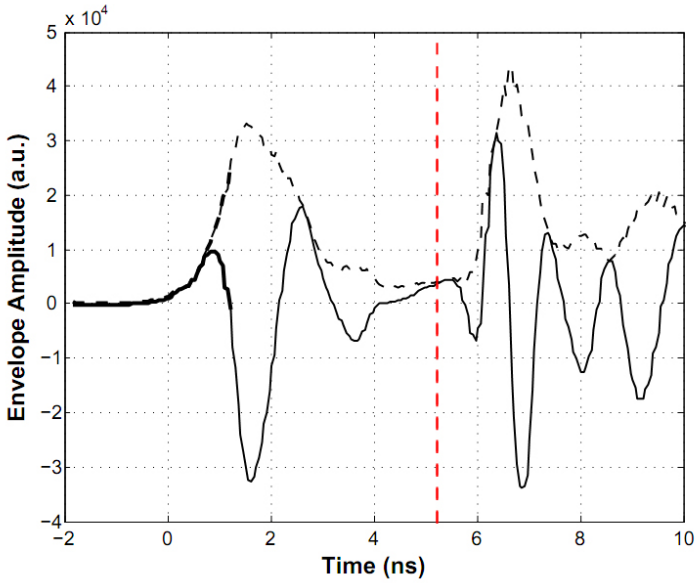

Figure 4.7. Representative GPR acquired trace (solid line) and related Envelope Amplitude (dashed line). The first half-cycle bolded and the reflection from the investigated media bottom is highlighted by the red dashed line.

In this study, we have determined the early-time amplitudes for the traces by taking the maximum value of the envelope in a temporal window that coincides with the first half-cycle of the GPR signal (see the bold line in Figure 4.7). The choice of analysing the first half-cycle comes from previous experimental and theoretical studies (Di Matteo et al., 2008; Di Matteo et al., 2013; Ferrara et al., 2013a; Ferrara et al., 2013b; Pettinelli et al., 2014), where it was found that the first half-cycle is the part of the signal which exhibits the best correlation with the soil dielectric properties, maximizing the signal-to-noise ratio and minimizing interference from reflections caused by shallow interfaces. To determine the uncertainty associated with the GPR envelope amplitudes, we acquired a total of 1000 traces for each measurement. The data analysis showed that the envelopes follow a Gaussian distribution, with an associated relative uncertainty of 3%.

4.7 Comparison between Experimental and Simulated GPR Results

The acquired radar traces show the effect of different KCl concentrations (e.g., conductivities) on the coupled early-time air-ground wave signal, as illustrated in Figure 4.8a (the change of the colours for these curves is related to various salt concentrations). It is clear that the measured

waveforms (on the left) and the relevant envelope amplitudes (on the right) show that an increase in the conductivity concentration gives rise to a decrease in the signal amplitude.

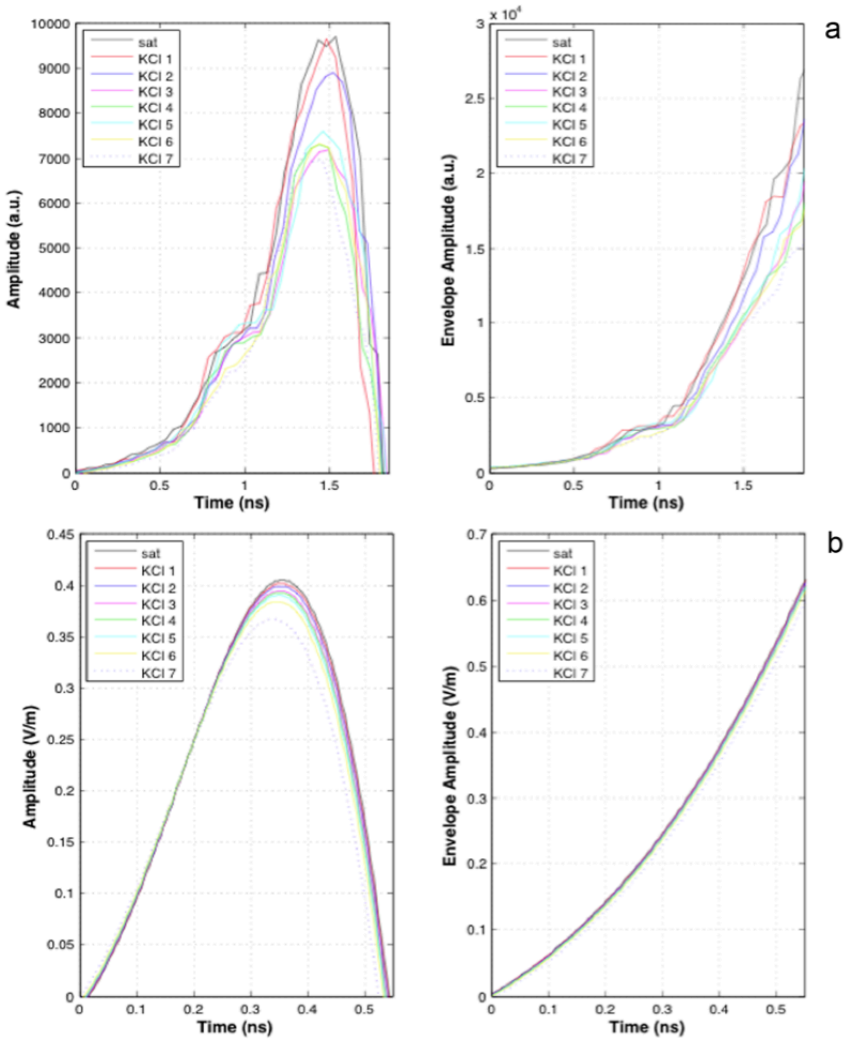

Figure 4.8. a) GPR averaged early-time first half cycle (on the left) and the related envelope (on the right) for different KCl concentrations (e.g., conductivities), acquired by measurements from the experimental setup; b) same quantities obtained by ad-hoc numerical simulations. Note that in the legend the term "sat" refers to deionised water and KCl1 and KCl7 refer to the lowest and the highest potassium chloride concentration, respectively.

The experimental setup discussed above has also been simulated by means of a suitable implementation of the CAD electromagnetic tool. To obtain results consistent with the measured data, the GPR antennas have expressly been designed and simulated, to provide a bandwidth similar to the commercial GPR system (0.5-1.5 GHz). The results of the signal traces deriving from this simulated environment, again as a function of various conductivities, are presented in Figure 4.8b.

From the comparisons between the measured and the simulated traces, together with their related envelopes, it is confirmed that the signal amplitudes are consistently affected by the conductivity variations. However, it is worth to note that the sensitivity of simulated data on salt concentration is

lower than for the experimental data. The observed discrepancies are likely due to the physical difference between the ideal simulated antennas and those used in the commercial GPR system.

To quantitatively compare the data, we estimated the degree of the exponential correlation between the GPR averaged envelope maximum of the first half-cycle and the TDR-derived conductivities. From this analysis we have found that an exponential function clearly represents both the experimental data (r=0.95), and the simulated data (r=0.99).

The variations of the electrical properties of the material can also be cross-checked by analysing the reflected wave from the investigated medium bottom. Figure 4.9 shows the exponential attenuation that conductivity causes in the GPR wave propagation.

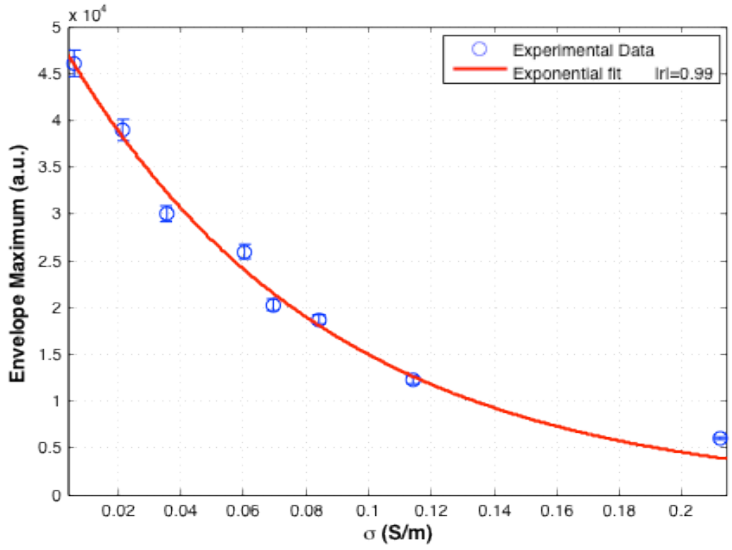

Figure 4.9. Envelope maximum of the reflected wave as a function of the corresponding conductivity values derived from the TDR measurements. The curve is the exponential data fitting.

4.8 Conclusions

In this work, the possibility to evaluate the soil dielectric-constant and conductivity features from the early-arrival signal attributes in ground-coupled radars is firstly studied with the implementation of a numerical setup. The reliability of the numerical implementation to adequately simulate the as similar as possible a real GPR system, was tested comparing experimental and simulated early-time signal waveform picked up by the antenna. In particular, we have considered the recently-developed GPR early-time amplitude technique to examine the signal sensitivity with respect to the variations of the subsurface electrical conductivity. We compared the envelope maximum of the acquired and simulated GPR signal first half cycle with the dielectric conductivity obtained from concurrently collected TDR measurements.

Our study has emphasised that the early-time can yield information about near-surface conductivity changes which are consistent with those obtained from TDR analysis. Moreover, the high correlation coefficient obtained between the GPR envelope and the TDR data points out that the early-time signal is rather sensitive to conductivity changes, confirming what has already been found in the previous theoretical study (Di Matteo et al., 2008; Di Matteo et al., 2013).

Based on these achievements, additional tests can be performed to further develop this approach. In particular, materials with higher conductivities and lower permittivities could be tested to better highlight the sensitivity of the conductivity effect on the early-time amplitudes. Moreover, it is worth to notice that the GPR early-time technique is system-specific and it should be properly calibrated for each radar equipment. Nevertheless, the results obtained here have shown that this technique could be used as an efficient tool for extracting the near-surface physical parameters of the materials.

Chapter 5

An Evaluation of Early-Time GPR Amplitude Technique for Shallow Soil Moisture Monitoring under Natural Field Conditions: Final Step

5.1 Executive Summary

It has been recently demonstrated that the early-time portion of the GPR signal, consisting of the direct air and ground wave events, is dependent on the shallow subsurface bulk electromagnetic properties of the material; these properties are strongly controlled by the water content in this material. While several controlled experiments have been conducted to study the effects of water content variations on the antenna-material coupling, they considered a limited range of moisture variations and soil textures. Further, those previous experiments did not consider highly dynamic shallow moisture responses that would be encountered under natural field conditions. For these reasons, general acceptance of this method requires that it be tested in 'real-life' applications. This work evaluates the early-time GPR technique under natural field conditions where surface roughness, lithology, lateral heterogeneities, vegetation and water content dynamics are not controlled. We assess the capacity of the early-time amplitude technique over a complete annual cycle of soil moisture conditions at three textural sites. To evaluate the sensitivity of the early-time amplitudes to subsurface water content variations, we compare the early-time results acquired using the enveloped amplitude of the first part of GPR signals with the bulk dielectric permittivity obtained from concurrently collected common-midpoint direct ground wave velocity and gravimetric water content measurements. Our results demonstrate that the early-time method can yield near-surface permittivity information that is consistent with that obtained from direct ground wave velocity measurements, and accurate predictions of shallow soil moisture conditions.

5.2 Introduction

Monitoring spatial-temporal variations in soil water content is a critical issue in the emerging discipline of hydropedology (Zhu et al., 2012). Soil water content is a fundamental parameter for determining biophysical and hydrological processes in the vadose zone (Vereecken et al., 2008); it

also plays a key role in understanding the impact of climatic change on water resources (Seneviratne et al., 2010). Given the value of soil water content data, a great deal of research has gone into the development of novel soil water content measurement techniques capable of providing accurate estimates of water content across a wide-range of spatial scales (Robinson et al., 2008; Vereecken et al., 2008; Bittelli, 2011; Zhu et al. 2012).

Conventional water content monitoring methods such as gravimetric sampling, thermal neutron probes and time-domain reflectometry (TDR) are generally invasive and give highly localized information due to their small sampling volumes. Hence, these techniques may not be appropriate for efficient acquisition of spatial data at the field-scale. Remote sensing imagery has the capacity to provide spatial information, but at a much larger scale (e.g., in the case of satellite remote sensing, averaging spatial data over many tens of meters or more). Further these remote methods are limited to the upper few centimetres of soil and are very sensitive to vegetative cover.

Given recent advancements in commercial geophysical systems, researchers are now exploring new spatial and temporal monitoring techniques capable of providing valuable soil water content information at the intermediate scales between point and remote sensing measurements. Water content estimation in this scale range is important in many hydrological processes such as water infiltration, percolation, runoff and evapotranspiration that affect soil erosion and flooding (Grayson and Western, 1998). In turn, soil water infiltration influences the transport of pesticides and other pollutants that can impact environmentally sensitive surface water bodies and ground water resources (Ritsema, 1999; Huisman et al., 2001; Tallon and Si, 2004). Moreover, soil water content is usually spatially variable at intermediate scale; therefore, monitoring techniques capable to provide a continuous and fast estimation of such a parameter can be very useful in different fields (e.g., geo-pedology, hydrology, agronomy and forestry).

Surface hydrogeophysical methods are highly suited for obtaining soil water content information at the intermediate scale due to their sampling volume (i.e., dm^3–m^3 scale), non-invasive nature and high resolving power. In particular, ground-penetrating radar (GPR) techniques have been shown to be very effective at monitoring soil water content at this scale (Huisman et al., 2003a; Weihermüller et al., 2007; Jol, 2009). While both GPR and TDR techniques are governed by the same electromagnetic (EM) properties, the larger GPR sampling volume and its non-invasive nature makes GPR techniques less-prone to the effects of macropores and air gaps compared to TDR probes (Robinson et al., 2003).

Monitoring soil water content in the shallow vadose zone directly below the air-soil interface is an important problem given its highly dynamic nature and the processes (e.g., evapotranspiration) taking place within this region. The direct ground wave (DGW) GPR technique uses EM waves that propagate along this interface; hence, it is well-suited for monitoring water content in shallow

root zone environments. While a number of studies (e.g., Grote et al., 2003; Huisman et al., 2003b; Galagedara et al., 2005; Weihermüller et al., 2007) have examined the capacity of this method to predict water content in this zone under limited ranges of conditions, an extensive field study by Steelman and Endres (2010) found significant temporal changes in the near-surface EM wavefield corresponding to seasonal and shorter-term variations in soil water content states. Steelman and Endres concluded that while the DGW velocity method can be successfully used to monitor soil water content dynamics over the annual cycle, the evolving near-surface EM wavefield can significantly complicate its application and analysis.

An alternative surface GPR method for monitoring soil water content directly below the air-soil interface has been proposed by Pettinelli et al. (2007). This technique analyses amplitude attribute information over the early-time portion of a GPR pulse obtained from conventional single-offset surface-coupled profiling. While this early-time technique has been tested at a controlled field site (Pettinelli et al., 2007) and under a laboratory setting (Ferrara et al., 2013), there is an obvious need to evaluate this method under natural field conditions where surface roughness, lithology, lateral heterogeneities, vegetation and water content dynamics are allowed to change with the natural environment.

Data acquired as part of a broader study (i.e., Steelman and Endres, 2010, 2011; Steelman et al., 2012) to assess the capacity of surface GPR techniques to monitor soil moisture dynamics over multiple annual cycles provide an exceptional opportunity to examine our early-time amplitude technique. The aim of this study is to assess the sensitivity of the early-time amplitude technique to subsurface water content variations over the annual cycle of soil water content conditions using that extensive set of reflection profiling data acquired at three sites with different soil textures. The results of our early-time analysis demonstrate that this portion of the GPR signal is a potentially valuable method for quantitatively monitoring near-surface soil water content under natural field conditions.

5.3 Early-Time Technique Recall

The early-time technique is a new radar approach for the estimation physical properties of the near-surface materials, when the data are acquired using a fixed-offset ground-coupled GPR antenna configuration. The early-time portion of the GPR waveform is linked to the energy of the direct signal, that propagates between the transmitting and receiving antennas. From the analysis of the amplitude-attributes of this first part of the GPR signals it is possible to get information about soil EM parameters (e.g., Pettinelli et al., 2007; Di Matteo et al., 2008; Ferrara et al., 2013a; Ferrara et

al., 2013b). The amplitude information is obtained through complex trace analysis applied to the acquired GPR early-time signal (Taner et al., 1979). Note that, as the early-time amplitude is affected by EM parameters variations, and mainly by permittivity changes, it is possible to determine also the soil volumetric water content using an appropriate petrophysical relationship (Steelman and Endres, 2011).

The theoretical bases of this radar technique are described in Di Matteo et al., (2013), where one of the main findings was to define how the amplitude of the direct signal that propagates between the antennas is related to the relative soil dielectric permittivity ε_r. In particular, the explicit expression for the direct signal amplitude was found and that the waveform amplitude presents an inverse linear dependence on the permittivity values.

The study of Di Matteo et al. (2013) also has confirmed what was found from previous studies (Ferrara et al., 2013a; Ferrara et al., 2013b), that the best signal portion to be analysed with the early-time method is the first positive half cycle of the radar waveforms. Essentially, since the first arrival of the GPR signals is strongly dependent on shallow subsurface permittivity variations, the signal to noise ratio is maximised by minimizing the interference from reflections caused by shallow interfaces.

5.4 Elements of the DGW Method

The DGW method uses the GPR trasmitter placed along the air-ground interface; in this configuration, the energy radiates outward as a spherical wavefront through both the air and the ground. The rate of expansion of the wavefront depends on the dielectric properties of the subsurface. Figure 5.1 shows wavefronts created when the transmitter rests upon the ground surface. The energy is propagated though the air and the ground. Since the electromagnetic field at an interface must have continuity, the wavefront in air creates a lateral wave in the soil, and similarly the wavefront in the soil creates the evanescent ground wave in the air (Annan, 1973; Grote et al., 2010).

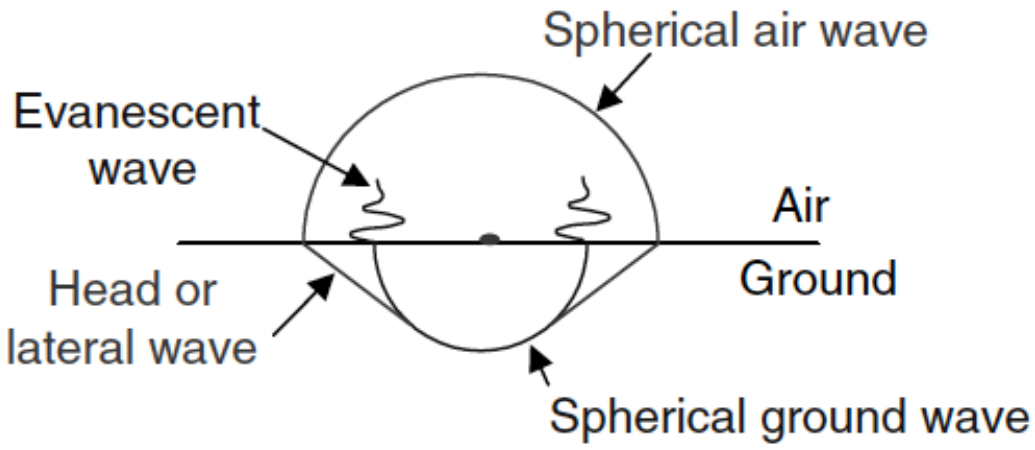

Figure 5.1. An illustration of the various wavefronts for a small electric dipole on the surface of a dielectric (Annan, 2002).

The fields at the ground surface are composed by two propagating components with one having the phase velocity of the air, and the other the velocity of the ground. The DGW is an interfacial wave represented by a combination of the spherical wave in the ground and the evanescent wave in the air which propagates along the air-ground interface between a transmitting and receiving antennae (Steelman and Endres, 2010).

The use of multi- offset CMP soundings, where the transmitting and receiving antenna are moved apart in opposite directions keeping a constant distance, allows the various wavefields to be distinctly separated. Figure 5.2 shows a representation of possible travel paths of GPR energy (Figure 5.2a) and a representative CMP data set (Figure 5.2b). Note that, systematically, varying the antenna separation, the signal path varies in the ground, enabling the estimation of wave properties. As the distance between the antennas increases with each measurement in a variable-offset survey, the time needed for the DGW to travel between antennas also increases. The airwave is energy traveling directly from the transmitter to the receiver, but it travels through the air at the speed of electromagnetic waves in free space; therefore, the airwave velocity is faster than the ground wave, so the airwave arrives earlier in time (Grote et al., 2003).

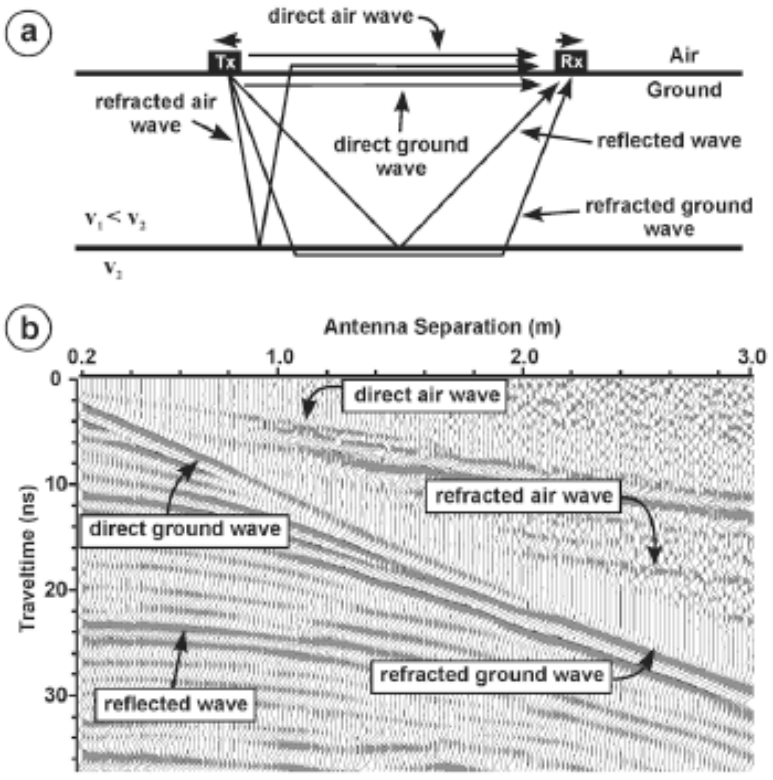

Figure 5.2. Schematic diagram showing the possible raypaths of GPR emitted signals and (b) a representative CMP soundings; direct air wave and DGW, critically refracted air and ground waves, and reflected ground waves are indicated (Steelman and Endres, 2010).

The DGW can be determined from CMP survey because it is characterized by a linear travel time–antenna offset relationship besides the inverse of its slope is equal to its velocity. The simplicity of a linear relationship (i.e., simple identification of the wavefield and straightforward linear curve fitting procedure) permits determination of EM wave velocity in near surface environments (Steelman and Endres, 2010).

Although several researchers have demonstrated the potential of GPR DGW methods for soil water content characterization, the efficacy of this technique is limited by the sampling depth uncertainty of GPR ground waves (Huisman et al., 2001; Hubbard et al., 2002; Grote et al., 2003; Galagedara et al., 2005a; Grote et al., 2010). Because of the unguided nature of this EM wave, it is difficult to quantify the soil volume influencing DGW propagation. Nevertheless, a number of studies have attempted to empirically define the effective DGW sampling depth (e.g., Du, 1996; Sperl, 1999; Galagedara et al., 2005b). Alternatively, van Overmeeren et al. (1997) used the similarity between GPR and seismic data to approximate the DGW sampling depth as half of the Fresnel zone, as it is accepted for seismic ground waves (Hagedoorn, 1954). This relationship proposes the equivalence of the DGW sampling depth (d) to half the Fresnel zone:

$$d = \frac{1}{2}\sqrt{\frac{vS}{f}} \qquad (5.1)$$

where v is the measured velocity of the DGW, S is the separation distance between the transmitting and receiving antenna, and f is the central frequency of the DGW signal. This relationship indicates that DGW sampling depth increases with decreasing soil permittivity (e.g., dry soils) and dominant central frequency (i.e., lower antenna frequencies); DGW sampling depth is also dependent on antenna separation distance. However, researchers have not reached a consensus for a functional relationship between DGW propagation and effective sampling depth (Steelman and Endres, 2010).

In a low-loss and non-magnetic material the propagation velocity of electromagnetic waves in a medium is determined from its relative dielectric permittivity (ε_r) (i.e., the effective permittivity ε of the bulk material relative to the free space permittivity ε_0) using the equation

$$v = \frac{c}{\sqrt{\varepsilon_r}} \qquad (5.2)$$

where c is the EM velocity in free space. Therefore, using EM wave velocity measurements it is possible to evaluate the material permittivity and, when the permittivity of liquid water ($\varepsilon_w = 78 - 88$) is much higher than permittivity of the other common components of the soil system (i.e., mineral soil grains $\varepsilon_s = 4 - 6$ and air $\varepsilon_a = 1$), as well as ice ($\varepsilon_i = 3.2$) (Cassidy, 2009), the DGW GPR methods can be also used to predict volumetric water content.

The estimation of soil water content from EM velocity, however, requires an appropriate petrophysical relationship to convert the bulk permittivity ε_r of the material into an accurate volumetric water content (θ) measurement (Steelman and Endres, 2010; Steelman and Endres, 2011).

5.5 Experimental Description

5.5.1 Field Site

The GPR data used in this study were acquired at three active agricultural field sites characterized by different soil textures: sand, sandy loam and silt loam. Both the sand (43°29'4.9"N, 80°38'34.4"W) and the sandy loam (43°29'1.3"N, 80°38'31.7"W) soil sites are 3 km west of Waterloo, Ontario, Canada, whereas the silt loam soil site (43°5'8.5"N, 80°45'22.3"W) is 2 km south of Woodstock, Ontario, Canada. The Waterloo sites are located on the Waterloo moraine,

which is characterized as an irregular tract of gently rolling to hummocky terrain with some exposures of ice- contact stratified sand and gravel deposits (Russell et al., 2007). Shallow core logs collected at the Waterloo sites showed that the sand site is characterized by a sequence of stratified sand deposits, whereas the sandy loam site grades downward into loamy sand below a depth of 0.4 – 0.5 m. The water table at the Waterloo site is believed to be 10 – 15 m below ground surface based on nearby springs. Precipitation and atmospheric temperature for the Waterloo sites were monitored using the University of Waterloo weather station located approximately 7 km east of the study sites. The Woodstock silt loam site is situated in a localized valley described as a glacio-fluvial outwash channel (Cowan, 1975); it is located 45 km southwest of the Waterloo sites. A nearby core log shows that this monitoring location is characterized by approximately 0.5– 0.7 m of silt loam grading downward into a silty gravel with sand. The water table varies seasonally between 2 and 3 m below ground surface based on water level data collected in the vicinity of the study area. Precipitation and atmospheric temperature was monitored using an on- site meteorological station located approximately 0.5 km west of the GPR monitoring site. Detailed information about these field sites and the weather conditions are found in Steelman and Endres (2010) and Steelman et al. (2012).

5.5.2 GPR Data Acquisition and Gravimetric Soil Sampling

For each survey date, a reflection profile and CMP sounding were collected along a fixed survey line at the three sites using a PulseEKKO 1000 GPR system (Sensors and Software, Inc.) equipped with high-frequency (900 MHz) bistatic antennas. The GPR data were collected using a time window of 100 ns, sampling interval of 0.1 ns and 64 stacks per trace. The reflection profiling data were collected using a standard antenna offset of 0.17 m (manufacturer's brackets), with a step size of 0.02 m along a 2 m profile resulting in 101 traces. For the CMP soundings, the transmitter and receiver antennas were manually separated at 0.02 m increments from 0.2 m to a maximum separation of 2.0 m.

The time periods covered by the GPR data were the following: May 2006-August 2007 for the silt loam site, August 2006-November 2007 for the sandy loam site and August 2006-October 2008 for the sand site. Each of these data sets cover the range of soil water content conditions commonly encountered during the annual cycle of a mid-latitude temperate climate. The sampling intervals during this acquisition program varied from 1 day to 4 weeks and resulted in 138, 28 and 32 concurrent pairs of reflection and CMP data at the sand, sandy loam and silt loam sites, respectively.

In addition to the GPR data, concurrent soil sampling was done in the vicinity of the survey lines (i.e., within 1–2 m of the line midpoint) to obtain gravimetrically-derived soil water contents. This sampling was performed during the first annual cycle at each site during unfrozen soil conditions, collecting 34 samples for the sand site, 23 samples for the sandy loam and 20 samples for silt loam sites (Steelman and Endres, 2010). These soil samples were extracted from the upper 0.5 m of soil at 0.1 m intervals.

5.5.3 GPR Data Processing and Analysis

To obtain the early-time amplitude information, we applied the complex trace analysis to the GPR reflection profiling data. In particular, this study used MATLAB® software to determine the early-time amplitude values for the traces by determining the maximum value of the enveloped amplitude in a time window that coincides with the first half-cycle of the GPR signal. It should be noted that the first half-cycle is the portion of the real trace between zero and the first zero crossing (Figure 5.3).

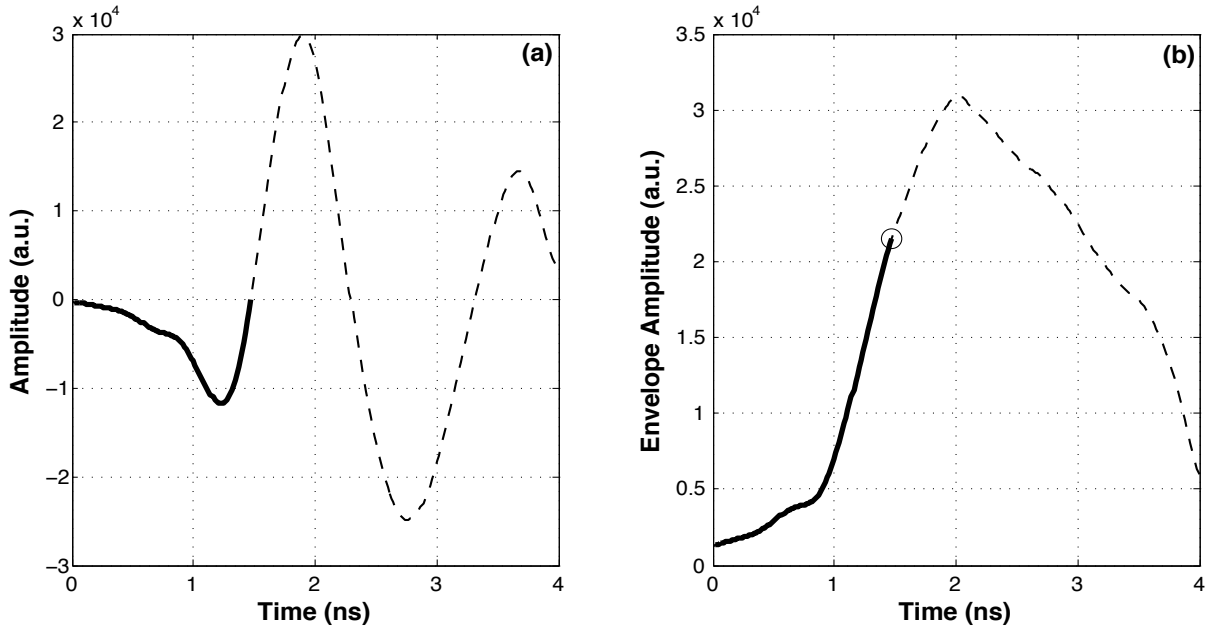

Figure 5.3. GPR waveform (a) and its related Envelope Amplitude (b). The first half-cycle duration is indicated in the panels using bold lines. The circle in (b) indicates the maximum amplitude value.

The choice of analysing the first half-cycle comes from previous experimental and theoretical studies on the early-time method (Ferrara et al., 2013a; Ferrara et al., 2013b; Di Matteo et al., 2013) where it was found that the first half-cycle is the part of the signal that has the highest correlation

with the soil dielectric properties, maximizing the signal-to-noise ratio and minimizing interference from reflections caused by shallow interfaces. Overall, the collected data are of good quality and did not require pre-processing before implementing our early-time analysis.

An early-time amplitude value based on the complex trace envelope was determined for each reflection profile and compared with the dielectric permittivity estimates obtained from the DGW velocity measurements and the gravimetrically-derived water contents. The DGW velocities have been taken from data presented in Steelman and Endres (2010) and Steelman et al. (2012); the methodology used for the DGW analysis is described in Steelman and Endres (2010). The water content data are taken from Steelman and Endres (2010) where a description of the measurement procedure and detailed soil descriptions can be found.

5.6 Results and Interpretation

5.6.1 Comparison between DGW and Early-Time Methods

Figure 5.4 shows representative examples of the acquired early-time radar traces at the sand site, for a range of dielectric permittivity values obtained from the corresponding DGW velocity measurements.

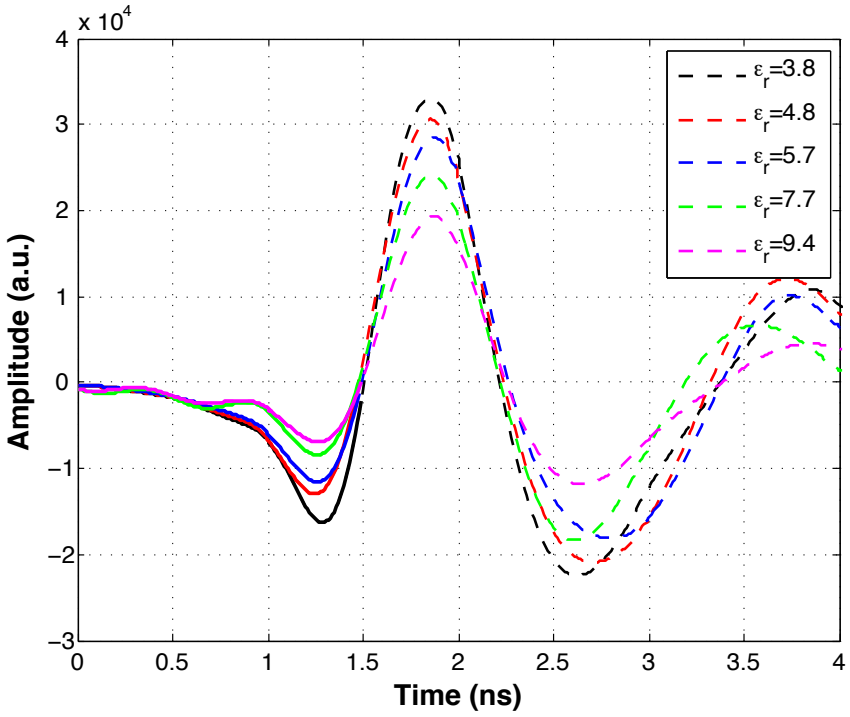

Figure 5.4. Representative early-time GPR signals for a range of soil dielectric permittivity values at the sand site. The permittivity values were obtained from the corresponding DGW velocity measurements. The first half-cycle is indicated with bold lines.

It can be clearly seen from this figure that the waveforms systematically evolve in terms of signal amplitude, such that a decrease in permittivity results in an increase in signal amplitude. Given the dependence between bulk dielectric properties of soil and water content, these early-time amplitude decreases correspond to water content increases. Figure 5.5 shows the computed amplitude envelope for the complex traces of the signals given in Figure 5.3.

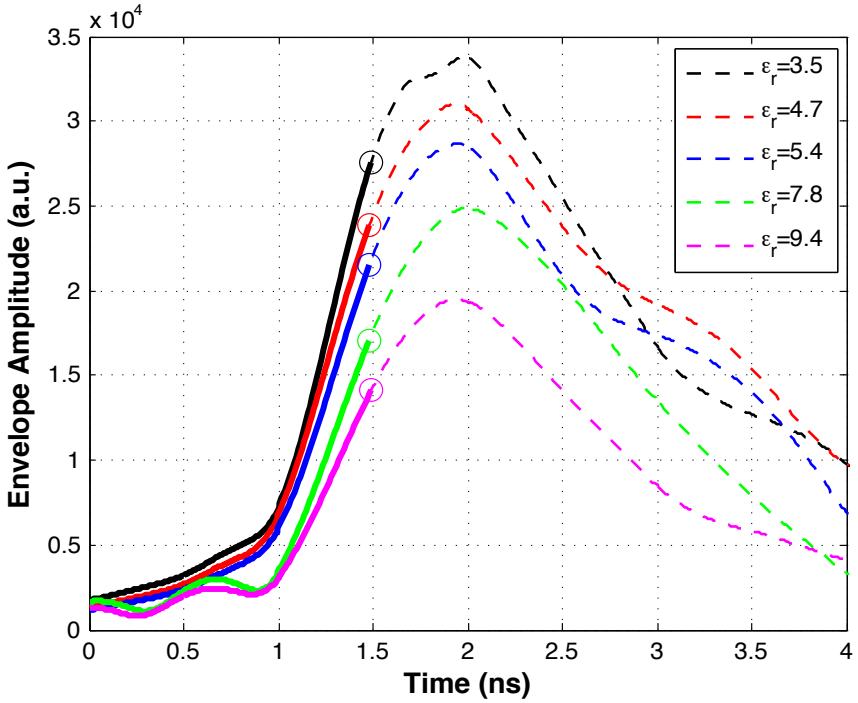

Figure 5.5. The complex trace amplitude envelopes for the GPR signals shown in Figure 2. The first half-cycle is highlighted with bold lines and the maximum amplitude values with circles.

Similarly, it is clear that the instantaneous-amplitude is strongly dependent on the dielectric permittivity of the soil. To obtain the early-time amplitude information, we determined the maximum value of the enveloped trace, such as the ones illustrated in Figure 3, in the time interval that corresponds to the signal first half-cycle.

For a better comparison, the envelope amplitude values were normalized to the maximum value encountered in our dataset. As would be expected, we found that the early-time amplitude measurements vary laterally along the profile line on each survey date. The nature of this variation can be appreciated from the histograms of the early amplitude measurements for two representative dates in Figure 5.6 corresponding to low and high permittivity values at the sand site.

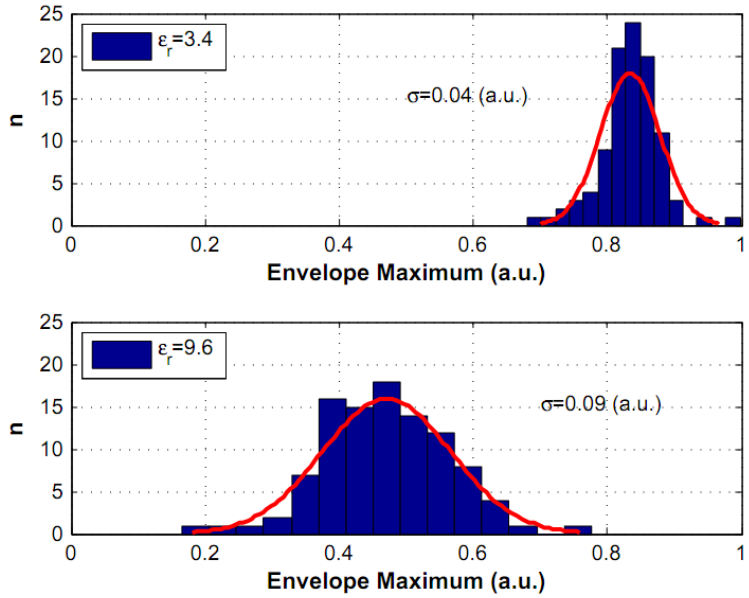

Figure 5.6. Histograms of the early-time envelope maximum values obtained along the survey line at the sand site for two dates (9 July 2008 and 16 May 2007, respectively) corresponding to low and high permittivity values based on the DGW velocity measurements.

From this figure, it appears that the degree of lateral variation increases with increasing permittivity. This trend is corroborated in Figure 5.7 where the standard deviation of the early amplitude signal for each survey is plotted as a function of the corresponding permittivity value obtained from the DGW velocity measurements.

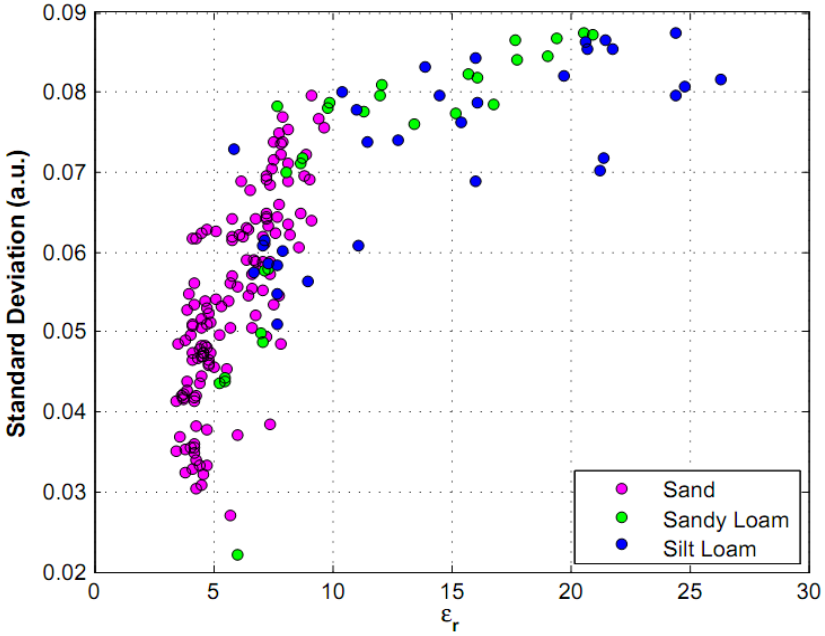

Figure 5.7. The standard deviation of the early-time envelope maximum measurements for each survey date as a function of the permittivity derived from the corresponding DGW velocity measurements for all the three sites.

For all three sites, there is a direct correlation between increasing standard deviation and higher permittivity. Given the dependence of bulk soil dielectric permittivity on water content, this trend suggests that the early-time amplitude technique is detecting more lateral variability during wetter conditions. While we do not have a definitive cause for this observation, such behaviour could reflect small-scale spatial variations in soil properties (e.g., grain-size distribution, porosity) that affect water retention as characterized the matric suction-saturation relationships. Given the large contrast in the dielectric permittivity of water and the other components (i.e., soil grains and air), one would expect these small-scale spatial variations to have greater impact on dielectric measurements under wetter conditions where they would produce corresponding pattern of water content variation (Di Pasquo et al., 2007).

The early-time envelope amplitude value was determined for all 101 traces along each reflection profile. To reduce the effects of variability in the early-time amplitude along each profile due to localized changes in near surface conditions, the average value of this quantity over the 101 traces (i.e., 2 meters) was used. Further, this lateral averaging window is identical to the spatial coverage of the CMP sounding used for the DGW measurements, making the comparison between these two quantities more consistent. Horizontal averaging can be used to compensate for the effects of small-scale lateral variations in the early amplitude measurements. To investigate the effect of horizontal averaging, we have determined the correlation coefficient for the inverse relationship between early-time amplitude and dielectric permittivity predicted by the theoretical work of Di Matteo et al. (2013) for progressively averaging window lengths. The averaging window is always centred at the midpoint of the reflection profile and is incrementally expanded until the entire profile line is used. The results of this analysis illustrated in Figure 5.8 clearly show that correlation coefficient increases rapidly as the width of the horizontal averaging window increases, indicating that the averaging process is effectively attenuating the effects of laterally varying surface conditions.

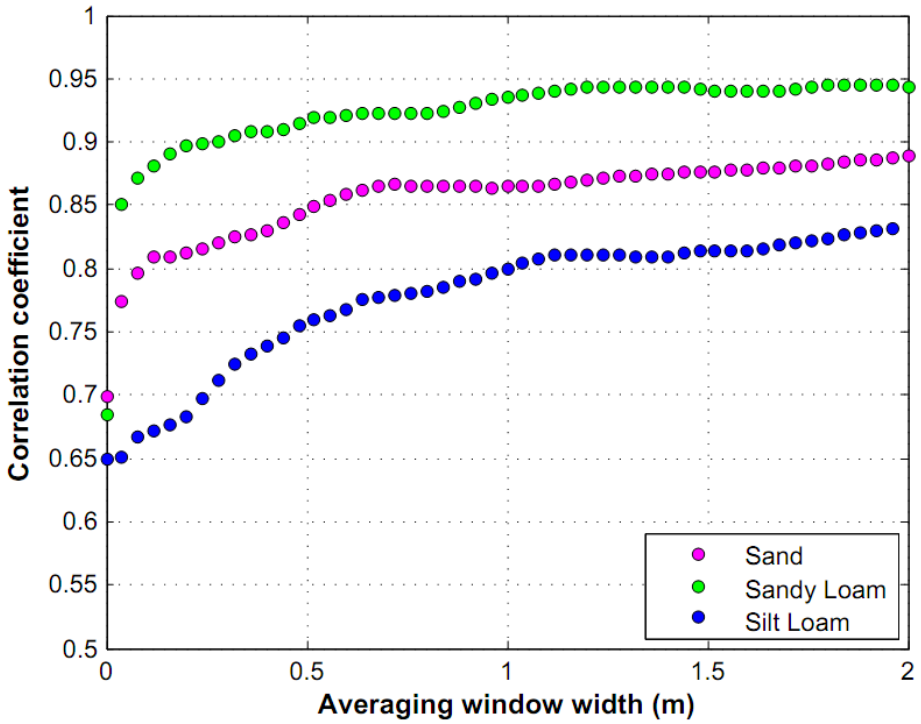

Figure 5.8. Correlation coefficient for the inverse relationship between the average envelope maximum in the first half-cycle and the CMP derived averaged permittivities as a function averaging window width.

Most of the improvement in the correlation coefficient is obtained once the window width is 0.50-1.00 meters. While we use an averaging window of 2.00 meter in the remainder of this work to be consistent with the spatial coverage of the CMP sounding used for the DGW measurements, the results in Figure 6 suggest that smaller windows could be used at these three sites to preserve the lateral resolution of an early-time survey without significantly impacting the correlation between early-time amplitude and permittivity.

Using the two-meter window width, an average early-time envelope maximum value was determined for each survey date at the three sites; the resulting time-series are given in Figure 5.9.

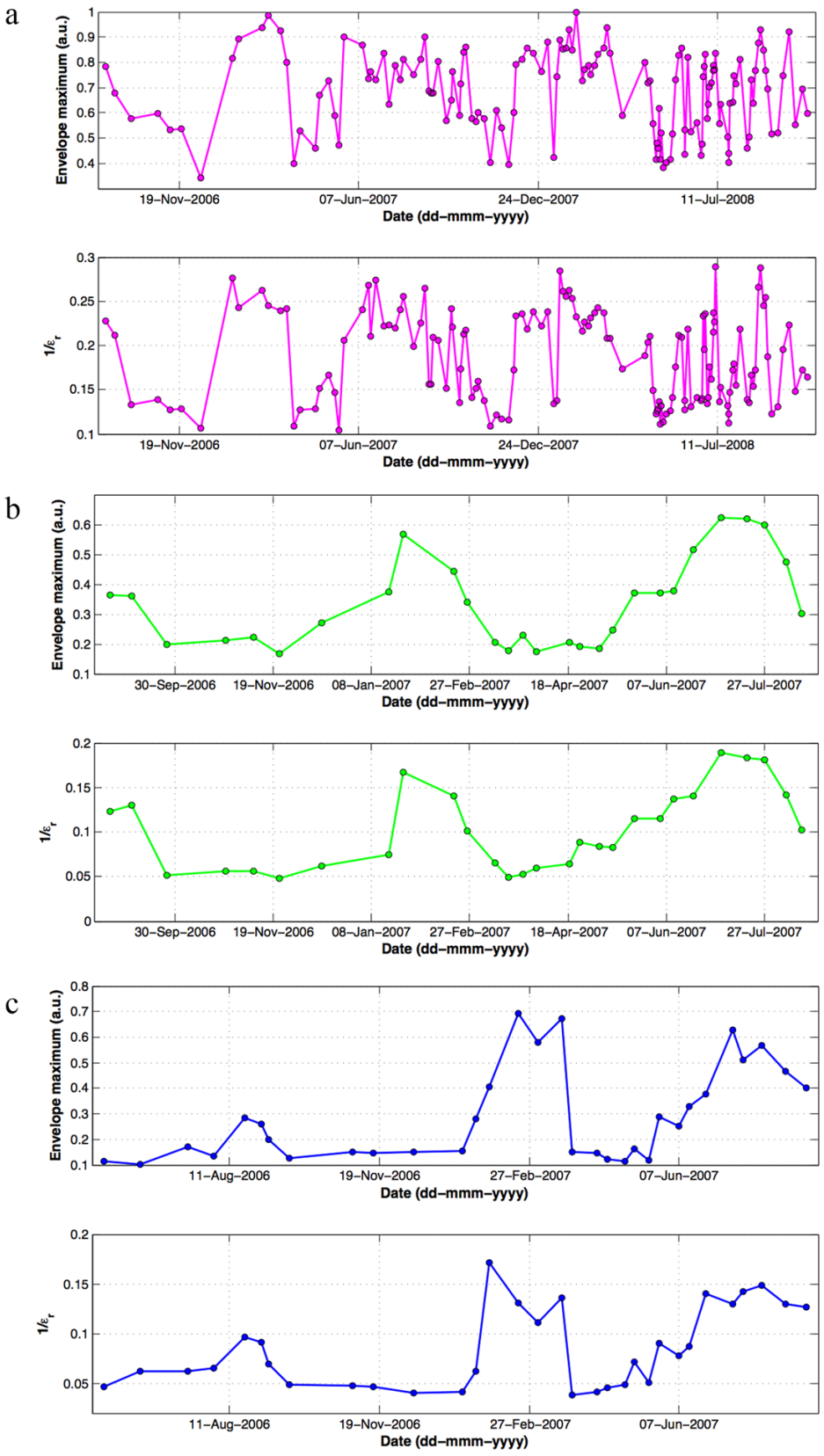

Figure 5.9. Temporal variation in the early-time envelope maximum and the corresponding $\frac{1}{\varepsilon_r}$ values derived from the DGW velocity measurements for (a) sand, (b) sandy loam and (c) silt loam sites. The error bars for the envelope maximum values are based on the standard deviation of the mean value for each date and are very small and not shown. Error bars for $\frac{1}{\varepsilon_r}$ values are very small (see Steelman and Endres, 2010 for further details) and not shown.

For comparison, the corresponding time-series for the reciprocal of the permittivity $\frac{1}{\varepsilon_r}$ derived from the DGW velocity measurements are also given. It can be observed that both time series exhibit very similar long-term (i.e., seasonal) and short-term (i.e., semi-monthly) variations that coincide with changing soil water content conditions. The similarities of these time-series provide further evidence that the early-time amplitude method can be used to extract near-surface permittivity information.

To quantify the relationship between early-time envelope maximum $E_{\max}$ and the permittivity values from the DGW velocity measurements, we have fitted these data using $E_{\max} = 1/(m\varepsilon_r + q)$ which is a form consistent with the theoretical results of Di Matteo et al. (2013). The values of the parameters determined with 95% confidence bounds for the fitted inverse relationship are m=0.25±0.03 and q=0.14±0.13, and results of this analysis are shown in Figure 5.10.

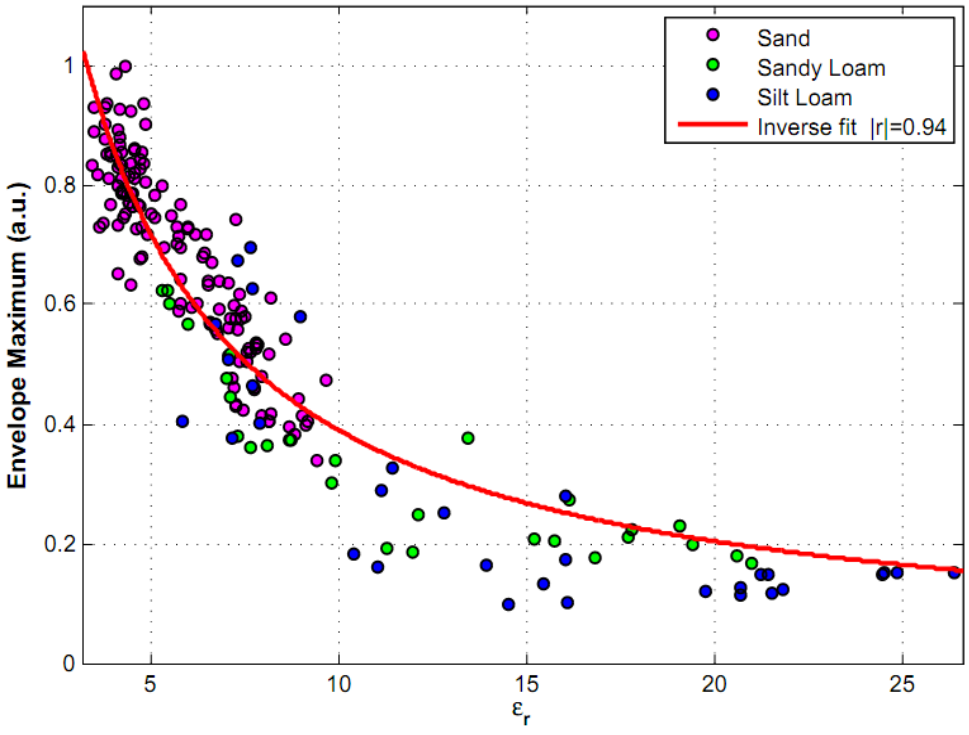

Figure 5.10. Early-time envelope maximum as a function of the corresponding ε_r values derived from the DGW velocity measurements for all three sites. Curve is the best fitting version of the relationship based on previous theoretical work (Di Matteo et al., 2013). Error bars for the envelope amplitude values are very small and not shown.

It can be seen in this figure that this derived relationship gives a good fit to the data that has a high correlation coefficient of r = 0.94. This semi-empirical relationship fits well the data collected in the three sites during different seasons and is also in agreement with previous studies where radar data were acquired on different materials using different radar systems (Pettinelli et al., 2007; Ferrara et al., 2013a). It is important to note that the sensitivity of the early-time technique seems to be higher for ε_r lower than about 12, whereas above this value the same relative variation in bulk soil permittivity produces a smaller change in the envelope maximum. This could also be an explanation for the increased variability observed under wet conditions (Figure 5.6).

5.6.2 Estimation of Soil Water Content

To examine the value of the early-time amplitude method for monitoring soil water content conditions through its dependence on near-surface permittivity, we have used our fitted relationship to convert the envelope maximum $E_{\max}$ data into permittivity values. These values were used to predict the soil water content employing the Topp equation (Topp et al., 1980); the comparison of various petrophysical relationships – equation (5.3-7) (Topp et al., 1980; Nadler et al., 1991; Roth et al. 1992; Curtis et al., 2001; Jacobsen and Schjønning 1993) –, found that the Topp equation provided accurate predictions of water content at these three sites using the DGW-derived permittivity values (Steelman and Endres, 2011).

$$\theta = -5.3\cdot10^{-2} + 2.92\cdot10^{-2}\varepsilon_r - 5.5\cdot10^{-4}\varepsilon_r^2 + 4.3\cdot10^{-6}\varepsilon_r^3 \quad (5.3)$$

$$\theta = -7.25\cdot10^{-2} + 3.67\cdot10^{-2}\varepsilon_r - 12.3\cdot10^{-4}\varepsilon_r^2 + 15\cdot10^{-6}\varepsilon_r^3 \quad (5.4)$$

$$\theta = -7.28\cdot10^{-2} + 4.48\cdot10^{-2}\varepsilon_r - 19.5\cdot10^{-4}\varepsilon_r^2 + 36.1\cdot10^{-6}\varepsilon_r^3 \quad (5.5)$$

$$\theta = -2.86 + 2.435\varepsilon_r - 3.421\cdot10^{-2}\varepsilon_r^2 + 2.37\cdot10^{-4}\varepsilon_r^3 \quad (5.6)$$

$$\theta = -7.01\cdot10^{-2} + 3.47\cdot10^{-2}\varepsilon_r - 11.6\cdot10^{-4}\varepsilon_r^2 + 18\cdot10^{-6}\varepsilon_r^3 \quad (5.7)$$

Our early-time amplitude prediction of water content was then compared with measured water contents over a range of depth intervals obtained from the gravimetric analysis of the soil samples. The results of this comparison are shown in Figure 5.11 for five depth intervals with the corresponding root mean square errors (*RMSE*) for each interval listed in Table 5.1. It can be seen in Figure 5.11 that the predictions cluster along the $\theta_w^{predicted} = \theta_w^{measured}$ line in all cases.

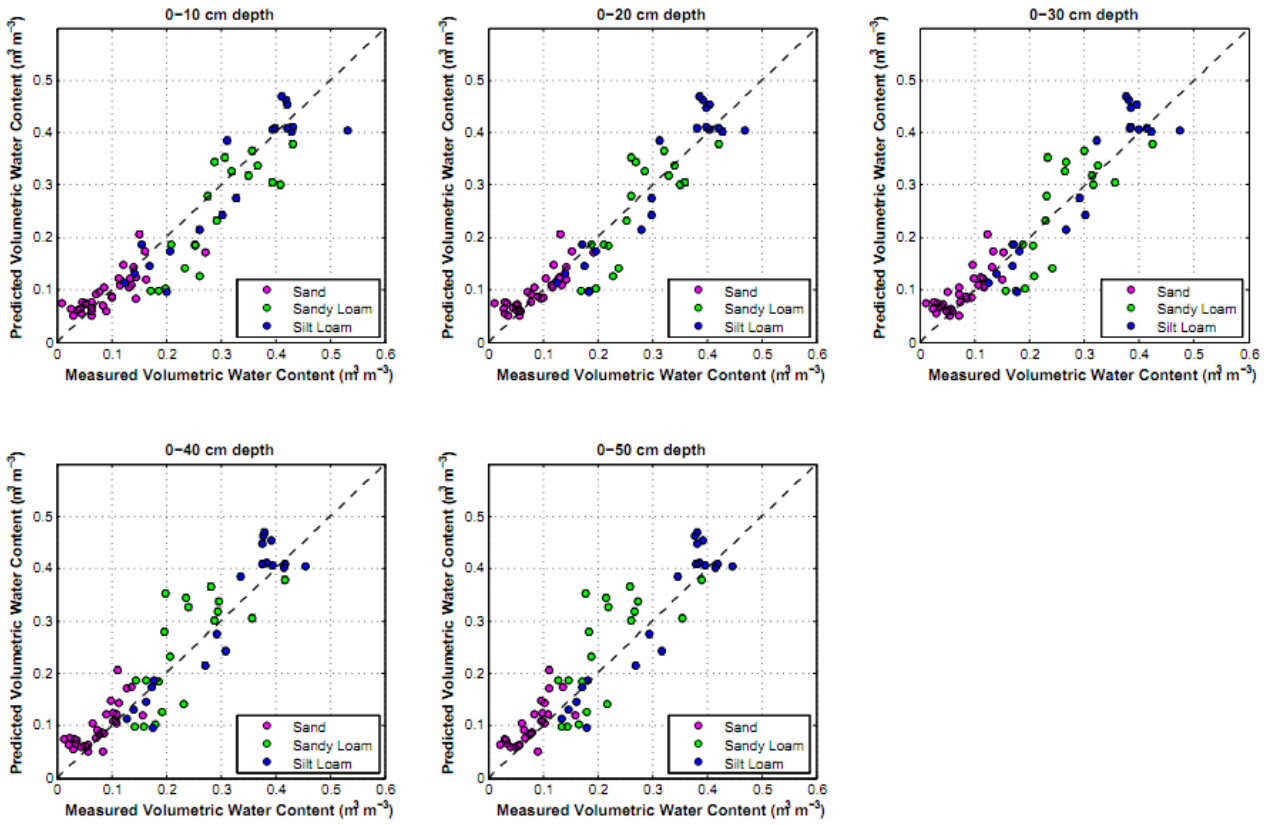

Figure 5.11. Comparison between the predicted volumetric water content from the early-time amplitude measurements and the volumetric water content derived from soil sampling for cumulative depth intervals to 0.50 meters. The black dashed line indicates $\theta_w^{predicted} = \theta_w^{measured}$ data. The error bars for the early-time predicted water content values are very small and not shown.

Table 5.1. Values of the root mean square error (RMSE) between the early-time predicted water content values and the field water content measurements for intervals in the upper 0.5m of soil.

INTERVAL	RMSE
0 - 10 cm depth	0.049
0 - 20 cm depth	0.044
0 - 30 cm depth	0.045
0 - 40 cm depth	0.049
0 - 50 cm depth	0.054

However, differences are discernible in the RMSE values where the minimum error was determined for the depth interval 0.00-0.20 meters, suggesting that this zone could correspond to the effective sampling depth of this technique using the 900 MHz antennas. This results are also confirmed by the GPR penetration depths calculated according to different models (Figure 5.12) proposed by proposed by Du (1996), Van Overmeeren et al. (1997), Sperl (1999), Galagedara et al. (2005), and Grote et al. (2010). Indeed, Figure 5.12 shows the predicted sampling depth for each of the models discussed above for data acquired with a 900 MHz antenna over the range of permittivities that were observed in dry to saturated soils. This figure shows that these relationships predict significantly different sampling depths, especially for drier soils (lower permittivity) (Grote et al., 2010). The sampling depths predicted by these models correspond to the upper 0.20 meters of soil, in agreement with sampling depths estimated using both the DGW method (Steelman and Endres, 2010) and the early-time technique, used at these three sites.

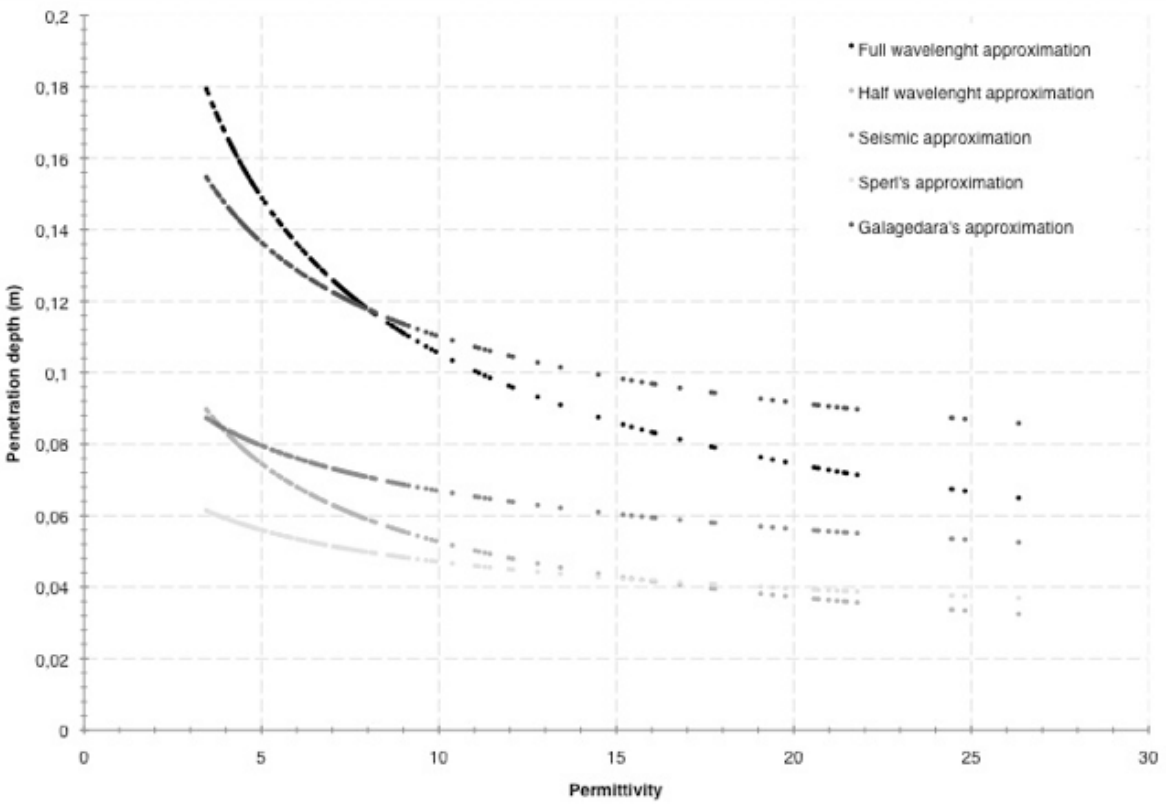

Figure 5.12. Penetration depth of the GPR signal according to different models: Full wavelength approximation, Half wavelength approximation, Van Overmeeren's (or seismic) approximation, Sperl's approximation, Galagedara's approximation.

5.6 Conclusions

In this work, we have examined the use of the early-time amplitude technique for GPR under natural field conditions using a data set that covers the range of near-surface conditions for three different soil textures. This method uses the envelope maximum of the complex trace in a temporal window that coincides with the first half cycle of the GPR signal to monitor near-surface dielectric permittivity. Our study shows that this technique can yield information from reflection profiling data that is consistent with results obtained from the DGW velocity analysis using CMP sounding data done by Steelman and Endres (2010) and Steelman et al. (2012). Further, we have shown that by calibrating the envelope maximum data using the dielectric permittivity estimates from the DGW measurements and a relationship based on a theoretical analysis by Di Matteo et al. (2013), accurate predictions of soil water content can be obtained from the widely used equation of Topp et al. (1980).

While both the early-time amplitude and DGW techniques have the capacity to monitor shallow soil water content variations, the use of the early-time amplitude method has some practical advantages in its uses. The DGW method is a "time of flight" approach that requires accurate identification of a specific phase of this event. This requirement can be difficult to achieve if there is either significant spatial and temporal variation in the near-surface wavefield; these conditions could make it difficult to determine an appropriate antenna offset to obtain this objective, impeding the application of the DGW method. In particular, these conditions would complicate the use of the fixed-offset DGW method used to gather spatial data. The use of the near-field waveform by the early-time amplitude method avoids this limitation and potentially allows its application over a wide range of surface conditions. Further, early-time amplitude method could be performed using lower-cost or cart-mounted GPR systems without separable antennas for shallow soil water content mapping if the antenna separation meets the near-field requirements.

Our study also examined the variability of the envelope maximum along the two-meter survey line for each survey date. The amount of variability grew with increasing near-surface permittivity, suggesting that a larger degree of heterogeneity will form in near-surface conditions as the soil becomes wetter. Lateral averaging with window widths of 0.5-1.0 meters can significantly attenuate this small-scale variability. While the physical mechanism for this variability has not been established, it may contain useful information about small-scale heterogeneity in soil properties. This observation could also be due to the increased uncertainty of the method with increased water content.

Our results clearly indicate that, once calibrated, the early-time amplitude technique could provide the type of near-surface dielectric permittivity information obtained from DGW analysis without the inherent complications of that technique. In addition, early-time amplitude technique can be applied to standard reflection profiling, permitting the extraction of shallow near-surface information while simultaneously obtaining reflection data from deeper intervals.

Chapter 6

Final Remarks and Conclusions

This thesis has focused on the study and application of electromagnetic (EM) techniques for estimating the material EM parameters and, in particular, on a novel use of GPR (Ground Penetrating Radar) analysis to obtain valuable information on the dielectric properties of an investigated medium. For comparison and calibration, other techniques like NMR (Nuclear Magnetic Resonance), TDR (Time Domain Reflectometry), more conventional GPR data analysis (e.g., CMP - Common Mid Point, etc.), and gravimetric measurements were also applied to measure the soil dielectric permittivity, conductivity, and water content.

The aim of this thesis was to validate previous observations regarding the ability of GPR to characterize the soil EM parameters aided by a novel data analysis approach: the so-called early-time method. It uses the amplitude attribute information of the early-time part of a GPR signal acquired with a standard common-offset ground-coupled antenna configuration.

Under these conditions, where the antenna offsets are small, the direct signal (i.e., the early-time signal) is a complex combination of the air and ground waves and carries information on the physical properties of the surrounding material. This is because amplitude, shape, and duration of this signal, change as a function of the EM properties of the material.

This novel GPR data analysis method uses the complex trace analysis principles, and each acquired waveform is considered as the real part of a complex trace, whose imaginary part is given by the quadrature component (obtained through a Hilbert transform) of the real part. In particular, the envelope amplitude, which is given by the module of the resultant complex transient waveform, is used as an early-time signal attribute, function of the shallow subsurface permittivity and conductivity.

If chapter 2, after an overview about GPR technique fundamentals, focuses on the early-time technique explanation and data analysis methodology, chapter 3 demonstrates the reliability of this approach to evaluate the shallow permittivity variations in an investigated medium. A controlled, lab-scale experiment was performed using a portable unilateral NMR as a control technique to verify the ability of the GPR early-time signal method to detect the lateral variations of the dielectric properties produced, changing the water content in the shallow portion of the tested

material. In this experimental first work a very high correlation was obtained between NMR signal intensity and the average envelope of the early-time radar signal.

The main results of this chapter have verified that:

- the systematic change in amplitude and time length of ground-coupled GPR early-time signals is induced by spatial variations in shallow soil dielectric properties, which, in this specific case, depends only on the water content distribution in the medium subsurface;
- the correlation between the dielectric parameter values and the early-time GPR amplitude attribute is very strong in the first half cycle of the GPR signals;
- the proposed early-time GPR technique can be used for quantitative analysis of surface soil moisture content, where the method can be calibrated using an independent procedure;
- this new GPR data analysis approach is highly suitable to create detailed maps of the shallow subsurface electric permittivity (e.g., water content) variations;
- the evaluation of the shallow soil dielectric properties using this novel technique instead of more traditional configuration radar systems, could represent a practical way for fast and high spatial resolution materials characterization.

Chapter 4 shows, in a more systematic way, the reliability of this approach to evaluate the shallow dielectric permittivity and conductivity variations in an investigated medium. In particular, numerical and experimental investigations are discussed with the aim of analysing the features related to the early-time method. The obtained results (both simulated and experimental), and a strong correlation between the early-wavelet amplitudes and the shallow-soil dielectric conductivity, derived from TDR measurements, have confirmed that the near-surface electromagnetic properties of the material could be directly extracted from the GPR early-time amplitude technique.

The main goals of this chapter were:

- the realization of an efficient and accurate simulation setup for the numerical analysis of the early-time features, paying a specific attention to simulate systems as similar as possible to real GPRs;
- the check of the numerical implementation reliability to adequately simulate the commercial GPR system, comparing experimental and simulated early-time signal waveform picked up by the antenna;
- the calculation of how the ground dielectric constant is varied in the early-time traces, finding, again, an inverse relationship between the early-time envelope amplitudes and dielectric constant always occurs;
- the possibility to evaluate, for the first time, not only permittivity variations, but also the soil dielectric conductivity changes using the first-arrival signal attributes analysis;

- an excellent agreement between both the experimental and numerical early-wavelet amplitudes and the shallow-soil dielectric conductivity derived from TDR measurements;
- the possibility to use this alternative approach as a efficient and high precision tool also to characterize the shallow subsurface conductivity variations.

Until now, several controlled experiments and numerical simulations have been conducted to study the effects of EM parameter variations on the antenna-material coupling. Thus, it is necessary to test the early-time technique in 'real-life' applications.

The work in this thesis is concluded with Chapter 5, in which is presented an extensive and exceptional field study to examine the early-time amplitude technique under natural field conditions. The early-time results acquired using the enveloped amplitude of the first part of GPR signals were compared with the bulk dielectric permittivity obtained from concurrently collected CMP and gravimetric water content measurements, to monitor a complete annual cycle of soil water content variations typical of mid-latitude climates at three sites with different soil textures. The obtained results demonstrate that from the early portion of the GPR signal analysis is possible to achieve near-surface permittivity information consistent with results obtained from direct ground wave velocity measurements, and accurate predictions of shallow soil moisture conditions.

The main outcomes of this chapter were:

- the capacity of the early-time GPR technique to assess a complete annual cycle of soil moisture conditions in three different textural sites, under natural field conditions, and for a complete range of seasonal soil conditions, where surface roughness, lithology, lateral heterogeneities, vegetation and water content dynamics are not controlled;
- the practical advantages of the use of the early-time amplitude technique in a wide range of surface conditions and system configurations. It can provide the type of near-surface dielectric permittivity information obtained from DGW analysis without the inherent complications of that technique (e.g., separable antennas, etc.): early-time amplitude method could be performed using lower-cost and cart-mounted GPR systems without separable antennas for shallow soil water content mapping. In addition, early-time amplitude technique can be applied to standard reflection profiling, allowing the extraction of shallow near-surface information, obtaining simultaneously reflection data from deeper intervals;
- the variability of the early-time signal attributes along the two meter survey line for each survey date. The amount of variability grows with increasing near-surface permittivity, suggesting that a larger degree of heterogeneity will be in near-surface conditions once the soil becomes wetter, including also useful information in the early-time signals about small-scale heterogeneity of soil properties;
- the potential of the early portion of the GPR signal to be a valuable method for

quantitatively monitoring near-surface soil water content under natural field conditions;

- the capability of the early-time GPR technique for accurate predictions of shallow soil water content.

The main findings of this thesis have established the effectiveness of the early-time GPR signal technique to determine EM material parameters and therefore soil water content. If this new radar approach represent an efficient non-invasive soil dynamics monitoring tool, the unique results presented in this thesis could represent a new operating and processing strategies to evaluate in a fast and high-resolution way EM material parameters.

Moreover, demonstrating the capacity of early-time GPR method for characterizing shallow EM parameters, both in controlled lab-scale and field scale experiments, and with numerical simulations, further field studies should be conducted with the aim of providing a more detailed evaluation of the influence of a larger range of EM parameters and water content values on the GPR response. Moreover, more improvements on numerical modeling should be achieved by better simulating real GPR antennas and by considering additional system parameterizations. Nevertheless, even if other improvements need to be done to further develop and test this approach, the early-time amplitude technique has the potential to be an efficient means of using GPR data for obtaining an estimation of soil information in a variety of different applications in geophysics and hydro-geophysics, environmental studies, civil engineering, mineral exploration, snow and ice controlling and/or water resources management.

References

Annan, A.P. 1973. Radio interferometery depth sounding: Part I – Theoretical discussion. Geophysics, 38, 557–580.

Annan, A.P. 2002. GPR-History, Trends, and Future Developments, Subsurface Sensing Technologies and Applications 3 (4), 253-270.

Annan, A. P. 1992. Ground Penetrating Radar Workshop Notes. Sensors and Software Inc., Mississauga, Ontario.

Annan, A.P. 2004. Ground Penetrating Radar Principles, Procedures & applications. Sensors & Software Inc., Canada.

Annan, A.P. 2005. Ground-Penetrating Radar. In D.K. Butler, (Ed.), Near-Surface Geophysics, 357–438. Tulsa (OK): Society of Exploration Geophysicists.

Annan, A.P., and S.W. Cosway. 1992. Ground penetrating radar survey design, Proceedings of the Symposium on the Application of Geophysics to Engineering and Environmental Problems, SAGEEP'92, Oakbrook, IL, April 26–29, 329–351.

Annan, A.P., and S.W. Cosway. 1994. GPR frequency selection. Proceedings of the Fifth International Conference on Ground Penetrating Radar, Kitchener, Ontario, Canada, June 12–16, 747–760.

Annan, A.P., and J.L. Davis. 1978. High frequency electrical methods for the detection of freeze-thaw interfaces. In Proceedings of the Third International Conference on Permafrost, 1, 495–500.

Annan, A.P., W.M. Waller, D.W. Strangway, J.R. Rossiter, J.D. Redman, and R.D. Watts. 1975. The electromagnetic response of a low-loss, 2-layer, dielectric earth for horizontal electric dipole excitation. Geophysics, 40, 2, 285–298.

Barone P.M., A. Di Matteo, F. Graziano, E. Mattei, and E. Pettinelli. 2010. GPR application to historical buildings structural control. Near Surface Geophysics, 8(5), 407–413. doi: 10.3997/1873-0604.2010017

Benson, R.C., Glaccum, R.A. and Noel, M.R., 1984. Geophysical Techniques for Sensing Buried Wastes and Waste Migration. US EPA Contract No. 68-03-3053. Environmental Monitoring Systems Laboratory. Office of R&D. US EPA, Las Vegas, Nevada 89114, 236.

Bevington, P.R. 1969. Data Reduction and Error Analysis for the Physical Sciences. McGraw-Hill Book Co.

Bittelli, M., 2011. Measuring soil water content: a review. HortTechnology 21(3), 293-300.

Blümich, B., S. Anferova, K. Kremer, S. Sharma, V. Hermann, and A.L. Segre. 2003. Unilateral nuclear magnetic resonance for quality control: The NMR-MOUSE. Spectroscopy 18, 18–29.

Blümich, B., P. Blümler, G. Eidmann, A. Guthausen, R. Haken, U. Schmitz, et al. 1998. The NMR MOUSE: Construction, excitation, and applications. Magnetic Resonance Imaging 16, 479–484.

Blümich, B., F. Casanova, M. Dabrowski, E. Danieli, L. Evertz, A. Haber, et al. 2011. Small-scale instrumentation for nuclear magnetic resonance of porous media. New Journal of Physics 13, 015003.

Brewster, M.L. and Annan, A.P. 1994. Ground-penetrating radar monitoring of a controlled DNAPL release: 200 MHz radar : Geophysics 59, 1211-1221.

Campbell, J.E. 1990. Dielectric properties and influence of conductivity in soils at one to fifty megahertz. Soil Science Society of America Journal 54, 332–341.

Capitani, D., N. Proietti, M. Gobbino, L. Soroldoni, U. Casellato, M. Valentini, and E. Rosina. 2009. An integrated study for mapping the moisture distribution in an ancient damaged wall painting. Analytical and Bioanalytical Chemistry 395, 2245–2253.

Cassidy, N.J. 2009. Electrical and Magnetic Properties of Rocks, Soils and Fluids. In H.M. Jol, (Ed.), Ground Penetrating Radar: Theory and Applications, 41–72. Amsterdam: Elsevier.

Chelidze, T.L. and Gueguen, Y., 1999. Electrical spectroscopy of porous rocks: A review – I. Theoretical models. Geophysical Journal International 137, 1–15.

Chelidze, T.L., Gueguen, Y. and Ruffet, C. 1999. Electrical spectroscopy of porous rocks: A review – II. Experimental results and interpretation. Geophysical Journal International 137, 16–34.

Clennell, B., A. Borysenko, I. Burgar, R. Sedev, and J. Ralston. 2007. Dielectric and combined NMR/capillary pressure methods for monitoring liquid/air and liquid/liquid interface evolution: Application to rock and mineral wettability studies. International Symposium of the Society of Core Analysts (SCA2007-39), Calgary, Canada.

Comite, D., A. Galli, C. Ferrara, and E. Pettinelli, 2014. Relations Between GPR Early-Time Signal Attributes and Ground Permittivity: A Numerical Investigation. Proceedings of the 8th European Conference on Antennas and Propagation (EuCAP), The Hague, April 2014.

Conyers, L.B., and D. Goodman. 1997. Ground-Penetrating Radar: An Introduction for Archaeologists. Altimira Press, Walnut Creek.

Cook, J.C., 1973. Radar Exploration Through Rock in Advance of Mining, Trans. Society Mining Engineers, AIME 254, 140-146.

Cowan, W.R. 1975. Quaternary geology of the Woodstock area. Southern Ontario. Ontario. Ministry of Natural Resources, Division of Mines.

Curtis, J.O. 2001. Moisture effects on the dielectric properties of soils. IEEE Trans. Geosci. Remote Sens. 39, 125–128.

Dane J.H., and G.C. Topp. 2002. Methods of Soil Analysis, Part4 – Physical Methods. SSSA BOOK SERIES NO.5, Wisconsin, USA.

Daniels, J.J., Brower, J., Baumgartner, F., 1998. High resolution GPR at Brookhaven National Laboratory to delineate complex subsurface targets. J. Environ. Eng. Geophys. 3 (1), 1–5.

Daniels, D.J. (editor), 2004. Ground Penetrating Radar – 2nd Edition. The Institution of Electrical Engineers, London, UK.

Davis, J.L., and A.P. Annan, 1989. Ground penetrating radar for high-resolution mapping of soil and rock stratigraphy. Geophysical Prospecting 37, 531–551.

de Coulon, F. 1986. Signal theory and processing, Artech House, Dedham (MA) 11, 381–391.

Di Matteo, A., E. Pettinelli, and E.C. Slob. 2008. Early-Time GPR Signal Measurements and Simulations to Estimate Shallow Soil Permittivity. Proceedings of the 12th Conference on Ground Penetrating Radar. June 16-19. Birmingham, UK.

Di Matteo, A., E. Pettinelli, and E.C. Slob. 2013. Early-time GPR signal attributes to estimate soil dielectric permittivity: a theoretical study. IEEE Transactions on Geoscience and Remote Sensing 51(3), 1643-1654.

Di Pasquo, B., E. Pettinelli, G. Vannaroni, A. Di Matteo, E. Mattei, A. De Santis, P.A. Annan, D.J. Redman. 2007. Design and construction of a large test site to characterize the GPR response in the vadose zone. Proceedings of the 2007 4th International Workshop on Advanced Ground Penetrating Radar. June 27-29. Naples, Italy.

Di Tullio, V., N. Proietti, M. Gobbino, D. Capitani, R. Olmi, S. Priori, et al. 2010. Non- destructive mapping of dampness and salts in degraded wall paintings in hypogeous building: The case

of St. Clement at mass fresco in St. Clement Basilica, Rome. Analytical and Bioanalytical Chemistry 396, 1885–1896.

Du, S. 1996. Determination of water content in the subsurface with the ground wave of ground penetrating radar. PhD thesis, Fakultät für Geowissenschaften der Ludwig-Maximilians-Universität München.

Du Trémolet de Lacheisserie É., D. Gignoux, and M. Schlenker. 2005. Magnetism Fundamentals, USA: Springer.

Engheta, N., C.H. Papas, and C. Elachi. 1982. Radiation patterns of interfacial dipole antennas. Radio Science 17, 1557–1566.

Farrar, T.C., and E.D. Becker. 1971. Pulse and Fourier Transform NMR. Academic Press, London.

Ferrara, C., P.M. Barone, S.E. Lauro, D. Capitani, V. Di Tullio, E. Mattei, N. Proietti, and E. Pettinelli. 2011. Integrated GPR and unilateral NMR approach to estimate water content in a porous material, in Proceedings of the 6th International Workshop on Advanced Ground Penetrating Radar, Aachen.

Ferrara, C., V. Di Tullio, P.M. Barone, E. Mattei, S.E. Lauro, N. Proietti, D. Capitani, and E. Pettinelli. 2013a. Comparison of GPR and Unilateral NMR for water content measurements in a laboratory scale experiment. Near Surface Geophysics 11. doi: 10.3997/1873-0604.2012051

Ferrara, C., D. Comite, P.M. Barone, S.E. Lauro, E. Mattei, G. Vannaroni, A. Galli, and E. Pettinelli. 2013b. An Evaluation of the Early-Time GPR Amplitude Technique for Electrical Conductivity Monitoring, in Proceedings of the 6th International Workshop on Advanced Ground Penetrating Radar, Nantes 2013.

Ferrara, C., P.M.Barone, C. Steelman, E. Pettinelli, and A.L. Endres, 2013c. Monitoring shallow soil water content under natural field conditions using the early-time GPR signal technique, in Vadose Zone Journal, DOI:10.2136/vzj2012.0202

Galagedara, L.W., G.W. Parkin, J.D. Redman, P. von Bertoldi, and A.L. Endres. 2005. Field studies of the GPR ground wave method for estimating soil water content during irrigation and drainage. Journal of Hydrology 301, 182–197. doi: 10.1016/j.jhydrol.2004.06.031

Giese K, and R. Tiemann. 1975. Determination of the complex permittivity from thin-sample time domain reflectometry improved analysis of the step response waveform. Advances Molecular Relaxation Processes 7, 45–59.

Goodman, D. 1994. Ground-Penetrating Radar Simulation in Engineering and Archaeology, Geophysics 59, 224-232.

Grayson, R.B., and A.W. Western. 1998. Towards areal estimation of soil water content from point measurements: time and space stability of mean response. Journal of Hydrology 207(1-2), 68-82.

Grote, K., S. Hubbard, and Y. Rubin. 2003. Field-scale estimation of volumetric water content using ground-penetrating radar ground wave techniques. Water Resources Research 39 (11), 5.1-5.13. doi:10.1029/2003WR002045

Grote, K., T. Crist, and C. Nickel. 2010. Experimental estimation of the GPR groundwave sampling depth, Water Resources Reasearch 46, W10520.

Holliger, K., and T. Bergmann. 2000. Finite-difference modelling of borehole georadar data. Proc. SPIE 4084, Eighth International Conference on Ground Penetrating Radar, 836 (April 27, 2000); doi:10.1117/12.383525; http://dx.doi.org/10.1117/12.383525

Holser, W.T., R.J.S. Brown, F.A. Roberts, O.A. Fredrikkson, and R.R. Unterberger. 1972. Radar logging of a salt dome, Geophysics 37, 889-906.

Huisman, J.A., S.S. Hubbard, J.D. Redman, and A.P. Annan. 2003a. Measuring soil water content with ground penetrating radar: a review. Vadose Zone Journal 2, 476–491.

Huisman, J.A., J.J.J.C. Smepvangers, W. Bouten, and G.B.M. Heuvelink. 2003b. Monitoring temporal development of spatial soil water content variation: comparison of ground penetrating radar and time domain reflectometry. Vadose Zone Journal 2, 519–529.

Huisman, J. A., C. Sperl, W. Bouten, and J.M. Verstraten. 2001. Soil water content measurements at different scales: accuracy of time domain reflectometry and ground-penetrating radar. Journal of Hydrology 245, 48-58.

Hwang, Y.K., A.L. Endres, S.D. Piggott, and B.L. Parker. 2008. Long-Term Ground Penetrating Radar Monitoring of a Small Volume DNAPL Release in a Natural Groundwater Flow Field Journal of Contaminant Hydrology 97 (1-2), 1-12. doi:10.1016/j.jconhyd.2007.11.004

Jacobsen, O.H., and P. Schjønning. 1993. A laboratory calibration of time domain reflectometry for soil water measurements including effects of bulk density and texture. J. Hydrol. 151, 147–157.

Jones, S.B., J.M. Wraith, and D. Or. 2002. Time domain Reflectometry measurement principles and applications, Hydrological Processes 16, 141-153. doi:10.1002/hyp.513

Jol, H.M. 1996. Digital Ground Penetrating Radar (GPR): A New Geophysical Tool for Coastal Barrier Research (Examples from the Atlantic, Gulf and Pacific Coasts U.S.A.), Journal of Coastal Research, Fall 1996.

Jol, H.M. 2009. Ground Penetrating Radar: Theory and applications, Elsevier, UK.

Ju, W., P. Gao, J. Wanga, Y. Zhou, and X. Zhang. 2010. Combining an ecological model with remote sensing and GIS techniques to monitor soil water content of croplands with a monsoon climate. Agricultural Water Manage 97(8), 1221-1231. doi: 10.1016/j.agwat.2009.12.007

Klysz, G., X. Ferrieres, J.-P. Balayssac, and S. Laurens. 2006. Simulation of direct wave propagation by numerical FDTD for a GPR coupled antenna, NDT&E International, 39(4), 338–47.

Lambot, S., E.C. Slob, D. Chavarro, M. Lubczynski, and H. Vereecken. 2008. Measuring soil surface water content in irrigated areas of southern Tunisia using full-wave inversion of proximal GPR data. Near Surface Geophysics 16, 403-410. doi: 10.3997/1873-0604.2008028

Lampe, B. and K. Holliger. 2000. Finite-difference modelling of ground-penetrating radar antenna radiation , 556 bis 560, Proceedings of the 8th International Conference on Ground Penetrating Radar, Gold Coast, Australia, May 23-26, 2000.

Legchenko A., and P. Valla. 2002. A review of the basic principles for proton magnetic resonance sounding measurements. Journal of Applied Geophysics 50, 3–19.

McNaughton, C.H. 2011. Monitoring a Shallow Gasoline Release using GPR at CFB Borden, Ph.D. Thesis, Department of Earth and Environmental Science, University of Waterloo, Ontario, Canada.

McNeill, J.D. 1980. Electrical conductivity of soils and rock. Technical Note TN-5, Geonics Limited, Mississauga, Ontario, Canada, 21 p.

Müller-Petke M., R. Dlugosch, and U. Yaramanci. 2011. Evalauation of surface nuclear magnetic resonance-estimated subsurface water content. New Journal of Physics 13, 095002.

Nadler, A., S. Dasberg, and I. Lapid. 1991. Time domain reflectometry measurements of water content and electrical conductivity of layered soil columns. Soil Science Society of American Journal 55, 938–943.

Neal, A. 2004. Ground-penetrating radar and its use in sedimentology: principles, problems and progress. Earth-Science Reviews 66, 261–330.

Oden, C.P., G.R. Olhoeft, D.L. Wright, and M.H. Powers. 2008. Measuring the electrical properties of soil using a calibrated ground-coupled GPR system. Vadose Zone Journal 7, 171–183.

Olhoeft, G.R. 1992. Geophysical detection of hydrocarbon and organic chemical contamination. Proceedings of the Symposium on the Application of Geophysics to Engineering and Environmental Problems: 2, April 26–29, Oak Brook, IL. Society of Engineering and Mining Exploratino Geophysics, Golden, CO, 587–595.

Olhoeft, G.R. 1998. Electrical, magnetic, and geometric properties that determine groundpenetrating radar performance. Proceedings, Seventh International Conference on Ground-Penetrating Radar, May 27–30, 1998, University of Kansas, Lawrence, Kansas, USA, 177–182.

Peters, L. Jr., J.J. Daniels, J.D. Young. 1994. Ground penetrating radar as a subsurface sensing tool. Proc. IEEE 82 _12, 1802–1822, December.

Pettinelli, E., G. Vannaroni, B. Di Pasquo, E. Mattei, A. Di Matteo, A. De Santis, and A.P. Annan. 2007. Correlation between near-surface electromagnetic soil parameters and early-time GPR signals: an experimental study. Geophysics 72 (2), A22-A28. doi: 10.1190/1.2435171

Pettinelli, E., A. Di Matteo, S.E. Beaubien, E. Mattei, S.E. Lauro, A. Galli, and G. Vannaroni. 2014. A controlled experiment to investigate the correlation between early-time signal attributes of

ground-coupled radar and soil dielectric properties. Journal of Applied Geophysics, 101, 68-76, 2014.

Rabiner, L.R., and B. Gold. 1975. Theory and Application of Digital Signal Processing. Englewood Cliffs, N.J., Prentice Hall.

Redman, J.D., E.W. Kunert, M. Gilson, J.A. Pilon, A.P. Annan. 1996. Borehole Radar for Environmental Applications: Selected Case Studies : Proceedings of the Sixth International Conference on Ground Penetrating Radar (GPR.96), September 30-October 3,1996, Sendai, Japan.

Reynolds, J.M. 1997. An introduction to Applied and Environmental Geophysics, John Wiley and Sons Ltd, Chichester.

Ridler, M.E., I. Sandholt, M. Butts, S. Lerer, E. Mougin, F. Timouk, L.Kergoat, and H. Madsen. 2012. Calibrating a soil–vegetation–atmosphere transfer model with remote sensing estimates of surface temperature and soil surface moisture in a semi arid environment. Journal of Hydrology 1-12, 436–437. doi:10.1016/j.jhydrol.2012.01.047

Ritsema, C.J., 1999. Special issue: preferential flow of water and solutes in soils. Journal of Hydrology 215(1-4), 1-3.

Robinson, D.A., C.S. Campbell, J.W. Hopmans, B.K. Hornbuckle, S.B. Jones, R. Knight, F. Ogden, J. Selker, and O. Wendroth. 2008. Soil moisture measurements for ecological and hydrological watershed scale observatories: A review. Vadose Zone Journal 7, 358–389. doi:10.2136/vzj2007.0143

Robinson, D.A., S.B. Jones, J.M. Wraith, D. Or, and S.P. Friedman. 2003. A review of advances in dielectric and electrical conductivity measurement in soils using time domain reflectometry. Vadose Zone Journal 2, 444–475. doi: 10.2113/2.4.444

Roth, C.H., M.A. Malicki, and R. Plagge. 1992. Empirical evaluation of the relationship between soil dielectric constant and volumetric water content as the basis for calibrating soil moisture measurements by TDR. J. Soil Sci. 43, 1–13.

Rubin, Y., and S.S. Hubbard. 2005. Hydrogeophysics. Springer, New York.

Russell, H.A.J., Sharpe, D.R., and Bajc, A.F. 2007. Sedimentary signatures of the Waterloo Moraine, Ontario, Canada. In M.J. Hambrey, P. Christoffersen, N.F. Glasser, and B. Hubbard (Eds.), Glacial Sedimentary Processes and Products (pp. 85–108), Special Publication Number 39 of the Internatioinal Association of Sedimentologists.

Sbartai, Z.M., S. Laurens, J. Rhazi, J.P. Balayssac, and G. Arliguie. 2007. Using radar direct wave for concrete condition assessment: Correlation with electrical resistivity. Journal of Applied Geophysics 62, 361–374.

Sheriff, R.E., and R.E. Geldart. 1982. Exploration Seismology, Volume 1: History, Theory, and Data Acquisition, Cambridge University Press, NewYork, 253 pp.

Sperl, C. 1999. Determination of spatial and temporal variations of the soil water content in an agro-ecosystem with ground penetrating radar (in German). PhD dissertation, Technische Universitat München, Munich, Germany.

Seneviratne, S. I., T. Corti, E.L. Davin, M. Hirschi, E.B. Jaeger, I. Lehner, B. Orlowsky, and A. J. Teuling. 2010. Investigating soil moisture climate interactions in a changing climate: A review. Earth Sci. Rev. 99, 125–161. doi:10.1016/j.earscirev.2010.02.004

Sharma, S., F., Casanova, W. Wache, A.L. Segre, and B. Blümich. 2003. Analysis of historical porous building materials by NMR MOUSE. Magnetic Resonance Imaging 21, 249.

Smith, G.S. 1984. Directive properties of antennas for transmission into a material half-space: IEEE Trans. Antennas propagate, Vol. AP-32, pp. 232–246.

Steelman, C.M., and A.L. Endres. 2010. An examination of direct ground wave soil moisture monitoring over an annual cycle of soil conditions. Water Resources Research 46, W11533. doi:10.1029/2009WR008815

Steelman, C.M., and A.L. Endres. 2011. Comparison of petrophysical relationships for soil moisture estimation using GPR ground waves. Vadose Zone J. 10, 270–285. doi: 10.2136/vzj2010.0040

Steelman, C.M., A.L. Endres, and J.P. Jones. 2012. High-resolution ground-penetrating radar monitoring of soil moisture dynamics: Field results, interpretation, and comparison with unsaturated flow model. Water Resources Research 48, W09538. doi:10.1029/2011WR011414

Steelman, C.M. 2012. Evaluating Vadose Zone Moisture Dynamics using Ground-Penetrating Radar, Ph.D. Thesis, Department of Earth and Environmental Science, University of Waterloo, Ontario, Canada.

Tallon, L.K., and B.C. Si. 2004. Representative Soil Water Benchmarking for Environmental Monitoring. Journal of Environmental Informatics 4 (1), 28-36.

Taner, M.T., F. Koehler and R.E. Sheriff. 1979. Complex seismic trace analysis. Geophysics 44, 1041-1063. doi: 10.1190/ 1.1440994

Taylor, J.R. 1997. An Introduction to Error Analysis. The Study of Uncertainties in Physical Measurements. Second Edition, University Science Book.

Thierbach, R., 1974. Electromagnetic Reflections in Salt Deposits. J. Geophys. 40, 633-637.

Topp, G.C., J.L. Davis, and A.P.Annan. 1980. Electromagnetic determination of soil water content: Measurements in coaxial transmission lines. Water Resour. Res. 16, 574–582.

Turin, G.L. 1960. An introduction to matched filters, IRE Trans. Information Theory, 6, 311–329.

Turner, G. 1993. The influence of subsurface properties on ground penetrating radar pulses. PhD dissertation, Macquarie University, Sydney.

Ulriksen, C.P.F., 1982. Application of Impulse Radar to Civil Engineering, Unpublished Ph.D. Thesis, Dept. of Engr, Geol., U. of Technology, Lund, Sweden, p. 175.

Unterberger, R.R., 1978. Radar propagation in rock salt. Geophys. Prosp. 26, 312-328.

Valerio, G., A. Galli, P. M. Barone, S. E. Lauro, E. Mattei, and E. Pettinelli. 2012. GPR detectability of rocks in a Martian-like shallow subsoil: a numerical approach, Planetary Space Science 46, 31-40.

van der Kruk, J., A. Klotzsche, F. Lavoué, G.A. Meles, A. Mester, R.W. Jacob, J.A. Doetsch, N. Linde, H. Maurer, A.G. Green, and H. Vereecken. 2011. High resolution hydrogeophysical imaging and characterization. Proceedings of the 15th International Water Technology Conference. IWTC-15. March 31 - April 02. Alexandria, Egypt.

van Overmeeren, R., S. Sariowan, and J. Gehrels. 1997. Ground penetrating radar for determining volumetric soil water content; results of comparative measurements at two test sites. Journal of Hydrology 197, 316–338.

Vereecken, H., J.A. Huisman, H. Bogena, J. Vanderborght, J.A. Vrugt, and J.W. Hopmans. 2008. On the value of soil moisture measurements in vadose zone hydrology: A review. Water Resources Research 44, W00D06. doi:10.1029/2008WR006829

Waite, A.H. and Schmidt, S.J., 1961. Gross errors in height indication from pulsed radar altimeters operating over thick ice or snow , IRE International Convention Record, Part 5, 38-54.

Walsh, D.O., E. Grunewald, P. Turner, and I. Frid. 2010. Javelin: A slim-hole and microhole NMR logging tool. Fast Times 15, 3, 67–72.

Wharton, R.P., G.A. Hazen, R.N. Rau, and D.L. Best. 1980. Electromagnetic propagation logging: Advances in technique and interpretation. The Society of Petroleum Engineers, 55th Annual Fall Meeting, Dallas, Texas, SPE 9267.

White, R. 1991. Properties of instantaneous seismic attributes, The Leading Edge 10, 7, 26-32.

Watanabe, K., and T. Wake. 2009. Measurement of unfrozen water content and relative permittivity of frozen unsaturated soil using NMR and TDR. Cold Regions Science and Technology 59, 34–41.

Watson, A.T., and C.T.P. Chang. 1997. Characterizing Porous Media with NMR Methods. Progress in Nuclear Magnetic Resonance Spectroscopy 31, 343–386.

Weihermüller, L., J.A. Huisman, S. Lambot, M. Herbst, and H. Vereecken. 2007. Mapping the spatial variation of soil water content at the field scale with different ground penetrating radar techniques. Journal of Hydrology 340, 205–216. doi:10.1016/j.jhydrol.2007.04.013

Xu, J., X. Ma, S.D. Logsdon, and R. Horton. 2012. Short, Multineedle Frequency Domain Reflectometry Sensor Suitable for Measuring Soil Water Content. Soil Science Society of American Journal 76(6), 1929-1937. doi:10.2136/sssaj2011.0361

Yaramanci U. 2004. New technologies in groundwater exploration – Surface Nuclear Magnetic Resonance. Geologica Acta 2, 109–120.

Yaramanci U., G. Lange, and M. Hertrich. 2002. Aquifer characterisation using Surface NMR jointly with other geophysical techniques at the Nauen/Berlin test site. Journal of Applied Geophysics 50, 47– 65.

Yilmaz O. 2001. Seismic data analysis. Society of Exploration Geophysicists, Tusla, OK.

Yoshikawa, K. and P.P. Overduin. 2005. Comparing unfrozen water content measurements of frozen soil using recently developed commercial sensors. Cold Regions Science and Technology 42, 250-256.

Zhang, T., P. Ligneul, B. Nicot, F. Pairoys, and M. Akbar. 2010. Dielectric Response of Carbonate Core-Plugs-Influence of Heterogeneous Rock Properties on Permittivity. SPE/DGS Saudi Arabia Section Technical Symposium and Exhibition, Al-Khobar, Saudi Arabia. doi:10.2118/136941-MS

Zhu, Q., K. Liao, Y. Xu, G. Yang, S. Wu and S. Zhou. 2012. Monitoring and Prediction of Soil Moisture Spatial-Temporal Variations from a Hydropedological Perspective: A Review. Soil Research 50(8), 625-637. doi:10.1071/SR12228